DESIGN OF POLYMERIC CARRIERS BASED ON GREEN TEA CATECHIN FOR CANCER THERAPY

LIANG KUN

NATIONAL UNIVERSITY OF SINGAPORE

2014

DESIGN OF POLYMERIC CARRIERS BASED ON GREEN TEA CATECHIN FOR CANCER THERAPY

LIANG KUN

(B.S.E), Duke University

A THESIS SUBMITTED

FOR THE DEGREE OF DOCTOR OF PHILSOPHY

NUS GRADUATE SCHOOL FOR INTEGRATIVE SCIENCES

AND ENGINEERING

NATIONAL UNIVERSITY OF SINGAPORE

2014

Declaration

I hereby declare that the thesis is my original work and it has been written by me in its entirety. I have duly acknowledged all the sources of information which have been used in the thesis.

This thesis has also not been submitted for any degree in any university previously.

_____

Liang Kun

18 Mar 2015

Acknowledgements

First and foremost, I would like to express my sincere gratitude to my Ph.D. supervisor Dr. Motoichi Kurisawa for his constant encouragement, support and guidance throughout the course of my endeavor. I would also like to thank my main supervisor, Associate Professor Lee Dong Yup (BTI / ChBE, NUS) and TAC chairman, Associate Professor Cao Tong (Dentistry, NUS) for their kind suggestions.

I would like to extend my appreciation to all the members of Nanomedicine group in Institute of Bioengineering and Nanotechnology (IBN) and Dr Gao Shujun. Their technical help, advice and support have been instrumental in helping me overcome all the challenges and motivating me to keep going. I am also grateful for the help from the students from IBN's Youth Research Program whom I mentored and all my colleagues from IBN for their useful discussions. And I would like to acknowledge all the aforementioned people for their advice about work and life that made my otherwise arduous Ph.D. journey much more pleasant and enjoyable. I would also like to thank A*STAR Graduate Academy for providing the scholarship for my studies and IBN for the financial support for my research.

Last but not least, I want to express my heartfelt appreciation to my family and friends for all of my work would not have been possible without their unwavering love and support.

Table of Contents

Summary

Many Drug Delivery Systems (DDS) have been developed over recent years to achieve the intended site-specific delivery of anticancer therapeutics to target tumor sites. For the delivery of small molecule anticancer drug to tumor tissues, many DDS formulations demonstrated significant toxicity towards cancer cells *in vitro* and even *in vivo*, but have been unsuccessful in clinical stages due to undesirable side effects that arise as a result of carrier instability. In addition, existing carriers suffer from low drug loading capacity leading to carrier inefficiency. On the other hand, for delivery of proteins and DNAs intracellularly, efficacy of such DDS is still not satisfactory, which may be attributed in part to inability to attain the desired stability to facilitate both transport and release. Thus the goal of a clinically approved vector remains elusive. In addition, few are equipped with cancer cell targeting ability. Complex formation between the therapeutic cargoes and the carrier may be an important consideration to overcome these issues. Many approaches have been explored to achieve optimal interaction between cargo and carrier either by chemical conjugation or physical interactions.

Here, we are inspired to use green tea catechin (-)-epigallocatechin-3-gallate (EGCG), in the design of novel polymeric complexes for cancer therapy. First, EGCG has been widely reported to possess anti-oxidative and anti-carcinogenic effects. Furthermore, the multiple-ringed structure of EGCG confers it the ability to interact favorably with small molecular anticancer drugs, protein and DNA through a wide range of non-covalent interactions including hydrophobic, hydrogen bonding and π-π stacking. Thus incorporating EGCG in polymer carrier system is predicted to enhance interactions between cargo and carrier, leading to better loading,

higher stability of the carrier formulation. To this end, two different polymer carrier systems based on EGCG for cancer therapy were developed.

The first drug carrier system was an amphiphilic polymer comprising of two EGCG molecules conjugated to the terminal end of linear polyethylene glycol (PEG) chain to form PEG-EGCG conjugates. Self-assembled PEG-EGCG micelles physically encapsulating the small molecule anticancer drug, doxorubicin (Dox) were prepared. As a result of strong interactions between Dox and EGCG, these nanosized PEG-EGCG micelles were observed to have an exceptionally high drug loading capacity, high stability and slow drug release. Further evaluation in a murine xenograft tumor model revealed that these micelles achieved tumor growth inhibition with no significant loss in body weight. In addition, micelle exhibited higher anticancer efficacy and reduced toxicity compared to optimal dosages of two clinically relevant Dox formulations such as free Dox and PEGylated liposomal Dox - DOXIL.

In the second system, EGCG was grafted onto the side chain of hyaluronic acid (HA) to synthesize HA-EGCG conjugates. EGCG was utilized for its strong interactions with protein. HA was exploited for its ability to target CD44 receptors overexpressed on many cancer cells. HA-EGCG conjugate self-assembled spontaneously in aqueous solution with the protein Granzyme B (GzmB) and linear polyethyleneimine (PEI) to form a nanogel complex. The nanogel complexes selectively delivered GzmB intracellularly into the cytoplasm of cancer cells *via* CD44 receptor-mediated endocytosis, and subsequently resulted in apoptosis of cancer cells.

HA-EGCG conjugates were also investigated for gene delivery. Self-assembled HA-EGCG/PEI/DNA nanogel complexes were prepared. Strong interactions between HA-EGCG and PEI/DNA gave rise to increased stability of complexes. These complexes achieved significant

enhancement in gene transfection than PEI/DNA binary complexes in CD44 overexpressing cancer cells as a result of increased uptake *via* CD44 receptor-mediated endocytosis. HA-EGCG nanogel complexes also showed superior transfection efficiency over HA complexes because of improved stability. Thus, we expect that this nanogel system could potentially be used to achieve targeted delivery of apoptosis inducing suicide genes to kill cancer cells.

In summary, we developed two EGCG based polymeric carrier systems and demonstrated their efficacy in delivery of small molecule drugs, protein and DNA for cancer therapy. They have the potential to be effective strategies to potentially overcome the challenges of current DDS.

List of Tables

List of Figures

List of Abbreviations

CLSM	Confocal laser scanning microscopy
CMC	Critical micelle concentration
CQ	Chloroquine
CSC	Cancer Stem Cell
DDS	Drug delivery system
DLS	Dynamic light scattering
DMEM	Dulbecco's Modified Eagle's medium
DMF	Dimethylformamide
DNA	Deoxyribose nucleic acid
Dox	Doxorubicin
EGCG	(-)-Epigallocatechin-3-gallate
EDC	*N*-(3-dimethylaminopropyl)-*N′*-ethylcarbodiimide hydrochloride
EPR	Enhanced permeability and retention
EtOH	Ethanol
FBS	Fetal bovine serum
FITC	Fluorescein-5-isothiocyanate
GFP	Green fluorescent protein
GzmB	Granzyme B
HA	Hyaluronic acid
Mw	Molecular weight
NaCl	Sodium chloride
NHS	N-hydroxysuccinimide
NMR	Nuclear magnetic resonance
PBS	Phosphate buffer saline
PEG	Poly(ethylene) glycol
PEI	Polyethyleneimine
PTK	Protein tyrosine kinase
RES	Reticulo-endothelial system
RGD	Arginine-glycine-aspartic acid
SDS	Sodium dodecyl sulfate
TEA	Triethylamine

Chapter 1: General Introduction

1.1. Cancer

Cancer is generally considered a growth system malfunction that originates within a patient's body. It manifests in many forms but is governed by one universal characteristic: the ability to divide and proliferate indefinitely. In normal tissues, this uncontrollable growth is offset by tumor-suppressor mechanisms in which diseased or infected cells go through a process programmed cell death or “apoptosis” [1]. In cancers, many of the cells lost the ability to undergo apoptosis thus leading to disruption of the balance between self-renewal and destruction [2]. With the impairment of apoptosis signaling, cancer cells continuously divide to create large cell masses also known as tumors. The exact reasons for signal failure in cancer are usually unclear but can be attributed to alterations in multiple complex cellular pathways [3].

Unlimited and unregulated cell growth is detrimental because it can cause the disruption of normal tissues and organs function by competing with healthy cells for the space, supply of oxygen and nutrients. In addition, cancers are malicious because they can spread throughout the body by invasion and metastasis [4, 5]. Invasion refers to the migration by cancer cells into tissues that are adjacent to them and directly causing them to become cancerous. On the other hand, metastasis refers to the permeation and distribution of cancer cells into lymphatic and blood vessels, which then transport them by the bloodstream to invade other normal tissues elsewhere in the body.

While numerous treatments have been developed to treat and delay the course of the disease, cancer currently has no complete cure. Drug treatment has only been met with limited success because cancer cells have been found to be extremely heterogeneous. Many different types of cancer cells exist within a tumor and different cancers may vary in characteristics and properties (e.g. cellular interactions and signaling complexities) [6, 7]; they either mutate or

develop drug resistance after prolonged drug exposure [8, 9]. While drug treatment may kill a large percentage of cells, even a small portion of resistant cells can cause cancer to relapse and regrowth. And it was discovered that drug resistance could also be mediated by cancer stem cell populations that exist within solid tumors [9]. In addition, it is well known that cancer cells can migrate from their original location and metastasize to reach various parts of the body [10]. All these obstacles make the task of cancer eradication particularly challenging.

1.2. Cancer treatments

It was estimated that there were 14.1 million cancer cases and 8.2 million cancer deaths worldwide in 2012 and it is expected to rise to 19.3 million new cancer cases per year by 2025 [11]. The four most common causes of cancer - lung, liver, stomach, and bowel - account for nearly half (46 %) of all cancer death. Despite the prevalence of cancer, the progress in disease management has been encouraging. The 5-year relative survival rate for all cancers in the US diagnosed between 2003 and 2009 was 68 %, up from 49 % in 1975 - 1977 [12], in large part due to the tremendous progress in diagnosis and treatment. Currently, the most common treatments of cancer include surgery, radiation therapy and chemotherapy.

1.2.1. Surgery

Surgery is the most established treatment for cancer and involves an invasive operation in which the cancerous tissue is removed. Common examples of surgical procedures for cancer include mastectomy for breast cancer and pneumonectomy (entire lung removal) or lung segmentectomy (removal of portions of lobe) for non-small cell lung cancer. Theoretically, cancers can be cured if all infected cells are removed by surgery, but this is not always possible. Often, cancer cells metastasize and spread rapidly to other parts of the body. Unless surgery is performed prior to any metastasis, complete surgical excision of cancer is impossible [13]. Nevertheless, surgery offers the greatest chance for survival, especially for early stage cancer patients. Performing tumor excision by surgery is also very challenging, especially in sensitive areas such as the brain or in areas where the access to the tumor is impeded. But with advancements in surgical techniques and instrumentation, surgeons have been able to overcome

some of these difficulties. One example is the use of ultrasound to assist in surgical procedures in hard-to-reach areas and this has led to improved clinical outcomes [14].

1.2.2. Radiation therapy

Radiation therapy refers to the method of killing cancer cells by a beam of high energy radiation. X-rays and gamma rays are the common types of radiation used [15]. The radiation may be delivered by a machine from outside the body (external-beam radiation therapy), or it may come from radioactive material placed in the body near cancer cells or injected into the blood stream (internal radiation therapy, also called brachytherapy). Radiation therapy destroys cancer cells by damaging their DNA, thus making it impossible for these cells to continue to grow and divide. However, radiation kills cells indiscriminately so any normal cells in the vicinity of the beam will be harmed as well. In order to reduce damage to nearby healthy tissue, radiation therapy is usually given in many fractions, so as to allow healthy tissue to recover between fractions. Radiation dosage is also adjusted carefully depending on the radiosensitivity of cancer and the presence of surrounding organs. Some acute side effects that may result from radiation therapy include skin irritation in the areas surrounding irradiated region and hair loss while long term adverse effects include scarring, fibrosis and memory loss [16, 17].

1.2.3. Chemotherapy

Chemotherapy generally refers to the use of cytotoxic drugs to kill cancer cells. This form of cancer treatment arose in the last century following the progress in drugs synthesis and discovery led by the pharmaceutical industry [18]. Many forms of drugs are used clinically for treatment including small molecule compounds and proteins. Patients undergoing chemotherapy

take these drugs at regular intervals to keep cancer under control. However, chemotherapeutic drugs typically exhibit toxicity against all fast-growing, proliferative cells. While the uncontrollable growth of cancer cells makes them suitable targets for these drugs, many active healthy cells may suffer collateral damage, leading to multiple side effects such as hair loss, weakness and bleeding [19]. Furthermore, many stand-alone chemotherapy drugs suffer from numerous other problems including rapid *in vivo* metabolism and/or excretion, failure to migrate and partition into deep cancer tissues, and nonspecific uptake by healthy cells as they circulate in the bloodstream. Very often, a large percentage of cytotoxic anticancer drugs administered to the patient does not reach the tumor site but rather is distributed throughout the rest of the body. The severity of toxic side effects from drugs migrating to healthy tissues further limits the dosage drug to be administered and compromise the efficacy of treatment. As such, a drug-free period is normally necessary following chemotherapy. This reduces possibility of complete eradication as cancer cells revive during that time [20].

Even though survival rates have improved with the advent of conventional chemotherapy, the clinical outcomes thus far are modest at best. Nonetheless as we continue to make progress in understanding of the pharmacokinetics and pharmacodynamics of anticancer drugs as well as underlying principles of cancer biology, it is expected that the efficacy of chemotherapy will be increased significantly.

1.2.3.1. Conventional anticancer drugs

Among the various chemotherapeutic drugs, conventional anticancer compounds are the most established [18, 21]; with the first documented chemotherapy drug being nitrogen mustards in the treatment of lymphoma in 1946 [22]. Later on, anti-metabolites such as methotrexate was

discovered to cure choriocarcinoma [23]. These conventional anticancer drugs are typically of small molecular weight (Molecular Weight (Mw) < 1000 g/mol), hydrophobic and can diffuse across membranes (both cell and nuclear) readily and interrupt cellular function by various mechanisms, as listed in Table 1-1. Some have modes of action within the nucleus and impact the DNA directly [24, 25]. For instance, doxorubicin (Dox) is a topoisomerase II inhibitor that intercalates DNA and hinders replication; cisplatin is an alkylating agent that crosslinks DNA while methotrexate and gemcitabine are anti-metabolites that interfere with DNA and RNA production by purine synthesis inhibition and pyrimidine substitution respectively. Other conventional small molecule drugs disrupt components of the cytoskeleton in the cytoplasm [24, 25]. For example, paclitaxel belongs to the category of anti-microtubule agents that inhibit cell division by stabilizing microtubule formation.

One issue with these conventional anticancer compounds is their limited solubility. Since most of the drugs are given intravenously, inability to dissolve in aqueous solution limits the amount of drug that can be administered. For instance, the surfactant Cremophor EL (polyethoxylated castor oil) is currently used as an excipient to dissolve paclitaxel [26]. Even though Cremophor EL successfully overcome the solubility issue, using this formulation has led to a new set of unwanted side effects such as hyperlipidaemmia, abnormal lipoprotein aggregation of erythrocyte, neurotoxicity and cardiotoxicity [26].

But by far the biggest problem with using these classical chemotherapeutic drugs is high toxicity toward normal cells as mentioned previously. One approach to overcome this problem is to design targeted anticancer drugs to improve the specificity toward cancer cells.

Table 1-1. Types of conventional anticancer drugs.

Generic	Trade Name	Mw (g/mol)	Class	Target
Doxorubicin	Adriamycin	544	Topoisomerase II inhibitor	DNA replication
Cisplatin	Platinol	300	Alkylating agent	DNA binding
Gemcitabine	Gemzar	263	Anti-metabolites	DNA/RNA synthesis
Methotrexate	Trexall	454	Anti-metabolites	DNA/RNA synthesis
Paclitaxel	Taxol	854	Anti-microtubule agent	Microtubule synthesis

1.2.3.2. Targeted chemotherapy

With the goal of selectively killing cancer cells in mind, a new generation of molecular-targeted anticancer therapeutics is being developed. They are designed specifically to interfere with cancer cellular functions, such as inhibition of growth factor proteins, or specific molecules that are key players in signal transduction, in the cell cycle or in other important cellular pathways of cancer cells [27, 28]. Generally, there are two classes of therapeutic agents for targeted cancer treatment - small molecule anticancer compounds and monoclonal antibodies.

1.2.3.2.1. Targeted small molecule anticancer drugs

Targeted small molecule anticancer drugs are synthetic molecules designed to target cancer biomarkers. Most notable among these biomarkers are protein tyrosine kinases (PTKs), an important family of signaling proteins involved in many protein-protein interactions. Examples of PTKs include: members of the human epidermal growth factor receptor family (HER1-4),

vascular endothelial growth factor receptor (VEGFR), platelet-derived growth factor receptor (PDGFR), epidermal growth factor receptor (EGFR) and mast/stem cell growth factor receptor (SCFR/c-KIT) [28, 29]. PTKs are involved in cellular growth, proliferation, migration, differentiation, and apoptosis [30]. Currently several inhibitors of PTKs have been approved by the FDA for treatment of specific types of cancer (Table 1-2), and others are being studied in clinical trials. One of the most successful small molecule tyrosine kinase inhibitor – Imatinib, was approved by FDA in 2001 for the treatment of chronic myeloid leukemia. It was found to drastically improve patient response and survival rate [31].

In general these targeted anticancer drugs are less toxic than conventional drugs and their side effects are usually mild, including nausea, headache, fluid retention [32]. However one concern with regards to their use is the development of resistance to these inhibitors, which usually arise as a result of mutations to the protein kinases [33, 34]. It is proposed that a combination therapy with a second agent whose mechanism of action is different from the original drug could possibly overcome this problem [35].

Table 1-2. Types of targeted small molecule anticancer drugs.

Generic	Trade Name	Mw (g/mol)	Target	Cancer Type
Imatinib	Gleevec	494	PDGFR, c-KIT, Abelson kinase	Chronic Myeloid Leukemia, Gastrointestinal Stromal Tumor
Sunitinib	Sutent	398	VEGFR, PDGFR, c-KIT	Gastrointestinal Stromal Tumor, Renal Cell Carcinoma
Erlotinib	Tarceva	393	EGFR	Non-small Cell Lung Cancer, Pancreatic Cancer
Sorafenib	Nexavar	465	VEGFR, PDGFR, c-KIT	Hepatocellular Carcinoma, Renal Cell Carcinoma

1.2.3.2.1. Monoclonal antibodies

Besides small molecule drugs, monoclonal antibodies (mAb)s are another class of chemotherapeutic agents. They are proteins produced by immune cells that bind to specific target molecules – antigens overexpressed on cell surfaces. Many tumor antigens have been identified as possible targets for mAbs. For instance, Trastuzumab binds to Her2 receptor overexpressed in some types of breast cancer cells and Cetuximab binds to epidermal growth factor receptor (EGFR) that is overactive in many cancer cells. Both result in disruption of proliferation signaling. On the other hand, Bevacizumab inhibits the function of the vascular endothelial growth factor (VEGF) protein that is needed for angiogenesis (Table 1-3).

Despite the high selectivity of these novel targeted chemotherapeutics, a range of previously unknown and unpredictable side effects has emerged. Most of these side effects arise as a result of specific molecular target in normal tissues being inhibited or modulated by the drugs [28]. Inhibition of EGFR, which is involved in regulation of cell proliferation, leads to skin-related problems such as papulopustular eruption in patients [29] while targeting VEGF pathway affects normal blood vessel formation and leads to side effects including hypertension, arterial thromboembolic events [30].

Table 1-3. Types of monoclonal antibodies.

Generic	Trade Name	Type	Class	Target
Bevacizumab	Avastin	mAb	Anti-angiogenesis	VEGF
Trastuzumab	Herceptin	mAb	Tyrosine kinase inhibitor	HER2
Cetuximab	Erbitux	mAb	Tyrosine kinase inhibitor	EGFR

1.2.3.3. Anticancer drugs in development – proteins and DNA/siRNA for intracellular targets

A majority of the targeted chemotherapeutics developed were focused on extracellular targets, especially antibody-receptor binding interactions. This is an area where there is potential for new drug discovery is in regulating molecules that play key roles in the intracellular pathways of cancer cells. The most studied approach is to trigger cell death in cancer cells by activating apoptosis.[36, 37] Cancer cells proliferate uncontrollably due to changes in cell-death signaling pathways, in particular mutation or defects to the *Bcl-2* family proteins and *p53* signaling. One strategy is to regulate gene expression by gene transfection, RNA interference using siRNA (small interfering RNA), antisense oligonucleotides and DNA aptamers. Thus far, there has been some initial success in cancer treatment. Most notably the *Bcl-2* antisense oligonucleotide has shown anticancer efficacy in combination with other drugs or radiation therapy [38, 39]. Small molecule compounds and recombinant proteins have also been explored to target molecules involved in the apoptosis pathway including various caspases and cytochrome C (Cyt C) [40, 41]. For example, caspase-3 mediated cell killing is exploited for cancer therapy in which a target antigen is used to induce activation of the caspase-3 moieties bound to the antibody [42].

1.2.4. Delivery of chemotherapeutic drugs

Even though we are equipped with more effective anticancer therapeutics, their clinical outcomes have been modest. A shortfall in the efficacy of most drugs is their difficulty in completing their journey to tumor cells upon intravenous administration. While in circulation the drug must be able to bypass the routes of clearance including renal filtration, liver metabolism, and

the organs of the reticulo-endothelial system (RES). RES comprises of phagocytic cells such as monocytes and macrophages that are responsible for the routine removal of foreign substances from the blood stream [43]. Upon overcoming these obstacles, the remaining drugs may encounter the tumor vasculature and some of those may successfully diffuse out of the blood vessels to enter the tumor interstitial space [44]. The drug that has made it to this point must then penetrate into the tumor and encounter a target cell. For drugs with intracellular targets, they must then cross the phospholipid bilayer membrane, and finally localize in the cellular compartment relevant to the drug's mechanism of action in sufficient concentrations to cause cell death [44].

To address these limitations and improve performance of stand-alone drug, drug delivery systems were developed with the goal of acting as chaperons to transport drugs to the target sites.

1.3. Drug Delivery Systems (DDS)

1.3.1. Overview

A DDS (drug delivery system) is defined as a "formulation or a device that enables the introduction of a therapeutic substance in the body and improves its efficacy and safety by controlling the rate, time, and place of release of drugs in the body" [45]. It includes the process of administration, release and finally transport of the active therapeutic across biological membranes to site of action. DDS exists in many forms, oral capsules or protective coatings, implantable drug reservoirs, controlled release devices like hydrogels, or formulations such as drug carriers and they can be introduced via many anatomical routes including intravenous, subcutaneous, intra-muscular and transdermal [45, 46]. In this thesis, the scope would be mainly focused on DDS for anticancer therapeutics.

1.3.2. Concept of "Magic Bullet"

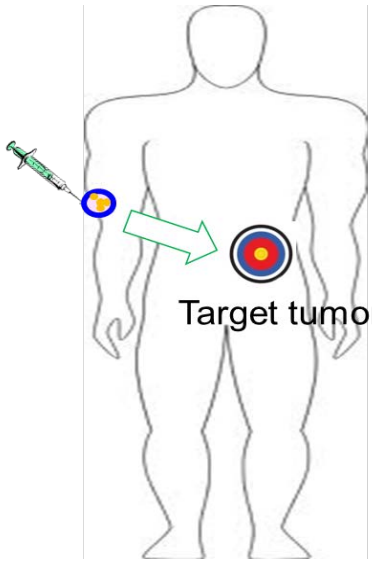

Figure 1-1. Pharmacologist interpretation of the "Magic Bullet" concept for chemotherapy where the goal of is to selectively deliver drugs to target tumor instead of healthy tissues and organs.

The criteria for the ideal DDS was first proposed by Paul Ehrlich in the early 19th century when he first introduced the term "Magic Bullet". This concept was first proposed by him in

immunology to describe the specificity of receptor antigen binding [47, 48]. Later on scientists adapted his idea of the magic bullet to illustrate the exclusive and highly specific manner in which a compound reaches its target [49]. Thus in the case of cancer drug delivery, the DDS had to bring the drug all the way to the tumor site where it exerts its biological activity while avoiding all healthy tissues along its journey (Figure 1-1) [50]. In this way, cytotoxic drugs will be directed only to tumors where they exert antitumor activity while the toxic effects on non-target site would be kept to a minimum.

One hundred years later, the vision of "Magic Bullet" still eluded us and the goal of achieving perfectly targeted DDS is far from realization [51]. Nevertheless, significant progress has been made along the way toward designing carriers for tumor-specific delivery.

1.3.3. Covalent drug delivery systems

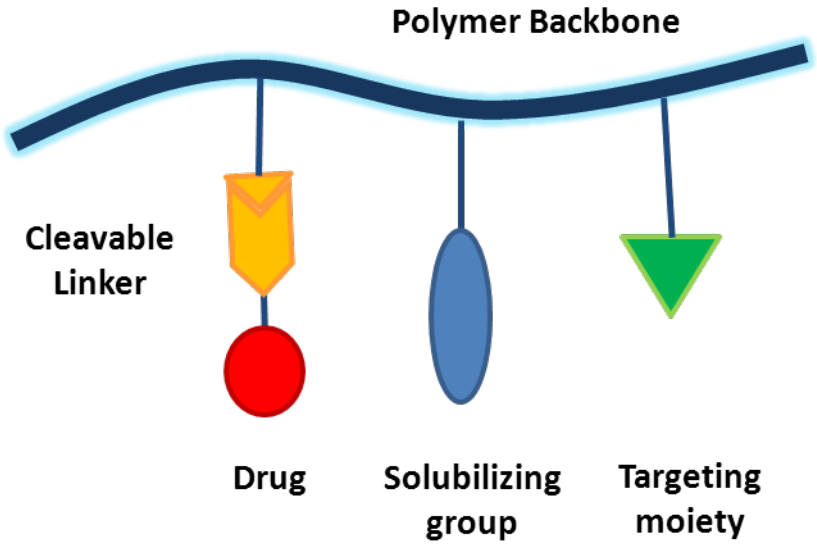

Figure 1-2. Ringsdorf's model for polymer-drug conjugate that comprises of the drug, solubilizing group, targeting moiety and cleavable linker bound to a polymer backbone.

To facilitate drug delivery to tumors, many drug delivery systems designs were explored. In 1975, Helmut Ringsdorf first proposed a general model for polymer-drug conjugate type of DDS using synthetic polymer for low-molecular weight drugs [52]. The drug was chemically

conjugated onto the polymer backbone together with other solubilizing groups and targeting moeties in a pendant chain configuration. In addition, a spacer was introduced between the drug and the polymer to facilitate release of drug after cellular uptake of the conjugates. Thereafter many polymer-drug conjugates were developed based on this model. In particular, Kopecek and his colleagues have done extensive research using the poly(*N*-(2-hydroxypropyl) methacrylamide) (HPMA) homopolymer as the polymer backbone. In one system, the anticancer drug Dox was conjugated onto poly(HPMA) via enzyme-degradable (Gly-Phe-Leu-Gly) linkages has been shown to have enhanced antitumor effect and prolonged survival time as compared to free drug [53, 54]. This promising polymer-drug conjugate has since progressed to Phase 2 of clinical trials [55]. Following the initial success, the usage of HPMA copolymers in polymer-drug conjugates has been further expanded by many other groups that made various modifications including switching to other pendant drugs such as cisplatin [56] and camptothecin [57], utilizing targeting molecules such as antibody fragments [58] as well as adopting a pH-responsive hydrazone linkage between the drug and the polymer [59, 60].

Despite the success of polymer-drug conjugates, one drawback for this type of DDS is the need for chemical modifications on the therapeutic payload since conjugation of drug onto polymer requires the formation of a covalent bond. Not all cargoes could be intact after conjugation. For macromolecules such as proteins, the structural conformations are important. Functionalization may potentially affect the three-dimensional structure of the protein and disturb its substrate binding sites or recognition areas resulting in loss of activity [61, 62].

A strategy to overcome this is to exploit the interactions between the modalities on the carriers and drugs to form non-covalent complexes. They can be prepared by controlled mixing of samples and followed by spontaneous self-assembly of the complexes over time [63, 64].

1.3.4. Non-covalent complexes for drug delivery

Formation of non-covalent inclusion complexes depends on the presence of physical interactions between the carrier and the drug payload, including van der Waals, hydrophobic interaction, H-bond, π-π stacking and electrostatic interactions [65]. A commonly used non-covalent complex is the polyethyleneimine (PEI) and DNA ionic complex, based on the condensation of anionic DNA with the cationic polymer [66]. In addition, the strength of interactions can be tuned by chemical modifications of the carrier. Hydrophobic functionalities can be grafted onto polymer backbones to enhance the interaction of carrier with hydrophobic drugs.

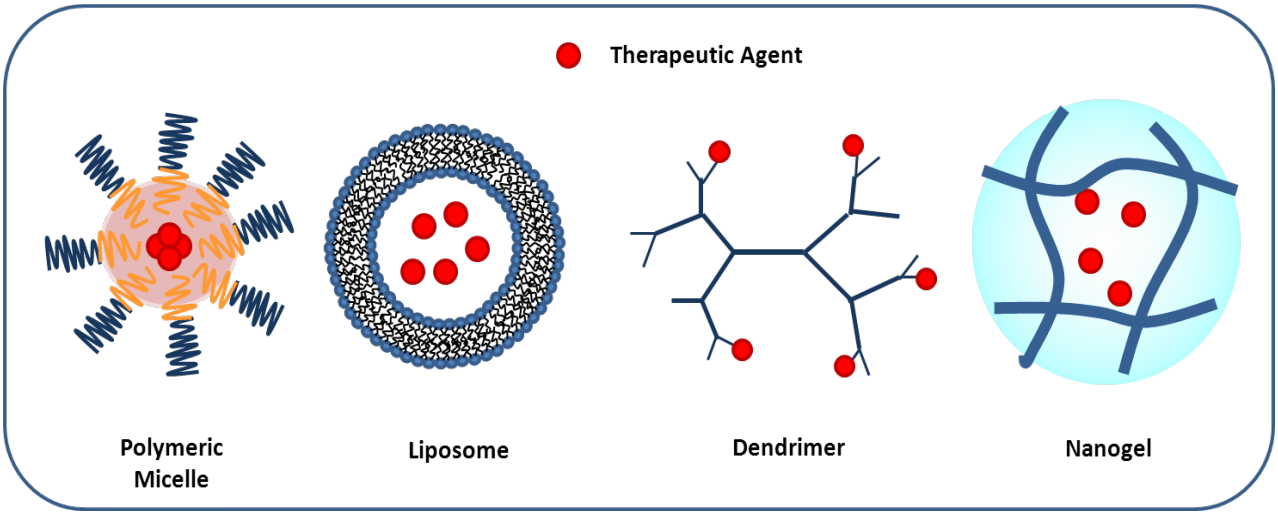

Figure 1-3. Representative types of non-covalent complexes for anticancer drug delivery.

Many classes of non-covalent polymeric complexes have emerged, such as polymeric micelles, liposomes, dendrimers and nanogels [67]. Among them, the two types of non-covalent polymeric complexes that are highlighted in this thesis are polymeric micelles and nanogels. Nanogels are composed of cross-linked three-dimensional polymer chain networks that are formed *via* covalent linkages or self-assembly processes [68]. In particular, hydrophilic polymers such as polysaccharides and poly(amino acids) are modified using hydrophobic moieties, such as

cholesteryl [69-71] and deoxycholic acid [72, 73] in order to form drug loading reservoirs where these hydrophobic molecules can reside. On the other hand, polymeric micelle has a core-shell structure that typically comes in the form of a block copolymer with one block forming the hydrophobic core and the other the hydrophilic corona or shell. The hydrophilic block is typically made up of poly(ethylene glycol) (PEG), whereas the hydrophobic block comprises of poly(amino acids) such as poly(aspartate) [74, 75] and poly(lactide-*co*-glycolide) (PLGA) [76, 77]. One common method of preparing polymeric micelles is by mixing the hydrophobic drug and polymer in organic solvent followed by dialysis against water to induce self-assembly of micelles [78]. In the micelle conformation, the inner hydrophobic core encapsulates the poorly water-soluble drug, while the outer hydrophilic corona provides solubility and protects the drug from being degraded in the aqueous environment [78, 79].

1.3.5. Passive targeting by EPR effect

Structure features are important design considerations for drug delivery systems. Nano-sized carrier formulations have been gathering more interest recently due to the advantage of passive targeting [80]. In the field of drug delivery, passive targeting generally refers to the passive accumulation of the drug carriers at the target tumor site. That is achieved by the EPR (Enhanced Permeability and Retention) effect [81-85]. Maeda *et al.* first introduced this concept of EPR effect in 1986 when they found that by conjugation of the anticancer protein neocarzinostatin (NCS) to a copolymer of styrene and maleic acid anhydride (SMA) to form SMANCS, they could achieve a much greater accumulation of (5-fold increase compared to free NCS at 24 hours) NCS in tumor tissues [81-83]. The explanation they proposed was that long circulating nanosized macromolecule drug carriers (< 200 nm) could be preferentially directed to tumor sites because of the tumor's leaky vasculature. In tumor sites, poorly developed vascular

endothelium due to excessive pro-angiogenic signaling and rapid growth of tumor and blood vessels creates much larger pores (400 nm - 1 μm) as compared to capillary pores of 1 nm [86, 87]. In addition, the poor lymphatic drainage at the tumor tissues as a consequence of physical forces arising from cancer and stromal cell proliferation transferred by the interstitial matrix also leads to build-up of the carriers. Ideally, upon reaching the tumor site the nanoparticle carriers would permeate into the tumor vasculature by the enlarged pores and they would accumulate at the tumor tissue due to the lack of lymphatic clearance. Subsequently, the drugs that are encapsulated within the carriers would gradually diffuse into tumor tissues and kill the cells.

Since its discovery, EPR strategy has been at the heart of the design criteria of many nanoparticle drug delivery systems. Kataoka *et al.* developed polymeric micelles of size range 100 - 200 nm encapsulating the anticancer drug Dox [74, 75, 88]. By leveraging on the EPR effect, they successfully demonstrated that micelles could selectively accumulate in tumor (the drug concentration in tumor was 2-fold that of free drug) and inhibit tumor growth in mice models [74, 89]. While passive targeting by using nano-sized drug carriers has become an important strategy for anticancer drug delivery, there are still other architectural features of carriers to consider for *in vivo* application.

1.3.6. Structural design considerations for drug carrier design *in vivo*

It is well-known that long blood circulation time is a pre-requisite [81, 90] for EPR effect. Many stand-alone chemotherapy drugs suffer from unfavorable biodistribution upon intravenous administration - they are rapidly cleared from circulation. By packaging drugs and presenting them in a different form, drug delivery systems could significantly improve the

pharmacokinetics and biodistribution of stand-alone drugs [91, 92]. However, it is important to note that several structural aspects of carriers can also influence the pharmacokinetics greatly.

1.3.6.1. Size

In order for a nanoparticle to exhibit prolonged circulation, the particle size has to be above the renal filtration cutoff size of 5.5 nm, observed using quantum dots [93]. The maximum size of particles is influenced by tumor vasculature and splenic filtration. As mentioned earlier, pores in tumor endothelium can vary from 400 nm - 1 μm while splenic clearance has a smaller size restriction. Particles larger than 200 nm in diameter will have difficulty passing through the inter-endothelial slits of sinusoidal spleen with width rarely exceeding 200 - 400 nm [94]. Furthermore, foreign particles can be recognized by opsonin proteins present in circulation. In a process known as opsonization, they adsorb onto surface of particles and present them to macrophages and monocytes at RES organs for phagocytosis [95]. It has been demonstrated by several groups that nanoparticles above 200 nm in diameter are readily recognized by opsonin proteins and subsequently cleared by the liver and spleen [96, 97].

Therefore it is generally believe that nanoparticles in the range of 20 – 200 nm would be ideal for anticancer drug delivery [98]. The effect of size in this range on pharmacokinetics and biodistribution has also been explored but with inconclusive results. Lee *et al.* found that 25 nm poly(ethylene glycol)-*block*-poly(ε-caprolactone) (PEG-*b*-PCL) block copolymer micelles was cleared faster from the plasma compared to 60 nm micelles (2.2-fold decrease in $T_{1/2}$), leading to an almost 2-fold decrease in their total tumor accumulation [99]. When Zhang *et al.* compared the pharmacokinetics of 20, 40 and 80 nm gold nanoparticles, 20 nm particles showed the longest blood circulation half-life and lowest RES uptake among them leading to significantly

higher tumor uptake than the other nanoparticles [100]. The discrepancies in the findings suggest that the relationship between size and blood circulation time is complex and other factors such as nanoparticle composition may also influence the pharmacokinetics of carriers.

Particle size also has a direct influence on tumor accumulation. In one study, Yue *et al.* reported that 36 nm and 72 nm fluorescently-labeled poly (ethylene glycol)-*b*-poly(l-lactide-*co*-2-methyl-2-hydroxy oxycarbonyl-propylene carbonate) [MPEG-*b*-P(LA-*co*-MHC)] micelles showed similar tumor tissue uptake but higher than 112 and 136 nm micelles [101]. Cabral *et al.* went further to show that while all sub-100 nm polymeric micelles carrying oxaliplatin had similar efficacy on highly permeable colorectal cancer; in poorly permeable pancreatic tumors, only the 30 nm micelles had antitumor activity [102]. They attributed this difference to the ability of the smaller 30 nm micelles to penetrate deeper into tumors with less porous vasculature. Thus smaller nanoparticles may be more suitable for passive targeting to less permeable tumors.

1.3.6.2. Surface charge

The overall charge on a surface of a particle, which is measured as zeta potential (ξ), can influence the pharmacokinetics and biodistribution significantly. In general, negative particles ($\xi \leq 10$ mV) exhibit strong RES uptake, and positive particles ($\xi \geq 10$ mV) will induce serum protein aggregation: neutral nanoparticles (within $\pm$ 10 mV) induces the least RES uptake and have the longest blood circulation time [98]. Levchenko *et al.* reported that liposomes exhibiting $\xi \sim 40$ mV exhibited more than 90% clearance in 10 min compared to 10% clearance for neutral ($\xi \pm 10$ mV) liposomes [103]. Xiao *et al.* also demonstrated that nanoparticles with high positive ($\xi \geq 20$ mV) or negative surface charge ($\xi \leq 20$ mV) were efficiently opsonized and cleared by

the liver from the blood circulation. In addition, Zhang *et al.* also found that positively charged complexes that form aggregates with serum proteins can lead to transient embolism in the lung capillaries [104].

1.3.6.3. Surface decoration by PEG

Surface decoration or coating is another important feature of nanoparticle carriers. Once administered intravenously, the circulating drug carriers are exposed to many blood components such as plasma proteins. As a result of protein opsonization and clearance by the RES organs [43], a large proportion of drug carriers would be cleared from the body without ever reaching the tumor tissue. In order to minimize opsonization and impart a stealth-shielding effect, hydrophilic PEG chains have been grafted onto the surface of nanoparticle carriers [95, 105]. The highly flexible PEG brushes rapidly switch from one conformation to the next providing a steric hindrance effect to repel protein attachment as well as inhibition of inter-molecular aggregation [106, 107]. As an additional benefit, attachment of PEG also helps to improve solubility of many hydrophobic drugs. PEGylated carriers have been demonstrated to increase blood circulation and reduce RES sequestration and in turn efficacy of treatment [108]. For instance, Sadzuko *et al*. found that PEGylation of liposomes led to a 3-fold reduction in RES uptake, a 6-fold higher plasma area under the curve (AUC), and a 3-fold increased tumor uptake of a liposomal drug [109]. Furthermore, it was also reported that the PEGylated liposomal carrier DOXIL® has an much improved elimination half-life time of 55 hours and an AUC of 900 $\mu g h m l^{-1}$ in patients, as compared to the non-PEGylated formulation - Myocet® with a half-life of 2.5 hours and AUC of 45 $\mu g h m l^{-1}$ [110, 111].

The density of PEG grafting also affected "Stealth" property. Essa *et al.* reported that an optimal 4 - 7 % PEG grafting density (mol/mol of lactic acid monomer) of poly(lactic acid) (PLA) could significantly reduce macrophage uptake [112]. Similarly, Gref *et al.* examined surface properties of PEG-PLA block copolymers also observed that PEG content of between 2 - 5 wt % of to be the optimal value for resisting protein adsorption [113]. These studies indicate that surface modification with a small amount of PEG is sufficient to confer "Stealth" property and there is no additional benefit with increase in PEG content.

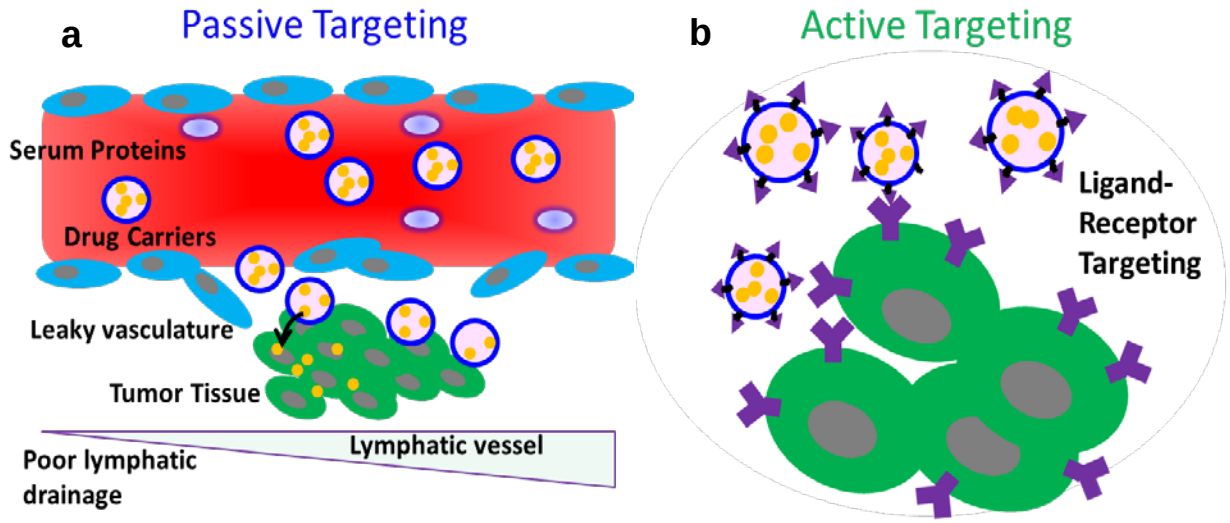

Figure 1-4. (a) Passive targeting of nanoparticle carriers containing anticancer drugs based on the Enhanced Permeability and Rentention (EPR) effect. Angiogenesis leads to large gaps between the endothelial cells in tumor blood vessels, leading higher accumulation of drug in tumors. (b) Active targeting based on ligand-receptor interaction to increase specificity of delivery.

1.3.7. Active targeting

Active targeting can be defined as "imparting to a nonspecific drug affinity towards its target by binding this drug with another molecule capable of specific recognition and binding to a target site. [114] " For anticancer drugs that have difficulty to cross the cancer cell membrane, the task of DDS is even more challenging as transporting them to the tumor site is insufficient. Even if we assume nanoparticle drug carriers can achieve tumor specific delivery by passive

targeting, these drugs still have to be taken up by the cells to their site of action. Hence active targeting strategy aims to exploit ligand-receptor, antigen–antibody and other forms of molecular recognition to deliver the drug to specific cells [114, 115]. For cancer therapy purposes, active targeting is especially beneficial because by improving the nanoparticle carrier's selectivity for cancer cells, it can potentially minimize the delivery of toxic drugs to healthy tissues and improve therapeutic outcome [116].

The overexpression of various receptors on the surface of cancer cell or tumor endothelial membrane [117] has inspired the design of many active targeting moieties against them. In particular, folate and transferrin ligands are among the most well-studied. As folate receptor is overexpressed in a variety of tumors especially ovarian cancer (80 - 90 %) [118] and binds folate molecule with extremely high affinity ($K_D \sim 10^{-9}$) [119], it has been used widely for tumor targeting. Yoo *et al.* reported the synthesis of folate receptor-targeting Dox micelles by conjugating folate moiety and Dox on either terminals of PEG-PLGA block copolymer respectively. These targeted micelles showed higher cellular uptake *in vitro* and greater tumor regression and consistently higher Dox accumulation (about 1.3-fold at 24 and 48 hours) in tumors compared to non-targeted micelles [76].

Transferrin (Tf) receptors, which are involved in the regulation of cell growth, are also highly expressed on cancer cells. Suzuki *et al.* found that Tf conjugated PEG-liposomes carrying the drug oxaliplatin decreased tumor volume more than non-targeted PEG-liposomes [120]. In addition, concentration of delivered drug in tumor was higher and maintained in the tumor for 72 hours after intravenous injection. The effect of Tf-targeting was also observed by Bartlett *et al.* They prepared Tf-targeting inclusion nanoparticle complexes containing luciferase-silencing

siRNA using Tf modified PEG-adamantane and β-cyclodextrin-polycation [121, 122]. Tumor luciferase activity in mice treated with Tf-targeted nanoparticles was 50 % lower than that in mice treated with non-targeted nanoparticles [122].

While active targeting is a promising strategy to reduce off-target effects, its effectiveness tend to be overestimated [123]. Since the primary mode of accumulation is passive extravasation based on EPR effect, tumor localization does not increase by addition of ligands that bind to cancer cells [124, 125]. Nevertheless, one major difference is that cellular uptake within tumors are improved with active targeting, as described by the folate and Tf systems mentioned [76, 122, 126]. This makes active targeting systems particularly attractive for intracellular delivery of therapeutics that are unable to enter cancer cells such as nucleic acids or proteins. For instance, Tf coated nanoparticles carrying siRNA (CALAA-01) for cancer treatment have been undergoing Phase I of clinical trials for solid tumors [127, 128].

Considerable research in the field of nanoparticle carriers has provided us with many useful insights on designing parameters for ideal anticancer drug carriers. Despite the progress in anticancer drug delivery, the use of carriers clinically for cancer therapy has been met with limited success thus far. The issues with the existing carriers will be revealed in the next section and new polymeric carrier designs which can help to overcome these problems will be discussed.

1.4. Issues with Existing Anticancer Drug Carriers

1.4.1. Delivery of the conventional small molecule anticancer drugs

In the area of small molecular hydrophobic drugs for chemotherapy, drug delivery systems provided many advantages such as increase in solubility, protection from hostile conditions and enzymatic degradation, and most importantly improvements in pharmacokinetics and biodistribution profile. Thus it is no surprise that over the past twenty years, many formulations entered clinical trials and several were successful in getting FDA approval for cancer treatment [115].

1.4.1.1. Existing carrier formulations and issues

Some of the carriers that have been approved for clinical use in cancer therapy are listed in Table 1-3. Most of the formulations are liposomal nanoparticles with particle size of ~ 100 nm with extended blood circulation time. Human trials using DOXIL® revealed that the plasma half-life was increased from 0.2 hours to 55 hours and AUC was enhanced 300-fold compared to free drug [129]. It was accompanied by a 4 to 16-fold enhancement of drug accumulation in malignant effusions. So far in clinical settings, these carriers have managed to attenuate the toxicity of the free drug and improved patient outcomes.

However, there are still some concerns with existing systems such as carrier stability and drug loading capacity. Table 1-3 describes some of the undesirable side effects associated with free drug toxicity for current formulations. Even though polymer drug carriers help to reduce the systemic cytotoxicity of chemotherapeutic drugs administered, low stability of the carrier formulation in circulation often results in leakage of drugs and extravasation of drugs in healthy tissues [51, 130]. In the *in vivo* environment, the presence of serum proteins induces instability of

carriers, possibly due to a variety of mechanisms including protein adsorption, protein penetration and drug extraction [131]. Therefore the carriers become ineffective because they may be either disintegrated or emptied of its payload by the time they reach the tumor tissue, thereby resulting in no efficacy. In addition, drugs that are leaked from carriers while in circulation also cause undesirable side effects as they are toxic toward healthy normal cells. Conjugation of drug to the polymer itself can improve the stability of the formulation but this often comes at the expense of difficulty in drug release at the target site [132].

Table 1-4. Commercially available carrier formulations for anticancer drugs.

Commercial Carrier	Drug	Carrier	Size (nm)	Drug Loading Capacity (%)	Half-life (h)	Side Effects	Ref.
DOXIL® / Caelyx®	Dox	PEGylated liposome	80-120	11-12	55	Palmar-Plantar Erythrodysesthesia (PPE), hand-foot syndrome, cardiomyopathy, local tissue necrosis	[111, 133]
Myocet®	Dox	Liposome	~100	~10	2-3	Palmar-Plantar Erythrodysesthesia (PPE), hand-foot syndrome, cardiomyopathy, myelosuppression, local tissue necrosis	[134, 135]
DaunoXome®	Daunorobicin	Liposome	40-60	7-8	4.4	Cardiomyopathy, allergies, fever, nausea, diarrhea	[67]
Abraxane®	Paclitaxel	Albumin	130	-	27	Neutropenia, fever, nausea, diarrhea	[67, 136]

Loading capacity refers to the weight percentage of drug payload in the formulation. Conventional polymeric carriers are designed improve the typical hydrophobic anticancer drugs' solubility in water, which is derived from hydrophobic interaction between hydrophobic polymer

blocks and drugs [137]. Often high molecular weight hydrophobic polymer units are used for the purpose. As such, the loading capacity of conventional polymeric micelle system is ~ 10 – 20 % (wt/wt) [78], and the commercial liposomal formulations are around 10 % (Table 1-3). The low drug loading capacity of polymer system compromises the efficiency of formulations, resulting in repeated injections or high dosages. Furthermore, it poses a problem when they are administered *in vivo*, as a large amount of polymers are required to deliver active drug molecules sufficient to antitumor activity. Although most polymers used for biomedical applications are biocompatible and non-toxic (certified by FDA), the effects of a large amount of polymers on the long-term side effects are not understood completely [138]. Even from the clinical point of view, it is predicted that the buildup of polymers in the body may lead to unfavorable host response. In particular, it was found that the prevalent usage of the polymer PEG has triggered immunogenic responses in some patients leading to production of anti-PEG immunoglobulin antibody (anti-PEG IgM) [139, 140]. Therefore, it is desirable to increase loading capacity of carrier formulations and improve carrier stability to achieve higher delivery efficiency as well as minimize potential toxicity.

1.4.1.2. Polymeric micelles for Doxorubicin

At the research level, many polymeric complexes have been studied for drug delivery to tumor tissue. Among them, polymeric micelles are considered a major class of promising delivery agents. Table 1-4 summarizes the various polymeric micelle formulations carrying the hydrophobic drug Dox. To encapsulate a hydrophobic molecule such as Dox, it is necessary to design block copolymers with adequate hydrophobicity. Therefore many micelle carriers that were developed tend to incorporate high molecular weight hydrophobic polymers to interact with Dox, hence decreasing the weight percentage of the drug in the carrier system considerably [141,

142]. Table 1-4 displays the loading capacity of typical Dox micelles developed by other researchers, which ranges from 3 – 20 %. This indicates that a large proportion of the mass of the formulation is made up of polymer (80 – 90 %). In addition, it was predicted that stability of the polymeric micelles could be improved with stronger drug-carrier interactions [143-145]. Thus it is possible that while trying to enhance the stability of polymeric micelles, the sizes of the hydrophobic portion is increased and as a result drug loading content is decreased.

Despite the improvement in antitumor efficacy of various Dox loaded polymeric micelles formulations (Table 1-4) over free Dox due to more favorable pharmacokinetics and biodistribution, little success has been seen in their advancement clinically [78, 79]. One possible issue with the drug loaded polymeric micelles is that the encapsulated drug leaks out from the carriers while circulating in the bloodstream, either by dilution effect or interaction with surfactant proteins in blood [145-147]. Chen *et al*. demonstrated that a polymeric micelle made of PEG-poly($_{D,L}$-lactic acid) (PEG-PDLLA) released its hydrophobic drugs 15 minutes after intravenous injection due to interaction with blood components [147]. Another preclinical trials of a particular type of block copolymer micelle comprising PEG (Mw 5,000) and polyaspartic acid (about 30 units) was found to be unstable after dilution in buffer and resulted in rapid release of drugs [148]. To improve the stability, the group modified the polymer backbone such that the drug was covalently conjugated to the carrier via a pH-sensitive hydrazone linker. Since tumor tissues have a slightly acidic pH [149, 150] compared to normal tissues, acid-degradable drug-polymer linkages can be employed to trigger drug release. The pH-responsive micelles were stable at physiological pH 7.4 but released increasingly more drugs with lower pH and achieved almost 100 % drugs release at pH 3 at 48 hours [151]. With this modification, the micelles exhibited tumor inhibition and 4-fold increase in maximum tolerated dosage compared

to free Dox (40 mg/kg vs. 10 mg/kg Dox concentration). Therefore the stability of polymeric micelles is an important design consideration for successful tumor delivery.

Table 1-5. Polymeric micelles developed for Dox delivery and their characterizations.

Polymer	Size (nm)	Drug Loading Capacity (%)	Drug Loading Efficiency (%)	Ref.
PEG-poly(Asp(Dox) Mixture of conjugated and encapsulated Dox	~50	7.3	~22	[88, 132]
PEG-poly(*b*-benzyl-*l*-aspartate) (PEG-PBLA)	45-67	12-20	58-67	[74, 152]
PEG-PLGA & Folate-PEG-PLGA	105-111	~19	-	[76]
PEG-poly(*b*-benzyl-*l*-glutamate) (PEG-PBLG)	72-138	3.6-13.2	61-75	[153]
PEG-PCL	25-104	3.1-4.3	-	[141]
PEG-PCL-PEG	50-92	3.7-8.5	26-57	[142]
PLA-PEG-PLA	120-140	~3	48-70	[154]
PEG-poly(*l*-histidine) and PEG-PLLA mixed micelle	50-80	15-17	75-85	[155]

1.4.2. Intracellular delivery of protein and DNA for cancer

As mentioned in the previous section, DNAs, siRNAs, and recombinant proteins constitute a major new therapeutic modality for chemotherapy. For the delivery of these anticancer therapeutics, more attention is needed to address the obstacles at the intracellular level since many of such drugs are focused targeting the apoptotic pathways within the cells. Pro-apoptotic proteins such as caspase-3 [42, 156] and Granzyme B (GzmB) [156, 157]; and *p53* gene [158, 159] which suppresses tumor growth are some prominent examples. To reach the targets within the cell, various barriers have to be overcome in the process, including the extracellular milieu that comprising various proteases and macrophages, cell membrane and endosomal membrane. The protein drug carriers therefore have to secure the passage the protein into the cytosol, circumventing all the barriers while maintaining the functionality of the protein [160, 161]. For delivery of genes, in addition to all these aforementioned barriers, there is an additional obstacle of the nuclear membrane. Intact DNA has to be deposited in the nucleus where it exerts its biological function [162, 163].

1.4.2.1. Existing carrier formulations for intracellular delivery

Table 1-5 summarizes some of the intracellular delivery agents that have been developed for both DNAs and proteins, including polycations, liposomes and cell penetrating peptides. However, none of them have been clinically approved at the moment. Many of these vehicles demonstrated some efficacy *in vitro* or even *in vivo* but still many problems remained.

Delivery of DNA using non-viral polymers has been examined extensively. Branched and linear PEIs are two cationic polymers routinely used for gene transfection *in vitro* [164, 165]. Unfortunately its high charge density and non-biodegradability often resulted in fairly high

toxicity, rendering it incompatible with clinical applications [163, 166]. For protein delivery, it is important to account for the characteristics of the protein of interest, including charge, molecular weight and hydrophobicity and then tailor the design of carrier to accommodate it. Many carriers intended for intracellular delivery of payload were positively charged to support adhesion to the negatively charged cell membrane before internalization [167, 168]. Although this feature facilitated the delivery of negatively charged proteins such as bovine serum albumin (BSA) as they can form complexes by electrostatic interaction, it becomes a challenge to deliver positively charged proteins. For instance, while several positively charged carriers such as pep-1 and Pulsin® was able to bind to negatively charged protein and transport them across the cell membrane into the cytoplasm [169-171]; only the liposomal carrier Bioporter® was reported to achieve delivery of positively charged proteins such as GzmB [156].

In addition to designing suitable carriers for different proteins, the stability of protein carrier complexes should also be considered. As physical interactions such as electrostatic or hydrophobic interactions play a dominant role in carrier-protein interactions, the strength of such interactions are easily affected by the environment. Presence of negatively charged serum albumin or other proteins can easily weaken the interactions and cause dissociation of the complex [172, 173]. Thus many of the carriers become unstable when exposed to external conditions, especially in the complex *in vivo* environment.

Lastly, the intracellular uptake of these nanoparticle complexes is based solely on affinity for cell membrane and not specific to any cell types [160, 172]. If the goal is to deliver a cytotoxic cargo to kill a specific group of cells e.g. cancer cells, it would be necessary for the carrier to recognize and selectively target those cells to minimize unwanted toxicity.

Table 1-6. Commercially available intracellular protein and DNA carriers.

Intracellular delivery agents	Carriers	Cargo	Advantages	Drawbacks	Ref.
Branched PEI Linear PEI (Exgen 500)	PEI polycation	Various genes RNase A, IgG,	Simple mixing of polycation and DNA "Gold Standard" for gene transfection	High amounts cause toxicity Efficiency can be rather low in some cell types Efficiency decreases with serum	[164, 165]
PULSin®	Cell Penetrating Peptide, Cationic amphiphile	GFP, Histone, Phycoerythrin, Anti-mouse IgG,	Simple mixing of carrier and protein	Charged induced instability Unstable in serum	[171]
BioPORTER® Pro-Ject™	Liposome	β-gal, GzmB, caspase-3, Cyt C, BSA, Phycoerythrin	Simple mixing of carrier and protein No toxicity Efficiency of up to 95%	Unstable in serum Highly positively charged or less hydrophobic cargo inefficient	[156]
Chariot™ / Pep-1	Cell penetrating peptide, Cationic amphiphile	GFP, β-gal, *P27* protein	Simple mixing of carrier and protein Average efficiency of 60-95%	Stability dependent on mixing ratio Positively charged cargo unstable	[169, 170]
Tat HIV-1	Protein Transduction Domain	β-gal, RNase A, HRP	Protein transduction done *in vivo*	Conjugation needed	[174, 175]

1.4.2.2. Polymeric complexes for protein and DNA delivery

Table 1-6 summarizes a variety of polymeric complexes used for intracellular protein and gene delivery. The two dominant types of non-covalent complexes here are based on electrostatic and hydrophobic interactions. In the former category are positively charged polymers such as PEI and lipopolyamine that depend on ionic interactions between the negatively charged

proteins/DNA with the carrier. To overcome the limitations of anionic cargo, Lee *et al.* developed charge-conversion polyionic complex (PIC) micelles [176]. In PIC micelles, the ε-amino group on lysine of positively charged Cyt C was modified with citraconic acid or cis-aconitic acid to turn Cyt C negatively charged so that it could complex with the positively charged block copolymer – PEG-poly[*N*-{*N*'-(2-aminoethyl)-2-aminoethyl}aspartamide] (PEG–pAsp(DET)). This modification generated acid-labile amide bonds that could be cleaved in acidic endosomal compartment upon endocytosis. After cleavage, the lysine group was restored and the protein was then released into the cytoplasm via electrostatic repulsion with the polymer PEG-pAsp(DET).

Complexes based on hydrophobic interactions are also commonly used. Ayame *et al.* developed polymeric nanogels comprising linear polysaccharide pullulan backbone functionalized with the hydrophobic cholesterol groups [69]. These cholesterol-bearing pullulan (CHP) polymer and protein self-assemble in water by physical crosslinking between the hydrophobic cholesterol moieties to form < 50 nm cationic nanogels [69, 71]. CHP nanogels complexes containing BSA and β-galactosidase (β-gal) were internalized into cells more efficiently than cationic liposomes and protein transduction domains (PTD); and endosomal escape of the proteins was also observed 18 hours after treatment.

To improve the stability of non-covalent complexes, complexes comprising of more than one kind of interaction were explored. Jong *et al.* designed a heparin-Pluronic nanogel system in which the negatively charged heparin can bind with positively charged proteins while the hydrophobic blocks of Pluronic create a hydrophobic core to retain hydrophobic molecules [177]. Using RNase A, they achieved a loading efficiency of > 78 % and demonstrated its delivery to the cytoplasm and even nucleus.

But stability can also be a double-edged sword. While high stability is desirable during cargo transport, the drawback is the difficulty in payload deposit at the target site. Once the complex enters the cell; the protein/DNA cargo has to be released in order to exert their biological functions. In fact, complexes that are found to be too stable cause a loss of delivery efficiency [178-180]. For example, Sato *et al.* observed that DNA/polygalactosamine (pGalN) formed highly stable complexes that were able enter cells but failed to dissociate and led to no transfection efficacy [179]. Therefore it is important to control the strength of physical interactions by optimizing the ratio of carrier in non-covalent complexes.

To deliver payload into designated cells, active targeting strategies were explored. One approach was to exploit integrin receptor-mediated endocytosis. The tripeptide Arg-Gly-Asp (RGD) motif is widely used for targeting integrins such as $a_v b_3$ and $a_v b_5$ overexpressed in many cancer cells [181, 182]. Using RGD-modified CHP nanogels, Shimoda *et al.* achieved significantly higher (10 times fluorescent intensity using FITC-BSA) delivery of proteins into cells than unmodified CHP [71]. Modification of heparin-Pluronic nanogels with RGD-ligand was also shown to increase the uptake of complexes into cells as compared to non-modified nanogels [183]. These two studies highlighted the possibility of chemical modification of polymeric carrier to accomplish selective delivery of intracellular cargo.

Table 1-7. Representative non-covalent complexes for intracellular delivery of proteins and DNA.

Type of Complex	Polymer	Cargo	Advantages	Drawbacks	Ref.
Cationic lipid based polymers	Lipopolyamine DOGS	BSA, β-gal, Phycoerythrin,	High efficiency comparable to commercial agents	Binds negatively charged proteins only Release of BSA inhibited Unstable in serum	[184]
Polyionic complex micelle (PIC)	PEG-p(Asp)(DET)	Anti-NPC IgG Cyt C	pH-responsive Non-toxic, nano-sized carriers Demonstrated endosomal escape ability	Chemical modification of protein needed Charge dependent -specific mixing ratio is required	[176, 185]
Nanoparticle complex	PLL-PEG-Folate Folate-*N*-trimethyl-chitosan nanoparticle	FITC-BSA	Active targeting to cancer cells Simple mixing of carrier and protein Non-toxic	Ionic interaction dependent on protein charge Serum free environment necessary	[186, 187]
	Protein Nanocapsule	eGFP HRP BSA	Engineered to be degradable or non-degradable Protect against protease degradation High efficiency comparable to CPP Stable nano-sized carrier	Chemical modification of protein needed	[188, 189]
Physically crosslinked nanogel	Heparin-Pluronic	RNase A	Simple mixing of carrier and protein Nano-sized carriers for passive targeting Non-toxic	Serum free environment necessary Efficiency not very high	[177, 183, 190]
	RGD-functionalized redox-sensitive Heparin-Pluronic	RNase A	RGD peptide active targeting Redox responsive for intracellular release Protection against denaturation Simple mixing of protein and carrier	Carrier itself has some toxicity Targeting moiety not specific to cancer	
	Pullulan nanogel	FITC-BSA β-gal p*Luc* gene	Stable nanosized carrier More effective than PTD or liposome Non-toxic at transfection conc. Endosomal escape function	Cationic carrier interacts well with anionic proteins mostly Lack of targeting (addressed using RGD)	[69, 191, 192]
	PEG-poly(HEMA-co-AC)	Cyt C	Reduction-sensitive, triggered release intracellular glutathione Non-toxic Stable in serum	Tedious preparation; also requires incubation temp of 50 ^{o}C and pH 8 during nanogel formation.	[193]

1.5. Drug carrier design based on (-)-Epigallocatechin-3-gallate (EGCG)

1.5.1. EGCG Overview

(-)-Epigallocatechin-3-gallate (EGCG) is the major component of green tea catechins and is well-known for its anti-oxidative, anti-mutagenic, anti-inflammatory and anti-carcinogenic properties [194-196]. EGCG is a small molecule compound with a Mw of 458 g/mol and its chemical structural comprises of 3 phenol rings and another 6-membered ring with many hydroxyl functional groups (Figure 1-5). This structure of EGCG confers it with the ability to engage in a multitude of non-covalent interactions with other molecules such as hydrophobic interaction [197-200], hydrogen bonding [197-200] and π-π stacking [201, 202] interactions. In particular, EGCG has been shown to bind with bioactive macromolecules such as proteins – lysozyme [197] and human serum albumin (HSA) [199, 200] through both hydrophobic interactions and hydrogen bonding. In light of this property of EGCG, integrating EGCG moiety as part of drug carriers for anticancer therapeutics could potentially lead to augmented interaction between the carrier and payload and address some of the shortcomings of the DDS mentioned in the previous section.

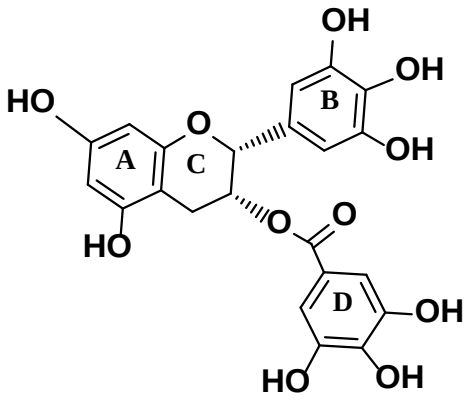

Figure 1-5. Chemical structure of (-)-epigallocatechin-3-gallate (EGCG).

1.5.2. EGCG as a component of drug carriers

The motivation for using EGCG in carrier design is the ability of EGCG to interact with a wide variety of therapeutic molecules such as small molecule drug, DNA or protein through physical interactions. It is expected that such favorable interactions with drugs/proteins/DNA would lead to formation of stable complexes with higher loading capacity.

The goal therefore is to develop polymeric carriers based on EGCG for cancer therapy. Two types of non-covalent polymeric complexes in which EGCG can be incorporated are polymeric micelles and nanogels. An approach to prepare polymeric micelles involves conjugation of EGCG moieties onto the terminal end of hydrophilic polymer blocks. The resultant amphiphilic conjugate can potentially self-assemble to form micelles with hydrophobic anticancer drugs encapsulated within the EGCG core. On the other hand, a nanogel can be formed by physical or chemical interactions between EGCG moieties grafted onto side groups of linear polymers. Various therapeutics can potentially be entrapped within the nanogel complex by physical interactions.

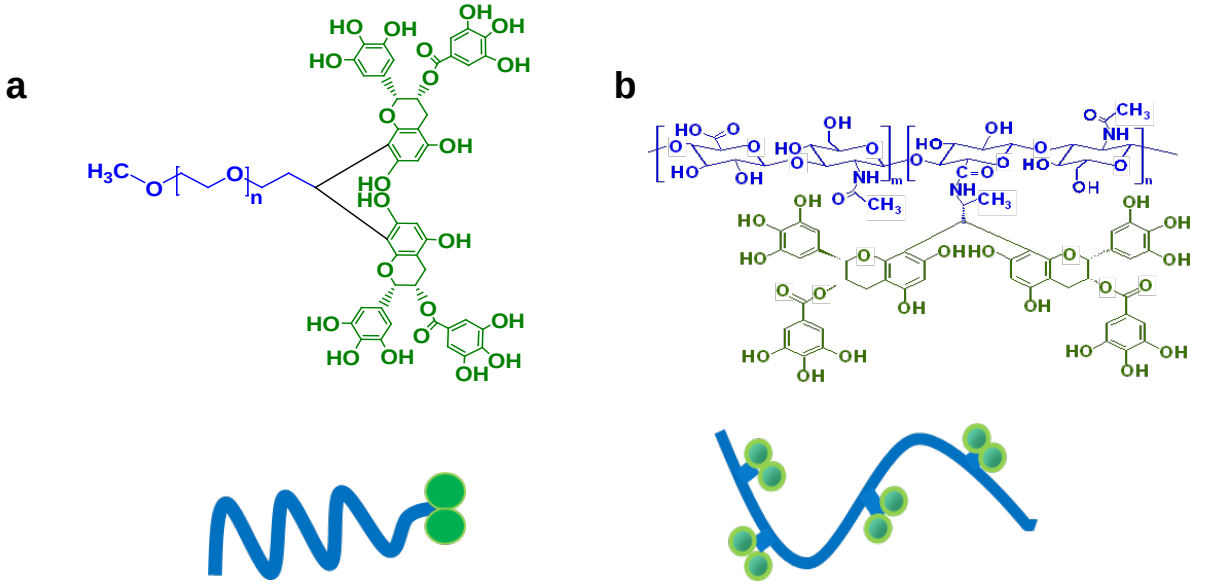

Figure 1-6. Structural formula and pictorial depiction of (a) PEG-EGCG conjugate and (b) HA-EGCG conjugate respectively.

To this end, two different EGCG based conjugates were developed - PEG-EGCG conjugate (polymeric micelle system) and hyaluronic acid (HA)-EGCG conjugate (HA-EGCG) (nanogel system) (Figure 1-6). These two different polymeric carriers were designed specifically to tackle the challenges associated with drug delivery to tumor and intracellular delivery of protein and DNA respectively.

1.5.3. PEG-EGCG carrier for Dox delivery

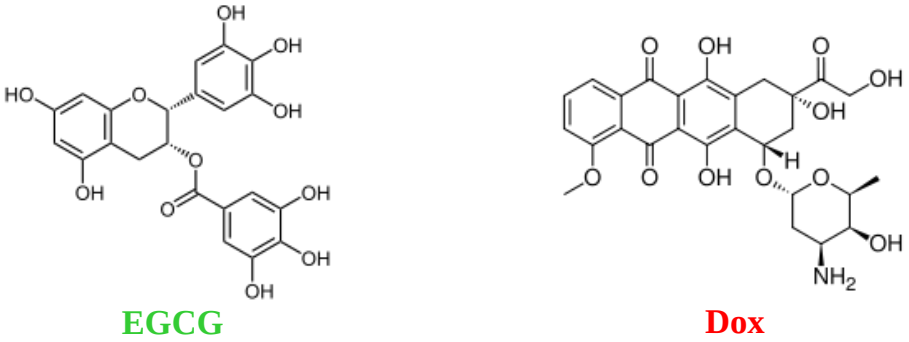

Figure 1-7. Structural similarity of EGCG and Dox, both comprising of multiple rings.

PEG-EGCG conjugate was designed to form polymeric micelles for the delivery of small molecular drugs to tumor tissues. Dox is chosen as the anticancer drug. Dox is an anthracycline antibiotic widely used for chemotherapy. It is a topoisomerase II inhibitor and it hinders DNA synthesis and replication by intercalating between base pairs of the DNA strand [25, 203]. Because of its high potency and non-selectivity, severe side effects are common, including cardiomyopathy and congestive heart failure [204, 205]. Thus many carrier formulations for Dox were developed but with limited success [206].

Among the issues related to Dox delivery systems, the two that are emphasized in this thesis are drug loading capacity and stability. In the section 1.4.1.2., it is suggested that the interaction between Dox and the carrier is an important factor in determining loading capacity

and stability. Thus it is postulated that EGCG moiety could be used to enhance interactions and facilitate Dox delivery. Figure 1-7 depicts the chemical structures of EGCG and the small molecular anticancer drug Dox which both share similar multiple rings. This similarity in structure could lead to favorable intermolecular interactions between the two compounds, in particular π-π stacking and hydrophobic interactions. Therefore EGCG was chosen as the component of the inner core of a polymeric micelle that interacts with Dox. The corona hydrophilic component composes of PEG chains that provide both solubility and "Stealth" property. With this EGCG core and PEG corona arrangement, PEG-EGCG conjugates and DOX would then self-assemble in aqueous environment to form Dox encapsulated micelles.

In contrast to other block copolymers listed in Table 1-4, instead of having a long-chained hydrophobic polymer block such as poly(ε-caprolactone) (PCL) or poly(*b*-benzyl-*l*-aspartate) (PBLA), EGCG moiety with a Mw of 458 g/mol, would be able to interact with Dox efficiently. This would drastically reduce the amount of polymeric carrier used and in turn the proportion of polymer in the drug formulation. Accordingly, the drug loading capacity can be significantly improved. In sum, as a result of the favorable physical interactions between EGCG and Dox in the hydrophobic core, PEG-EGCG polymeric micelles encapsulating Dox is expected to have high drug loading capacity and stability. Thus chemotherapy using stable Dox-loaded PEG-EGCG nanoparticle micelles could overcome the problem of carrier dissociation and drug leakage in circulation, thereby potentially reduce side effects and improve anticancer efficacy.

1.5.4. HA-EGCG carrier for intracellular delivery

HA-EGCG conjugate was designed for the targeted intracellular delivery of protein and DNA in the form of nanogel complexes. Two issues associated with delivery of intracellular anticancer therapeutics such as proteins and DNA to cancer cells are instability and non-

specificity. In the formation of non-covalent complexes, stability is dependent on the interactions between the carrier and the cargo. Since EGCG has the ability to bind both protein and DNA efficiently through hydrophobic interactions, hydrogen bonding and π-π stacking [197, 199, 200, 202, 207], it would be ideal to leverage on this property in designing polymeric carriers for protein delivery. It is expected that the physical interactions between EGCG and proteins/DNA would lead to more stable complex formation and enhance the delivery efficacy.

To improve cancer cell targeting, EGCG moieties were grafted onto hyaluronic acid (HA) polymer backbone. HA is a linear polysaccharide composed of *N*-acetylglucosamine and glucuronic acid disaccharide repeats of variable length [208, 209]. HA plays an important role in cancer biology and it is believed to be involved in biological functions related to cell proliferation, motility, angiogenesis and malignancy [209-212]. More importantly, it binds to HA-receptor, CD44 that are expressed abundantly on many types of cancer cells and enables the uptake of HA by CD44-mediated endocytosis [213, 214]. The application of HA to target cancer cells have been demonstrated extensively [215, 216].

In addition, cancer stem cells, which are a small group of tumor initiating cells within the tumor mass, also display elevated levels of CD44 receptors. Cancer stem cells (CSCs) have been recognized as important targets for cancer treatment because they are closely associated with proliferation and metastasis of cancer cells, as well as enhanced drug resistance and tumor relapse rate [217, 218]. Conventional chemotherapy that eliminates rapidly proliferative cells has little effect on these cells because CSCs are believed to be in a dormant state [219, 220]. By virtue of CD44 targeting, HA based therapeutics could potentially deliver anticancer therapeutics selectively to CSCs to achieve complete cancer eradication.

By grafting EGCG moiety onto the HA polymer backbone, we hypothesized that EGCG and protein/DNA interaction would serve as a driving force for the self-assembly of stable nanogel complexes. The resultant HA-EGCG nanogel complexes would be useful for CD44 targeting by specific delivery of anticancer therapeutics to cancer cells. Since CD44 is also a biomarker of CSCs, this nanogel system can potentially target CSCs to achieve more effective cancer elimination.

1.6. Objective

Our research focusses on using a novel compound - green tea catechin, EGCG as an ingredient of polymeric carriers for cancer therapy. EGCG has been shown to interact with a variety of bioactive molecules including proteins, DNA and small molecular drugs. Therefore we hypothesize that EGCG moiety can be leveraged in carrier design to deliver multiple therapeutic payloads (Figure 1-8).

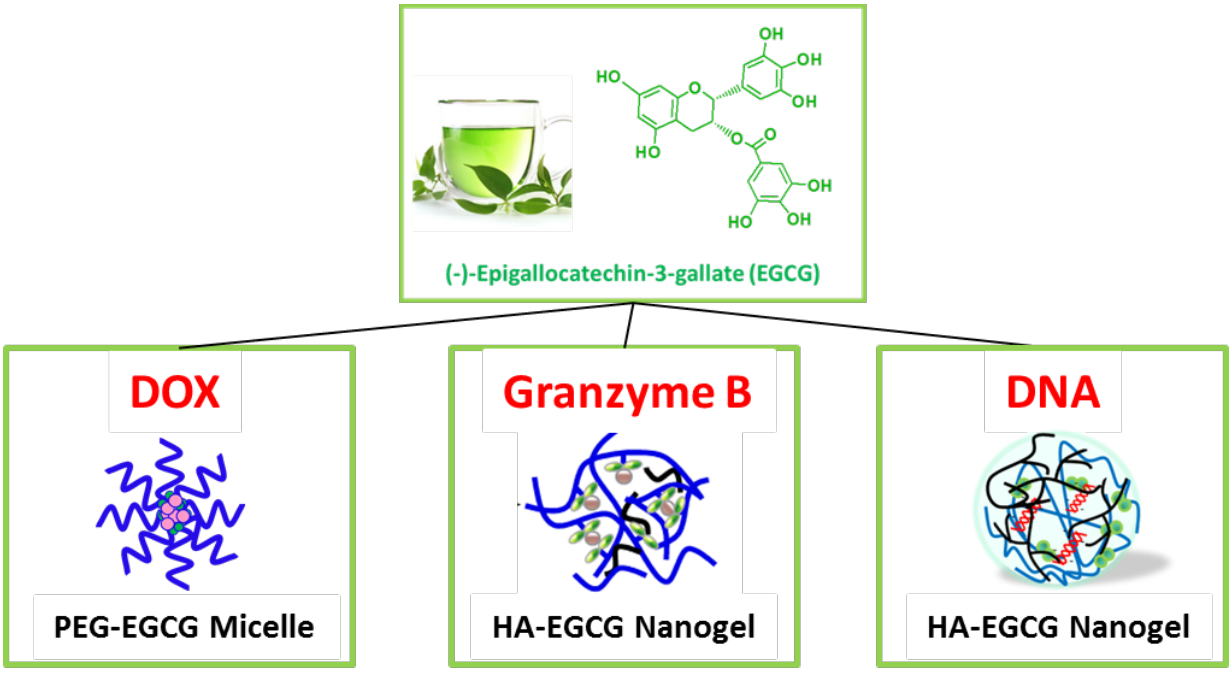

Figure 1-8. Design of EGCG based polymeric carriers for delivery of various anticancer therapeutics.

Hence, the overall objective is to develop polymeric carriers for the delivery of various cancer therapeutics based on EGCG. For this purpose, we synthesized two different EGCG based conjugates - PEG-EGCG and HA-EGCG; and explored the possibility of using them for the delivery of three types of cargo – small molecule drug Dox, protein and DNA. The specific aims within each of the three sections are outlined below:

- Delivery of Dox to tumor tissue using PEG-EGCG conjugates
  - Physically encapsulate Dox into PEG-EGCG polymeric micelles

  - Prepare Dox-loaded PEG-EGCG micelles of high drug loading capacity and high stability
  - Achieve significant antitumor efficacy using Dox-loaded PEG-EGCG micelles *in vivo* with little unwanted toxicity
- Intracellular delivery of protein by HA-EGCG conjugates
  - Investigate interactions between EGCG and the protein GzmB and form stable GzmB and HA-EGCG nanogel complexes
  - Demonstrate selective killing of CD44 overexpressing cancer cells by using the nanogel complexes to deliver GzmB into cytosol of those cells via CD44-mediated endocytosis
- Gene delivery by HA-EGCG conjugates
  - Prepare and characterize HA-EGCG/PEI/DNA nanogel complexes for gene delivery
  - Improve transfection efficiency of CD44 overexpressing cancer cells by exploiting CD44-mediated endocytosis to increase complex uptake

References:

1. Lowe, S.W., E. Cepero, and G. Evan, *Intrinsic tumour suppression.* Nature, 2004. **432**(7015): p. 307-315.
2. Ruddon, R.W., *Cancer biology*. 2007: Oxford University Press.
3. Hanahan, D. and R.A. Weinberg, *The Hallmarks of Cancer.* Cell, 2000. **100**(1): p. 57-70.
4. Fidler, I.J., *Tumor heterogeneity and the biology of cancer invasion and metastasis.* Cancer Research, 1978. **38**(9): p. 2651-2660.
5. Fidler, I.J., D.M. Gersten, and I.R. Hart, *The biology of cancer invasion and metastasis.* Adv cancer res, 1978. **28**(149): p. 6.
6. Dexter, D.L., et al., *Heterogeneity of cancer cells from a single human colon carcinoma.* The American journal of medicine, 1981. **71**(6): p. 949-956.
7. Weiss, L., *Cancer cell heterogeneity.* Cancer and Metastasis Reviews, 2000. **19**(3): p. 345-350.
8. Gottesman, M.M., *Mechanisms of cancer drug resistance.* Annual review of medicine, 2002. **53**(1): p. 615-627.
9. Dean, M., T. Fojo, and S. Bates, *Tumour stem cells and drug resistance.* Nature Reviews Cancer, 2005. **5**(4): p. 275-284.
10. Poste, G. and I.J. Fidler, *The pathogenesis of cancer metastasis.* Nature, 1980. **283**(5743): p. 139-146.
11. Ferlay, J., I. Soerjomataram, and M. Ervik, *GLOBOCAN 2012 v1. 0, Cancer Incidence and Mortality Worldwide: IARC CancerBase No. 11. Lyon, France: International Agency for Research on Cancer; 2013*. 2014.
12. He, Y., et al., *p53 mediated apoptosis by reduction sensitive shielding ternary complexes based on disulfide linked PEI ternary complexes.* Biomaterials, 2014. **35**(5): p. 1657-1666.
13. Wada, H., T. Fukuse, and S. Hitomi, *Long-term survival of surgical cases of lung cancer.* Lung Cancer, 1995. **13**(3): p. 269-274.
14. Lacy, A.M., et al., *Laparoscopy-assisted colectomy versus open colectomy for treatment of non-metastatic colon cancer: a randomised trial.* The Lancet, 2002. **359**(9325): p. 2224-2229.
15. DeVita, V.T., T.S. Lawrence, and S.A. Rosenberg, *Cancer: Principles and Practice of Oncology-Advances in Oncology*. Vol. 1. 2010: Lippincott Williams & Wilkins.
16. Cooper, J.S., et al., *Late effects of radiation therapy in the head and neck region.* International Journal of Radiation Oncology*Biology*Physics, 1995. **31**(5): p. 1141-1164.
17. Dougherty, T.J., et al., *Photoradiation Therapy for the Treatment of Malignant Tumors.* Cancer Research, 1978. **38**(8): p. 2628-2635.
18. DeVita, V.T. and E. Chu, *A History of Cancer Chemotherapy.* Cancer Research, 2008. **68**(21): p. 8643-8653.
19. Love, R.R., et al., *Side effects and emotional distress during cancer chemotherapy.* Cancer, 1989. **63**(3): p. 604-612.
20. Kerbel, R.S. and B.A. Kamen, *The anti-angiogenic basis of metronomic chemotherapy.* Nature Reviews Cancer, 2004. **4**(6): p. 423-436.
21. Chabner, B.A. and T.G. Roberts, *Chemotherapy and the war on cancer.* Nature Reviews Cancer, 2005. **5**(1): p. 65-72.
22. Goodman, L.S., et al., *NITROGEN MUSTARD THERAPYUse of Methyl-Bis (Beta-Chloroethyl) amine Hydrochloride and Tris (Beta-Chloroethyl) amine Hydrochloride for Hodgkin's Disease, Lymphosarcoma, Leukemia and Certain Allied and Miscellaneous Disorders.* Journal of the American Medical Association, 1946. **132**(3): p. 126-132.

23. Li, M.C., R. Hertz, and D.M. Bergenstal, *Therapy of Choriocarcinoma and Related Trophoblastic Tumors with Folic Acid and Purine Antagonists.* New England Journal of Medicine, 1958. **259**(2): p. 66-74.
24. Thurston, D.E., *Chemistry and pharmacology of anticancer drugs*. 2006: CRC press.
25. Boulikas, T., *Introduction to Anticancer Therapeutics*, in *Anticancer Therapeutics*. 2008, John Wiley & Sons, Ltd. p. 47-54.
26. Gelderblom, H., et al., *Cremophor EL: the drawbacks and advantages of vehicle selection for drug formulation.* European Journal of Cancer, 2001. **37**(13): p. 1590-1598.
27. Sawyers, C., *Targeted cancer therapy.* Nature, 2004. **432**(7015): p. 294-297.
28. Shawver, L.K., D. Slamon, and A. Ullrich, *Smart drugs: Tyrosine kinase inhibitors in cancer therapy.* Cancer Cell, 2002. **1**(2): p. 117-123.
29. Robinson, D.R., Y.-M. Wu, and S.-F. Lin, *The protein tyrosine kinase family of the human genome.* Oncogene, 2000. **19**(49): p. 5548-5557.
30. Lemmon, M.A. and J. Schlessinger, *Cell signaling by receptor-tyrosine kinases.* Cell, 2010. **141**(7): p. 1117-1134.
31. Druker, B.J., et al., *Five-Year Follow-up of Patients Receiving Imatinib for Chronic Myeloid Leukemia.* New England Journal of Medicine, 2006. **355**(23): p. 2408-2417.
32. Hartmann, J.T., et al., *Tyrosine kinase inhibitors-a review on pharmacology, metabolism and side effects.* Current drug metabolism, 2009. **10**(5): p. 470-481.
33. Bixby, D. and M. Talpaz, *Mechanisms of resistance to tyrosine kinase inhibitors in chronic myeloid leukemia and recent therapeutic strategies to overcome resistance.* ASH Education Program Book, 2009. **2009**(1): p. 461-476.
34. Sawyers, C.L., *Opportunities and challenges in the development of kinase inhibitor therapy for cancer.* Genes & Development, 2003. **17**(24): p. 2998-3010.
35. Baselga, J., *Targeting tyrosine kinases in cancer: the second wave.* Science, 2006. **312**(5777): p. 1175-1178.
36. Ricci, M.S. and W.-X. Zong, *Chemotherapeutic Approaches for Targeting Cell Death Pathways.* The Oncologist, 2006. **11**(4): p. 342-357.
37. Reed, J.C. and M. Pellecchia, *Apoptosis-based therapies for hematologic malignancies.* Blood, 2005. **106**(2): p. 408-418.
38. Raab, R., et al., *A Phase I Trial of Oblimersen Sodium in Combination With Cisplatin and 5-Fluorouracil in Patients with Advanced Esophageal, Gastroesophageal Junction and Gastric Carcinoma.* American journal of clinical oncology, 2010. **33**(1): p. 61.
39. Loriot, Y., et al., *Inhibition of BCL-2 in small cell lung cancer cell lines with oblimersen, an antisense BCL-2 oligodeoxynucleotide (ODN): in vitro and in vivo enhancement of radiation response.* Anticancer research, 2010. **30**(10): p. 3869-3878.
40. Kasibhatla, S. and B. Tseng, *Why Target Apoptosis in Cancer Treatment?* Molecular Cancer Therapeutics, 2003. **2**(6): p. 573-580.
41. Philchenkov, A., et al., *Caspases and cancer: mechanisms of inactivation and new treatment modalities.* Experimental oncology, 2004. **26**(2): p. 82-97.
42. Tse, E. and T.H. Rabbitts, *Intracellular antibody-caspase-mediated cell killing: an approach for application in cancer therapy.* Proceedings of the National Academy of Sciences, 2000. **97**(22): p. 12266-12271.
43. Van Furth, R., et al., *The mononuclear phagocyte system: a new classification of macrophages, monocytes, and their precursor cells.* Bulletin of the World Health Organization, 1972. **46**(6): p. 845.

44. Nichols, J. and Y. Bae, *Nanotechnology for Cancer Treatment: Possibilities and Limitations*, in *Cancer Targeted Drug Delivery*, Y.H. Bae, R.J. Mrsny, and K. Park, Editors. 2013, Springer New York. p. 37-56.
45. Jain, K., *Drug Delivery Systems - An Overview*, in *Drug Delivery Systems*, K. Jain, Editor. 2008, Humana Press. p. 1-50.
46. Tiwari, G., et al., *Drug delivery systems: An updated review.* International journal of pharmaceutical investigation, 2012. **2**(1): p. 2.
47. Ehrlich, P. and J. Morgenroth, *Ueber Hämolysine: vierte Mittheilung*. 1900: Schumacher.
48. Ehrlich, P., *Chemotherapeutische trypanosomen-studien*. 1907: L. Schumacher.
49. Winau, F., O. Westphal, and R. Winau, *Paul Ehrlich—in search of the magic bullet.* Microbes and Infection, 2004. **6**(8): p. 786-789.
50. Strebhardt, K. and A. Ullrich, *Paul Ehrlich's magic bullet concept: 100 years of progress.* Nat Rev Cancer, 2008. **8**(6): p. 473-480.
51. Bae, Y.H. and K. Park, *Targeted drug delivery to tumors: myths, reality and possibility.* Journal of Controlled Release, 2011. **153**(3): p. 198.
52. Ringsdorf, H., *Structure and properties of pharmacologically active polymers.* Journal of Polymer Science: Polymer Symposia, 1975. **51**(1): p. 135-153.
53. Seymour, L.W., et al., *The pharmacokinetics of polymer-bound adriamycin.* Biochemical Pharmacology, 1990. **39**(6): p. 1125-1131.
54. Duncan, R., et al., *Anticancer agents coupled to N-(2-hydroxypropyl)methacrylamide copolymers. 3. Evaluation of adriamycin conjugates against mouse leukaemia L1210 in vivo.* Journal of Controlled Release, 1989. **10**(1): p. 51-63.
55. Seymour, L.W., et al., *Phase II studies of polymer-doxorubicin (PK1, FCE28068) in the treatment of breast, lung and colorectal cancer.* International journal of oncology, 2009. **34**(6): p. 1629.
56. Gianasi, E., et al., *HPMA copolymer platinates as novel antitumour agents: in vitro properties, pharmacokinetics and antitumour activity in vivo.* European Journal of Cancer, 1999. **35**(6): p. 994-1002.
57. Caiolfa, V.R., et al., *Polymer-bound camptothecin: initial biodistribution and antitumour activity studies.* Journal of Controlled Release, 2000. **65**(1–2): p. 105-119.
58. Lu, Z.-R., P. Kopečková, and J. Kopeček, *Polymerizable Fab' antibody fragments for targeting of anticancer drugs.* Nature biotechnology, 1999. **17**(11): p. 1101-1104.
59. Ulbrich, K., et al., *HPMA copolymers with pH-controlled release of doxorubicin: In vitro cytotoxicity and in vivo antitumor activity.* Journal of Controlled Release, 2003. **87**(1–3): p. 33-47.
60. Vetvicka, D., et al., *Biological evaluation of polymeric micelles with covalently bound doxorubicin.* Bioconjugate Chemistry, 2009. **20**(11): p. 2090-2097.
61. Wong, S.S., *Chemistry of protein conjugation and cross-linking*. 1991: CRC press.
62. Jung, B. and P. Theato, *Chemical strategies for the synthesis of protein–polymer conjugates*, in *Bio-synthetic Polymer Conjugates*. 2013, Springer. p. 37-70.
63. Whitesides, G.M., J.P. Mathias, and C.T. Seto, *Molecular self-assembly and nanochemistry: a chemical strategy for the synthesis of nanostructures*. 1991, DTIC Document.
64. Elemans, J.A., A.E. Rowan, and R.J. Nolte, *Mastering molecular matter. Supramolecular architectures by hierarchical self-assembly.* Journal of Materials Chemistry, 2003. **13**(11): p. 2661-2670.
65. Cerny, J. and P. Hobza, *Non-covalent interactions in biomacromolecules.* Physical Chemistry Chemical Physics, 2007. **9**(39): p. 5291-5303.
66. Baker, A., et al., *Polyethylenimine (PEI) is a simple, inexpensive and effective reagent for condensing and linking plasmid DNA to adenovirus for gene delivery.* Gene therapy, 1997. **4**(8).

67. Haley, B. and E. Frenkel, *Nanoparticles for drug delivery in cancer treatment.* Urologic Oncology: Seminars and Original Investigations, 2008. **26**(1): p. 57-64.
68. Chacko, R.T., et al., *Polymer nanogels: A versatile nanoscopic drug delivery platform.* Advanced Drug Delivery Reviews, 2012. **64**(9): p. 836-851.
69. Ayame, H., N. Morimoto, and K. Akiyoshi, *Self-Assembled Cationic Nanogels for Intracellular Protein Delivery.* Bioconjugate Chemistry, 2008. **19**(4): p. 882-890.
70. Shimizu, T., et al., *Nanogel DDS enables sustained release of IL-12 for tumor immunotherapy.* Biochemical and Biophysical Research Communications, 2008. **367**(2): p. 330-335.
71. Shimoda, A., S.-i. Sawada, and K. Akiyoshi, *Cell Specific Peptide-Conjugated Polysaccharide Nanogels for Protein Delivery.* Macromolecular Bioscience, 2011. **11**(7): p. 882-888.
72. Na, K., et al., *Self-organized pullulan/deoxycholic acid nanogels: Physicochemical characterization and anti-cancer drug-releasing behavior.* Biotechnology and Bioprocess Engineering, 2006. **11**(3): p. 262-267.
73. Zhou, H., et al., *Synthesis and Characterization of Amphiphilic Glycidol−Chitosan−Deoxycholic Acid Nanoparticles as a Drug Carrier for Doxorubicin.* Biomacromolecules, 2010. **11**(12): p. 3480-3486.
74. Kataoka, K., et al., *Doxorubicin-loaded poly(ethylene glycol)–poly(β-benzyl-l-aspartate) copolymer micelles: their pharmaceutical characteristics and biological significance.* Journal of Controlled Release, 2000. **64**(1–3): p. 143-153.
75. Kataoka, K., A. Harada, and Y. Nagasaki, *Block copolymer micelles for drug delivery: design, characterization and biological significance.* Advanced Drug Delivery Reviews, 2001. **47**(1): p. 113-131.
76. Yoo, H.S. and T.G. Park, *Folate receptor targeted biodegradable polymeric doxorubicin micelles.* Journal of Controlled Release, 2004. **96**(2): p. 273-283.
77. Yoo, H.S. and T.G. Park, *Biodegradable polymeric micelles composed of doxorubicin conjugated PLGA–PEG block copolymer.* Journal of Controlled Release, 2001. **70**(1): p. 63-70.
78. Aliabadi, H.M. and A. Lavasanifar, *Polymeric micelles for drug delivery.* Expert Opinion on Drug Delivery, 2006. **3**(1): p. 139-162.
79. Mahmud, A., et al., *Polymeric micelles for drug targeting.* Journal of Drug Targeting, 2007. **15**(9): p. 553-584.
80. Soo, P., et al., *Nano-sized Advanced Delivery Systems as Parenteral Formulation Strategies for Hydrophobic Anti-cancer Drugs*, in *Nanotechnology in Drug Delivery*, M. Villiers, P. Aramwit, and G. Kwon, Editors. 2009, Springer New York. p. 349-383.
81. Matsumura, Y. and H. Maeda, *A New Concept for Macromolecular Therapeutics in Cancer Chemotherapy: Mechanism of Tumoritropic Accumulation of Proteins and the Antitumor Agent Smancs.* Cancer Research, 1986. **46**(12 Part 1): p. 6387-6392.
82. Fang, J., T. Sawa, and H. Maeda, *Factors and Mechanism of "EPR" Effect and the Enhanced Antitumor Effects of Macromolecular Drugs Including SMANCS*, in *Polymer Drugs in the Clinical Stage*, H. Maeda, et al., Editors. 2003, Springer US. p. 29-49.
83. Maeda, H., *The enhanced permeability and retention (EPR) effect in tumor vasculature: the key role of tumor-selective macromolecular drug targeting.* Advances in Enzyme Regulation, 2001. **41**(1): p. 189-207.
84. Maeda, H., et al., *Tumor vascular permeability and the EPR effect in macromolecular therapeutics: a review.* Journal of Controlled Release, 2000. **65**(1-2): p. 271-284.
85. Torchilin, V., *Tumor delivery of macromolecular drugs based on the EPR effect.* Advanced Drug Delivery Reviews, 2011. **63**(3): p. 131-135.
86. Jain, R.K., *Transport of molecules across tumor vasculature.* Cancer and Metastasis Reviews, 1987. **6**(4): p. 559-593.

87. Yuan, F., et al., *Vascular Permeability in a Human Tumor Xenograft: Molecular Size Dependence and Cutoff Size.* Cancer Research, 1995. **55**(17): p. 3752-3756.
88. Yokoyama, M., et al., *Characterization of physical entrapment and chemical conjugation of adriamycin in polymeric micelles and their design for in vivo delivery to a solid tumor.* Journal of Controlled Release, 1998. **50**(1–3): p. 79-92.
89. Nakanishi, T., et al., *Development of the polymer micelle carrier system for doxorubicin.* Journal of Controlled Release, 2001. **74**(1-3): p. 295-302.
90. Iyer, A.K., et al., *Exploiting the enhanced permeability and retention effect for tumor targeting.* Drug discovery today, 2006. **11**(17): p. 812-818.
91. Moses, M.A., H. Brem, and R. Langer, *Advancing the field of drug delivery: Taking aim at cancer.* Cancer Cell, 2003. **4**(5): p. 337-341.
92. Utreja, P., S. Jain, and A.K. Tiwary, *Novel drug delivery systems for sustained and targeted delivery of anti- cancer drugs: current status and future prospects.* Curr Drug Deliv, 2010. **7**(2): p. 152-61.
93. Choi, H.S., et al., *Renal clearance of quantum dots.* Nature biotechnology, 2007. **25**(10): p. 1165-1170.
94. Moghimi, S.M., A.C. Hunter, and J.C. Murray, *Long-Circulating and Target-Specific Nanoparticles: Theory to Practice.* Pharmacological Reviews, 2001. **53**(2): p. 283-318.
95. Owens Iii, D.E. and N.A. Peppas, *Opsonization, biodistribution, and pharmacokinetics of polymeric nanoparticles.* International Journal of Pharmaceutics, 2006. **307**(1): p. 93-102.
96. Liu, D., A. Mori, and L. Huang, *Role of liposome size and RES blockade in controlling biodistribution and tumor uptake of GM1-containing liposomes.* Biochimica et Biophysica Acta (BBA) - Biomembranes, 1992. **1104**(1): p. 95-101.
97. Moghimi, S.M., et al., *Enhanced hepatic clearance of intravenously administered sterically stabilized microspheres in zymosan-stimulated rats.* Journal of Leukocyte Biology, 1993. **54**(6): p. 513-7.
98. Li, S.-D. and L. Huang, *Pharmacokinetics and Biodistribution of Nanoparticles.* Molecular Pharmaceutics, 2008. **5**(4): p. 496-504.
99. Lee, H., et al., *The Effects of Particle Size and Molecular Targeting on the Intratumoral and Subcellular Distribution of Polymeric Nanoparticles.* Molecular Pharmaceutics, 2010. **7**(4): p. 1195-1208.
100. Zhang, G., et al., *Influence of anchoring ligands and particle size on the colloidal stability and in vivo biodistribution of polyethylene glycol-coated gold nanoparticles in tumor-xenografted mice.* Biomaterials, 2009. **30**(10): p. 1928-1936.
101. Yue, J., et al., *Size-dependent biodistribution and antitumor efficacy of polymer micelle drug delivery systems.* Journal of Materials Chemistry B, 2013. **1**(34): p. 4273-4280.
102. Cabral, H., et al., *Accumulation of sub-100 nm polymeric micelles in poorly permeable tumours depends on size.* Nature nanotechnology, 2011. **6**(12): p. 815-823.
103. Levchenko, T.S., et al., *Liposome clearance in mice: the effect of a separate and combined presence of surface charge and polymer coating.* International Journal of Pharmaceutics, 2002. **240**(1–2): p. 95-102.
104. Zhang, J.-S., F. Liu, and L. Huang, *Implications of pharmacokinetic behavior of lipoplex for its inflammatory toxicity.* Advanced Drug Delivery Reviews, 2005. **57**(5): p. 689-698.
105. Otsuka, H., Y. Nagasaki, and K. Kataoka, *PEGylated nanoparticles for biological and pharmaceutical applications.* Advanced Drug Delivery Reviews, 2003. **55**(3): p. 403-419.
106. Vlerken, L., T. Vyas, and M. Amiji, *Poly(ethylene glycol)-modified Nanocarriers for Tumor-targeted and Intracellular Delivery.* Pharmaceutical Research, 2007. **24**(8): p. 1405-1414.

107. Knop, K., et al., *Poly(ethylene glycol) in Drug Delivery: Pros and Cons as Well as Potential Alternatives.* Angewandte Chemie International Edition, 2010. **49**(36): p. 6288-6308.
108. Gref, R., et al., *Biodegradable long-circulating polymeric nanospheres.* Science, 1994. **263**(5153): p. 1600-1603.
109. Sadzuka, Y., S. Hirotsu, and S. Hirota, *Effect of liposomalization on the antitumor activity, side-effects and tissue distribution of CPT-11.* Cancer Letters, 1998. **127**(1): p. 99-106.
110. Hofheinz, R.-D., et al., *Liposomal encapsulated anti-cancer drugs.* Anti-Cancer Drugs, 2005. **16**(7): p. 691-707.
111. Barenholz, Y., *Doxil® — The first FDA-approved nano-drug: Lessons learned.* Journal of Controlled Release, 2012. **160**(2): p. 117-134.
112. Essa, S., J.M. Rabanel, and P. Hildgen, *Characterization of rhodamine loaded PEG-g-PLA nanoparticles (NPs): Effect of poly(ethylene glycol) grafting density.* International Journal of Pharmaceutics, 2011. **411**(1–2): p. 178-187.
113. Gref, R., et al., *'Stealth' corona-core nanoparticles surface modified by polyethylene glycol (PEG): influences of the corona (PEG chain length and surface density) and of the core composition on phagocytic uptake and plasma protein adsorption.* Colloids and Surfaces B: Biointerfaces, 2000. **18**(3–4): p. 301-313.
114. Torchilin, V., *Passive and Active Drug Targeting: Drug Delivery to Tumors as an Example*, in *Drug Delivery*, M. Schäfer-Korting, Editor. 2010, Springer Berlin Heidelberg. p. 3-53.
115. Peer, D., et al., *Nanocarriers as an emerging platform for cancer therapy.* Nat Nano, 2007. **2**(12): p. 751-760.
116. Gu, F.X., et al., *Targeted nanoparticles for cancer therapy.* Nano Today, 2007. **2**(3): p. 14-21.
117. Brannon-Peppas, L. and J.O. Blanchette, *Nanoparticle and targeted systems for cancer therapy.* Advanced Drug Delivery Reviews, 2004. **56**(11): p. 1649-1659.
118. Campbell, I.G., et al., *Folate-binding Protein Is a Marker for Ovarian Cancer.* Cancer Research, 1991. **51**(19): p. 5329-5338.
119. Hilgenbrink, A.R. and P.S. Low, *Folate receptor-mediated drug targeting: From therapeutics to diagnostics.* Journal of Pharmaceutical Sciences, 2005. **94**(10): p. 2135-2146.
120. Suzuki, R., et al., *Effective anti-tumor activity of oxaliplatin encapsulated in transferrin–PEG-liposome.* International Journal of Pharmaceutics, 2008. **346**(1–2): p. 143-150.
121. Bartlett, D.W. and M.E. Davis, *Physicochemical and Biological Characterization of Targeted, Nucleic Acid-Containing Nanoparticles.* Bioconjugate Chemistry, 2007. **18**(2): p. 456-468.
122. Bartlett, D.W., et al., *Impact of tumor-specific targeting on the biodistribution and efficacy of siRNA nanoparticles measured by multimodality in vivo imaging.* Proceedings of the National Academy of Sciences, 2007. **104**(39): p. 15549-15554.
123. Lammers, T., et al., *Drug targeting to tumors: principles, pitfalls and (pre-) clinical progress.* Journal of Controlled Release, 2012. **161**(2): p. 175-187.
124. Pirollo, K.F. and E.H. Chang, *Does a targeting ligand influence nanoparticle tumor localization or uptake?* Trends in Biotechnology, 2008. **26**(10): p. 552-558.
125. Kirpotin, D.B., et al., *Antibody Targeting of Long-Circulating Lipidic Nanoparticles Does Not Increase Tumor Localization but Does Increase Internalization in Animal Models.* Cancer Research, 2006. **66**(13): p. 6732-6740.
126. Choi, C.H.J., et al., *Mechanism of active targeting in solid tumors with transferrin-containing gold nanoparticles.* Proceedings of the National Academy of Sciences, 2010. **107**(3): p. 1235-1240.
127. Davis, M.E., *The first targeted delivery of siRNA in humans via a self-assembling, cyclodextrin polymer-based nanoparticle: from concept to clinic.* Molecular Pharmaceutics, 2009. **6**(3): p. 659-668.

128. Davis, M.E., et al., *Evidence of RNAi in humans from systemically administered siRNA via targeted nanoparticles.* Nature, 2010. **464**(7291): p. 1067-1070.
129. Gabizon, A., et al., *Prolonged circulation time and enhanced accumulation in malignant exudates of doxorubicin encapsulated in polyethylene-glycol coated liposomes.* Cancer Research, 1994. **54**(4): p. 987-992.
130. Kwon, I.K., et al., *Analysis on the current status of targeted drug delivery to tumors.* Journal of Controlled Release, 2012. **164**(2): p. 108-114.
131. Kim, S., et al., *Overcoming the barriers in micellar drug delivery: loading efficiency, in vivo stability, and micelle–cell interaction.* Expert Opinion on Drug Delivery, 2010. **7**(1): p. 49-62.
132. Fukushima, S., et al., *Roles of adriamycin and adriamycin dimer in antitumor activity of the polymeric micelle carrier system.* Colloids and Surfaces B: Biointerfaces, 1999. **16**(1–4): p. 227-236.
133. Drummond, D.C., et al., *Optimizing Liposomes for Delivery of Chemotherapeutic Agents to Solid Tumors.* Pharmacological Reviews, 1999. **51**(4): p. 691-744.
134. *Nano-Oncology: Clinical Application for Cancer Therapy and Future Perspectives.* Journal of Nanomaterials, 2011. **2011**.
135. Rivera, E., *Liposomal Anthracyclines in Metastatic Breast Cancer: Clinical Update.* The Oncologist, 2003. **8**(suppl 2): p. 3-9.
136. Kratz, F., *Albumin as a drug carrier: Design of prodrugs, drug conjugates and nanoparticles.* Journal of Controlled Release, 2008. **132**(3): p. 171-183.
137. Attwood, D., et al., *Block copolymers for drug solubilisation: Relative hydrophobicities of polyether and polyester micelle-core-forming blocks.* International Journal of Pharmaceutics, 2007. **345**(1–2): p. 35-41.
138. Bae, Y. and K. Kataoka, *Intelligent polymeric micelles from functional poly(ethylene glycol)-poly(amino acid) block copolymers.* Advanced Drug Delivery Reviews, 2009. **61**(10): p. 768-784.
139. Garay, R.P., et al., *Antibodies against polyethylene glycol in healthy subjects and in patients treated with PEG-conjugated agents.* Expert Opinion on Drug Delivery, 2012. **9**(11): p. 1319-1323.
140. Abu Lila, A.S., H. Kiwada, and T. Ishida, *The accelerated blood clearance (ABC) phenomenon: Clinical challenge and approaches to manage.* Journal of Controlled Release, 2013. **172**(1): p. 38-47.
141. Shuai, X., et al., *Micellar carriers based on block copolymers of poly(epsilon-caprolactone) and poly(ethylene glycol) for doxorubicin delivery.* Journal of controlled release : official journal of the Controlled Release Society, 2004. **98**(3): p. 415-26.
142. Cuong, N.-V., et al., *Synthesis and characterization of PEG–PCL–PEG triblock copolymers as carriers of doxorubicin for the treatment of breast cancer.* Journal of Applied Polymer Science, 2010. **117**(6): p. 3694-3703.
143. Gaucher, G., et al., *Block copolymer micelles: preparation, characterization and application in drug delivery.* Journal of Controlled Release, 2005. **109**(1): p. 169-188.
144. Aliabadi, H.M. and A. Lavasanifar, *Polymeric micelles for drug delivery.* 2006.
145. Allen, C., D. Maysinger, and A. Eisenberg, *Nano-engineering block copolymer aggregates for drug delivery.* Colloids and Surfaces B: Biointerfaces, 1999. **16**(1): p. 3-27.
146. Liu, J., F. Zeng, and C. Allen, *Influence of serum protein on polycarbonate-based copolymer micelles as a delivery system for a hydrophobic anti-cancer agent.* Journal of Controlled Release, 2005. **103**(2): p. 481-497.
147. Chen, H., et al., *Fast release of lipophilic agents from circulating PEG-PDLLA micelles revealed by in vivo forster resonance energy transfer imaging.* Langmuir, 2008. **24**(10): p. 5213-5217.

148. Tsukioka, Y., et al., *Pharmaceutical and biomedical differences between micellar doxorubicin (NK911) and liposomal doxorubicin (Doxil).* Cancer Science, 2002. **93**(10): p. 1145-1153.
149. Tannock, I.F. and D. Rotin, *Acid pH in Tumors and Its Potential for Therapeutic Exploitation.* Cancer Research, 1989. **49**(16): p. 4373-4384.
150. Gerweck, L.E. and K. Seetharaman, *Cellular pH gradient in tumor versus normal tissue: potential exploitation for the treatment of cancer.* Cancer Research, 1996. **56**(6): p. 1194-1198.
151. Bae, Y., et al., *Preparation and Biological Characterization of Polymeric Micelle Drug Carriers with Intracellular pH-Triggered Drug Release Property: Tumor Permeability, Controlled Subcellular Drug Distribution, and Enhanced in Vivo Antitumor Efficacy.* Bioconjugate Chemistry, 2004. **16**(1): p. 122-130.
152. Kwon, G., et al., *Block copolymer micelles for drug delivery: loading and release of doxorubicin.* Journal of Controlled Release, 1997. **48**(2): p. 195-201.
153. Jeong, Y.-I., et al., *Antitumor activity of adriamycin-incorporated polymeric micelles of poly(γ-benzyl l-glutamate)/poly(ethylene oxide).* International Journal of Pharmaceutics, 2009. **365**(1-2): p. 150-156.
154. Liu, L., et al., *Biodegradable polylactide/poly(ethylene glycol)/polylactide triblock copolymer micelles as anticancer drug carriers.* Journal of Applied Polymer Science, 2001. **80**(11): p. 1976-1982.
155. Lee, E.S., K. Na, and Y.H. Bae, *Polymeric micelle for tumor pH and folate-mediated targeting.* Journal of Controlled Release, 2003. **91**(1): p. 103-113.
156. Zelphati, O., et al., *Intracellular Delivery of Proteins with a New Lipid-mediated Delivery System.* J. Biol. Chem., 2001. **276**(37): p. 35103-35110.
157. Giesubel, U., et al., *Cell binding, internalization and cytotoxic activity of human granzyme B expressed in the yeast Pichia pastoris.* Biochem. J, 2006. **394**: p. 563-573.
158. Ramesh, R., et al., *Successful treatment of primary and disseminated human lung cancers by systemic delivery of tumor suppressor genes using an improved liposome vector.* Molecular Therapy, 2001. **3**(3): p. 337-350.
159. Prabha, S. and V. Labhasetwar, *Nanoparticle-mediated wild-type p53 gene delivery results in sustained antiproliferative activity in breast cancer cells.* Molecular Pharmaceutics, 2004. **1**(3): p. 211-219.
160. Torchilin, V., *Intracellular delivery of protein and peptide therapeutics.* Drug Discovery Today: Technologies, 2008. **5**(2–3): p. e95-e103.
161. Chou, L.Y., K. Ming, and W.C. Chan, *Strategies for the intracellular delivery of nanoparticles.* Chemical Society Reviews, 2011. **40**(1): p. 233-245.
162. Pack, D.W., et al., *Design and development of polymers for gene delivery.* Nature Reviews Drug Discovery, 2005. **4**(7): p. 581-593.
163. Morille, M., et al., *Progress in developing cationic vectors for non-viral systemic gene therapy against cancer.* Biomaterials, 2008. **29**(24–25): p. 3477-3496.
164. Godbey, W.T., K.K. Wu, and A.G. Mikos, *Poly(ethylenimine) and its role in gene delivery.* Journal of Controlled Release, 1999. **60**(2–3): p. 149-160.
165. Boussif, O., et al., *A versatile vector for gene and oligonucleotide transfer into cells in culture and in vivo: polyethylenimine.* Proceedings of the National Academy of Sciences, 1995. **92**(16): p. 7297-7301.
166. Lv, H., et al., *Toxicity of cationic lipids and cationic polymers in gene delivery.* Journal of Controlled Release, 2006. **114**(1): p. 100-109.
167. Harush-Frenkel, O., et al., *Targeting of nanoparticles to the clathrin-mediated endocytic pathway.* Biochemical and Biophysical Research Communications, 2007. **353**(1): p. 26-32.

168. Gratton, S.E., et al., *The effect of particle design on cellular internalization pathways.* Proceedings of the National Academy of Sciences, 2008. **105**(33): p. 11613-11618.
169. Morris, M.C., et al., *A peptide carrier for the delivery of biologically active proteins into mammalian cells.* Nat Biotech, 2001. **19**(12): p. 1173-1176.
170. Muñoz-Morris, M.A., et al., *The peptide carrier Pep-1 forms biologically efficient nanoparticle complexes.* Biochemical and Biophysical Research Communications, 2007. **355**(4): p. 877-882.
171. Weill, C., et al., *A practical approach for intracellular protein delivery.* Cytotechnology, 2008. **56**(1): p. 41-48.
172. Gu, Z., et al., *Tailoring nanocarriers for intracellular protein delivery.* Chemical Society Reviews, 2011. **40**(7): p. 3638-3655.
173. Du, J., et al., *Synthetic nanocarriers for intracellular protein delivery.* Current drug metabolism, 2012. **13**(1): p. 82-92.
174. Fawell, S., et al., *Tat-mediated delivery of heterologous proteins into cells.* Proceedings of the National Academy of Sciences, 1994. **91**(2): p. 664-668.
175. Wadia, J.S. and S.F. Dowdy, *Transmembrane delivery of protein and peptide drugs by TAT-mediated transduction in the treatment of cancer.* Advanced Drug Delivery Reviews, 2005. **57**(4): p. 579-596.
176. Lee, Y., et al., *Charge-Conversional Polyionic Complex Micelles—Efficient Nanocarriers for Protein Delivery into Cytoplasm.* Angewandte Chemie International Edition, 2009. **48**(29): p. 5309-5312.
177. Choi, J.H., et al., *Intracellular delivery and anti-cancer effect of self-assembled heparin-Pluronic nanogels with RNase A.* Journal of Controlled Release, 2010. **147**(3): p. 420-427.
178. Bowman, K. and K.W. Leong, *Chitosan nanoparticles for oral drug and gene delivery.* International journal of nanomedicine, 2006. **1**(2): p. 117.
179. Sato, T., T. Ishii, and Y. Okahata, *In vitro gene delivery mediated by chitosan. Effect of pH, serum, and molecular mass of chitosan on the transfection efficiency.* Biomaterials, 2001. **22**(15): p. 2075-2080.
180. Mao, H.Q. and K.W. Leong, *Design of Polyphosphoester-DNA Nanoparticles for Non-Viral Gene Delivery.* Advances in genetics, 2005. **53**: p. 275-306.
181. Ruoslahti, E., *RGD and other recognition sequences for integrins.* Annual review of cell and developmental biology, 1996. **12**(1): p. 697-715.
182. Pasqualini, R., E. Koivunen, and E. Ruoslahti, *αv integrins as receptors for tumor targeting by circulating ligands.* Nature biotechnology, 1997. **15**(6): p. 542-546.
183. Nguyen, D.H., et al., *Targeting ligand-functionalized and redox-sensitive heparin-Pluronic nanogels for intracellular protein delivery.* Biomedical Materials, 2011. **6**(5): p. 055004.
184. Dalkara, D., G. Zuber, and J.-P. Behr, *Intracytoplasmic Delivery of Anionic Proteins[ast].* Mol Ther, 2004. **9**(6): p. 964-969.
185. Lee, Y., et al., *Efficient Delivery of Bioactive Antibodies into the Cytoplasm of Living Cells by Charge-Conversional Polyion Complex Micelles.* Angewandte Chemie, 2010. **122**(14): p. 2606-2609.
186. Hwa Kim, S., et al., *Folate receptor mediated intracellular protein delivery using PLL–PEG–FOL conjugate.* Journal of Controlled Release, 2005. **103**(3): p. 625-634.
187. Zheng, Y., et al., *Preparation and characterization of folate conjugated N-trimethyl chitosan nanoparticles as protein carrier targeting folate receptor: in vitro studies.* Journal of Drug Targeting, 2009. **17**(4): p. 294-303.
188. Yan, M., et al., *A novel intracellular protein delivery platform based on single-protein nanocapsules.* Nat Nano, 2010. **5**(1): p. 48-53.

189. Biswas, A., et al., *Endoprotease-Mediated Intracellular Protein Delivery Using Nanocapsules.* ACS Nano, 2011. **5**(2): p. 1385-1394.
190. Dai Hai Nguyen, et al., *Disulfide-crosslinked heparin-pluronic nanogels as a redox-sensitive nanocarrier for intracellular protein delivery.* Journal of Bioactive and Compatible Polymers, 2011. **26**(3): p. 287-300.
191. Toita, S., S.-i. Sawada, and K. Akiyoshi, *Polysaccharide nanogel gene delivery system with endosome-escaping function: Co-delivery of plasmid DNA and phospholipase A< sub> 2</sub>.* Journal of Controlled Release, 2011. **155**(1): p. 54-59.
192. Shimoda, A., S.i. Sawada, and K. Akiyoshi, *Cell Specific Peptide-Conjugated Polysaccharide Nanogels for Protein Delivery.* Macromolecular Bioscience, 2011. **11**(7): p. 882-888.
193. Chen, W., et al., *In Situ Forming Reduction-Sensitive Degradable Nanogels for Facile Loading and Triggered Intracellular Release of Proteins.* Biomacromolecules, 2013. **14**(4): p. 1214-1222.
194. Tachibana, H., et al., *A receptor for green tea polyphenol EGCG.* Nat Struct Mol Biol, 2004. **11**(4): p. 380-381.
195. Yang, C., J. Lambert, and S. Sang, *Antioxidative and anti-carcinogenic activities of tea polyphenols.* Archives of Toxicology, 2009. **83**(1): p. 11-21.
196. Yang, C.S., et al., *Cancer prevention by tea: animal studies, molecular mechanisms and human relevance.* Nature Reviews Cancer, 2009. **9**(6): p. 429-439.
197. Ghosh, K.S., B.K. Sahoo, and S. Dasgupta, *Spectrophotometric studies on the interaction between (−)-epigallocatechin gallate and lysozyme.* Chemical Physics Letters, 2008. **452**(1): p. 193-197.
198. Sarni-Manchado, P. and V. Cheynier, *Study of non-covalent complexation between catechin derivatives and peptides by electrospray ionization mass spectrometry.* Journal of mass spectrometry, 2002. **37**(6): p. 609-616.
199. Maiti, T.K., K.S. Ghosh, and S. Dasgupta, *Interaction of (-)-epigallocatechin-3-gallate with human serum albumin: fluorescence, fourier transform infrared, circular dichroism, and docking studies.* Proteins, 2006. **64**(2): p. 355-362.
200. Trnková, L., et al., *Study on the interaction of catechins with human serum albumin using spectroscopic and electrophoretic techniques.* Journal of Molecular Structure, 2011. **985**(2): p. 243-250.
201. Porat, Y., A. Abramowitz, and E. Gazit, *Inhibition of amyloid fibril formation by polyphenols: structural similarity and aromatic interactions as a common inhibition mechanism.* Chemical biology & drug design, 2006. **67**(1): p. 27-37.
202. Zheng, X., et al., *Electrochemical studies of (−)-epigallocatechin gallate and its interaction with DNA.* Analytical and bioanalytical chemistry, 2006. **386**(6): p. 1913-1919.
203. Gewirtz, D., *A critical evaluation of the mechanisms of action proposed for the antitumor effects of the anthracycline antibiotics adriamycin and daunorubicin.* Biochemical Pharmacology, 1999. **57**(7): p. 727-741.
204. Saltiel, E. and W. McGuire, *Doxorubicin (Adriamycin) Cardiomyopathy—A Critical Review.* Western Journal of Medicine, 1983. **139**(3): p. 332.
205. Singal, P.K. and N. Iliskovic, *Doxorubicin-induced cardiomyopathy.* New England Journal of Medicine, 1998. **339**(13): p. 900-905.
206. Matsumura, Y. and K. Kataoka, *Preclinical and clinical studies of anticancer agent-incorporating polymer micelles.* Cancer Science, 2009. **100**(4): p. 572-579.
207. Abe, I., K. Kashiwagi, and H. Noguchi, *Antioxidative galloyl esters as enzyme inhibitors of p-hydroxybenzoate hydroxylase.* FEBS Lett, 2000. **483**(2-3): p. 131-4.
208. Girish, K. and K. Kemparaju, *The magic glue hyaluronan and its eraser hyaluronidase: a biological overview.* Life Sciences, 2007. **80**(21): p. 1921-1943.

209. Necas, J., et al., *Hyaluronic acid (hyaluronan): a review.* Veterinarni medicina, 2008. **53**(8): p. 397-411.
210. Bartolazzi, A., et al., *Interaction between CD44 and hyaluronate is directly implicated in the regulation of tumor development.* The Journal of experimental medicine, 1994. **180**(1): p. 53-66.
211. Sy, M.S., et al., *Interactions Between CD44 and Hyaluronic Acid: Their Role in Tumor Growth and Metastasis*, in *Attempts to Understand Metastasis Formation III*, U. Günthert, P. Schlag, and W. Birchmeier, Editors. 1996, Springer Berlin Heidelberg. p. 129-153.
212. Kultti, A., et al., *Therapeutic targeting of hyaluronan in the tumor stroma.* Cancers, 2012. **4**(3): p. 873-903.
213. Knudson, W., G. Chow, and C.B. Knudson, *CD44-mediated uptake and degradation of hyaluronan.* Matrix Biology, 2002. **21**(1): p. 15-23.
214. Ghosh, S.C., S. Neslihan Alpay, and J. Klostergaard, *CD44: a validated target for improved delivery of cancer therapeutics.* Expert opinion on therapeutic targets, 2012. **16**(7): p. 635-650.
215. Choi, K.Y., et al., *Hyaluronic acid-based nanocarriers for intracellular targeting: interfacial interactions with proteins in cancer.* Colloids and Surfaces B: Biointerfaces, 2012. **99**: p. 82-94.
216. Oh, E.J., et al., *Target specific and long-acting delivery of protein, peptide, and nucleotide therapeutics using hyaluronic acid derivatives.* Journal of Controlled Release, 2010. **141**(1): p. 2-12.
217. Dean, M., T. Fojo, and S. Bates, *Tumour stem cells and drug resistance.* Nat Rev Cancer, 2005. **5**(4): p. 275-284.
218. Jordan, C.T., M.L. Guzman, and M. Noble, *Cancer Stem Cells.* New England Journal of Medicine, 2006. **355**(12): p. 1253-1261.
219. Clevers, H., *The cancer stem cell: premises, promises and challenges.* Nat Med, 2011: p. 313-319.
220. Visvader, J.E. and G.J. Lindeman, *Cancer stem cells in solid tumours: accumulating evidence and unresolved questions.* Nature Reviews Cancer, 2008. **8**(10): p. 755-768.

Chapter 2: Development of doxorubicin-loaded poly(ethylene glycol)-green tea catechin polymeric micelles for cancer therapy

2.1. Introduction

Chemotherapy has been widely used for cancer treatment but is plagued by rampant toxicity [1]. Chemotherapeutic drugs damage all proliferating cells in the body non-specifically in hope that cancer cells are eliminated before normal cells [2, 3]. In addition, majority of the administered drugs do not reach their intended target tumors but are distributed throughout other parts of the body instead, contributing to adverse side effects such as nausea, hemorrhage and inflammation. The application of nanomedicine, in particular anticancer drug delivery systems, has been widely considered as a promising strategy to improve conventional chemotherapy [4]. Anticancer drugs packaged in nanoparticle formulations experienced drastically improved pharmacokinetics and tissue distribution over the stand-alone drug [5, 6], resulting in diminished toxicity. This has led to the eventual approval of liposomal nanocarriers such as DOXIL® for clinical use [7].

One class of nanocarriers that has garnered increasing interest is polymeric micelle. Polymeric micelles are well-defined core-shell structures consisting of a hydrophobic inner core for drug loading and a hydrophilic shell - typically comprising linear PEG that provides the "Stealth" property in circulation [8]. Micellar carriers confer several advantages, such as increased drug solubility, increased plasma half-life and reduced clearance by reticulo-endothelial system (RES) [8, 9]. In addition, their nanosizes (~ 100 nm) allow them to accumulate passively at tumor site *via* enhanced permeability and retention (EPR) effect [10]. One of the most successful micelle formulations for the delivery of various anticancer drugs developed by Kataoka *et al.*, based on the PEG-poly(aspartic acid) block copolymer, has since progressed to the clinical stages [11]. Despite the promises, several concerns still remain. First, typical polymer micelles have low drug loading capacities of 5 – 20 % (w/w) [8, 12] because

they generally encompass high molecular weight hydrophobic polymer units to interact favorably with hydrophobic drugs, leading to low drug loading and low carrier efficiency [13]. Second, upon intravenous administration polymeric micelles are confronted by many challenges in the blood stream that may disrupt their integrity [14, 15]. For instance, severe dilution to below the critical micelle concentration (CMC) may lead to dissociation of micelles [16]. In addition, they may be destabilized by blood plasma proteins through adsorption and core infiltration, leading to premature release of drugs [17, 18]. This instability not only hamper the delivery of anticancer drugs to tumor sites but may also lead to off-target toxicity [15, 19].

In our efforts to design micellar carriers to overcome these limitations, we are inspired to incorporate the molecule EGCG as a novel feature. EGCG is the main constituent of green tea catechins that is widely reported to possess anticancer and anti-oxidative properties [20, 21]. Dox is chosen as the anticancer drug. Dox is an anthracycline antibiotic widely used for chemotherapy. It is a topoisomerase II inhibitor and hinders DNA synthesis and replication by intercalating between base pairs of the DNA strand [22]. Both EGCG and Dox are small molecules and share similar aromatic multiple-ringed chemical structures. Based on reports of EGCG binding to aromatic residues of proteins through π-π stacking and hydrophobic interactions [23, 24], we expect that this similarity in structure could lead to favorable intermolecular interactions between the two molecules.

In this chapter, the formation of a novel polymeric anticancer drug carrier, Dox-loaded EGCG based micelle is described. PEG-EGCG conjugates - comprising two EGCG moieties chemically bonded to the terminal end of PEG chain, were synthesized and used to prepare Dox encapsulating micelles. We hypothesize that interactions between EGCG and Dox would support the formation of a core-shell micellar configuration in which EGCG and Dox could be

sequestered in the hydrophobic core surrounded by a hydrophilic PEG shell. As a result of the strong interactions between EGCG and Dox, these Dox-loaded PEG-EGCG micelles are expected to have enhanced drug loading capacity and stability. Hence, we investigated the physicochemical properties of the Dox-loaded PEG-EGCG micelles including size, drug loading capacity, drug release profile and stability. Most importantly, the anticancer effects of the Dox-loaded PEG-EGCG micelles were evaluated in HAK-1B liver carcinoma cells both *in vitro* and *in vivo,* with two clinically relevant Dox formulations - free Dox and the nanocarrier based DOXIL® as comparisons.

2.2. Materials and Methods

2.2.1. Materials

Dox·HCl was purchased from (Boryung Pharm. Inc, Korea). PEG-aldehyde (PEG-CHO) was bought from NOF Japan. EGCG (TEAVIGO) was purchased from DMS Nutritional Products Ltd Switzerland. AlamarBlue® was purchased from Invitrogen. All buffers, including phosphate buffer saline ((PBS) 150 mM, pH 7.3), and media were supplied by Biopolis Shared Facilities (BSF), Singapore.

2.2.2. Synthesis of PEG-EGCG Conjugate

PEG-EGCG was synthesized by conjugation between a terminal aldehyde group of PEG-CHO and the A ring of EGCG as described in a previous report [25]. Briefly, the aldehyde-terminated PEG (PEG-CHO, Mw 5000) and EGCG were separately dissolved in a mixture of acetic acid, water and DMSO. The reaction was initiated with the dropwise addition of the PEG-CHO solution, and was conducted at 20 °C (pH 2) under a nitrogen atmosphere for 48 h. The resulting products were dialyzed (Mw cut-off: 3500 Da) and lyophilized to give PEG-EGCG.

2.2.3. Preparation of Dox-loaded PEG-EGCG micelles

Dox·HCl was dissolved in 1 ml of DMF at final concentration of 12 mg/ml. Five mole ratio of TEA was added to the solution and the mixture was vortexed for 15 min. Subsequently, 6 different concentrations of PEG-EGCG (Mw 5,000) in the range of 0.5 - 24 mg/ml pre-dissolved in 1 ml of DMF were added and the final mixture was vortexed for another 1 h at room temperature. Following that, the mixtures were transferred into dialysis tubings (Mw cut-off:

3500 Da) (Spectrapor, Spectrumlabs, USA) and dialyzed against de-ionized water. Water was changed every 6 - 8 h. After 3 days of dialysis, the contents from the dialysis tubings were collected and freeze-dried.

An optimized batch of highly concentrated Dox-loaded PEG-EGCG micelles which comprised PEG-EGCG (Mw 10,000) (10kPE-1U) was also prepared. Both feed Dox and PEG-EGCG concentrations were lowered to 1 mg/ml by dissolving in 12 ml of DMF. After mixing, dialysis was performed for 6 h and then the contents from tubing were subjected to ultrafiltration using Amicon Ultra-15 centrifugal filter units (Millipore) to remove the free Dox from the micelle solution. The sample was then freeze-dried.

2.2.4. Determination of physiochemical properties of micelles

1. **NMR**

Freeze-dried Dox-loaded PEG-EGCG micelles were dissolved in D_2O or DMSO-d_6 for NMR analysis. Proton NMR signals were recorded with a Bruker 400 MHz Ultrashield Plus (Bruker BioSpin, MA, USA) and chemical shifts were expressed as parts per million (ppm).

2. **Particle size**

Dynamic light scattering (DLS) was used to determine the hydrodynamic size of the Dox-loaded PEG-EGCG micelles. The micelle solutions were passed through 0.2 μm microfilter before measurement. DLS measurements were performed using Zetasizer 3000 HAS (Malvern Instrument Ltd., Malvern, UK) equipped with a He–Ne laser beam at 658 nm (dynamic light scattering, scattering angle: 901). Measurements were performed in triplicates.

3. **Drug loading**

Freeze-dried micelles were re-dissolved in DMF for quantification of drug loading. The amount of Dox in the micelle was determined by measuring the absorbance at 480 nm using a UV–VIS spectrophotometer (Hitachi). Dox solutions of various concentrations in DMF were prepared, and the absorbance at 485 nm was measured to generate a standard curve to determine concentration of Dox in micelle samples. After obtaining the Dox amount in micelle, drug loading content (DLC) and drug loading efficiency (DLE) could be derived using formula 1 and formula 2 respectively.

$$\text{Drug loading content (DLC) (\%)} = \frac{\text{weight of drug in micelle}}{\text{total weight of micelle}} \times 100 \quad \text{----------} \quad \textbf{(1)}$$

$$\text{Drug loading efficiency (DLE) (\%)} = \frac{\text{weight of drug in micelle}}{\text{weight of drug in feed}} \times 100 \quad \text{-------} \quad \textbf{(2)}$$

4. **Fluorescence intensity**

Dox-loaded PEG-EGCG micelles were diluted in water to final Dox concentration of 200 µg/ml as determined by absorbance measurements. The micelles were then subjected to fluorescence measurements using a FluoroMax-4 spectrofluorometer (Horiba). The excitation wavelength was fixed at 480 nm and the emission wavelength range of 520 – 650 nm was monitored. Free Dox was used as control in both experimental settings.

5. **Critical micelle concentration (CMC)**

CMC was determined by dynamic laser scattering (DLS) using the Malvern Zetasizer, using a method described previously [26]. Detection was made using back scatter optical arrangement at an angle of 173°. A series of micelle solutions ranging from 2 to 0.05 µg/ml was prepared from an aqueous stock solution of Dox-loaded PEG-EGCG micelle. Hydrodynamic size was plotted against the concentration and the intersection of best fit lines drawn through the data

points correspond to the estimated CMC value of the micelle. All the measurements were performed in triplicates.

6. **Kinetic stability**

The kinetic stability of the Dox-loaded PEG-EGCG micelles was probed by two independent methods. The first method is to monitor the change in the hydrodynamic size of micelle caused by fetal bovine serum (FBS) destabilization. The micelles were diluted in PBS with 10 % FBS to reach a final concentration of 250 μg/ml and the sizes of the micelles were monitored up to 4 weeks.

In the second method, the scattered light intensity of the micelles in distilled water was measured in the presence of sodium dodecyl sulfate (SDS) acting as a destabilizing agent. Thirty μl of SDS solution (50 mg/ml) was added to 1 ml of the micelles (250 μg/ml) and the scattered light intensity of the resultant solution was monitored by DLS over a period of up to 4 weeks. All the measurements were performed in triplicates.

2.2.5. *In vitro* release study

Freeze-dried micelle samples were re-suspended in water and transferred into dialysis tubings (Mw cut-off: 1000 Da). Sample Dox concentrations were fixed at 200 μg/ml. The tubing was placed into 30 ml PBS solutions in a 50-ml centrifuge tube. The release of Dox was monitored at 37 ^{o}C in an incubator shaker. At selected time intervals, buffered solution outside the dialysis bag was removed for fluorescence measurements (Hitachi Spectroflurometer F-2500) and replaced with fresh buffer solution. A Dox standard curve at fluorescence intensity of 480 nm was generated and the Dox sample concentrations were calculated based on it.

2.2.6. Cell viability assay

HepG2 hepatocarcinoma cells were maintained in Dulbecco's modified Eagle's medium (DMEM) and HAK-1B liver carcinoma cells were maintained in RPMI medium 1640, both containing 10 % FBS and 1 % penicillin/streptomycin at 37 °C with 5 % $CO_{2.}$ For cytotoxicity assay, both cells were harvested and plated at a density of 10,000 cells per well in 96-well plates and incubated for 24 h. Cells were then exposed to a series of free Dox or micelle-encapsulated Dox at various concentrations for a designated period of time. The viability of cells was determined using the AlamarBlue® assay (Invitrogen) at the designated time-points. Briefly, cells were gently washed with PBS once before fresh medium with AlamarBlue® (10 % v/v) was added. The cells were incubated for another 2 h and fluorescence was measured using a Tecan Infinite Microplate Reader (Ex/Em: 545/590 nm). Cell viability was expressed as a percentage of untreated control cells and the data was reported as mean ± s.d. of quadruplicates.

2.2.7. Intracellular trafficking of DOX-loaded PEG-EGCG micelle

HAK-1B cells were seeded in an 8-well chamber slide (Lab-Tek®) and left to attach overnight. Free Dox (25 μg/ml) and Dox-loaded PEG-EGCG micelles (25 μg/ml of Dox equivalent concentration) were added to the cells and incubated for 4 or 24 h. Before confocal microscopy, cells were gently washed twice with cold PBS and the cell nuclei were subsequently stained with Hoechst 33342 (Molecular Probes). Finally, the cells were visualized using a confocal laser scanning microscope (Zeiss LSM 510 META).

2.2.8. *In vivo* tumor inhibition study

The *in vivo* study was performed on 6 – 8 weeks old BALB/c nude mice using a HAK-1B human liver carcinoma xenograft model. To establish the HAK-1B model, the mice were

injected subcutaneously in the right flank with 0.1 ml of cell suspension containing 10 million HAK-1B cells. When the tumors had grown to approximately 100 mm^3, the various treatments were administered (day 0). Tumor-bearing mice were randomly assigned to one of the following treatment groups (n = 8 - 10 mice per group): normal saline (control), free Dox: 1 mg/kg, 2 mg/kg, 5 mg/kg and 10 mg/kg, DOXIL: 1 mg/kg, 2 mg/kg, 5 mg/kg and 10 mg/kg and Dox-loaded PEG-EGCG micelles: 25 mg/kg and 50 mg/kg. All dosages were reported as Dox equivalent concentrations. Three dosages of various treatments were given through tail vein injection on day 0, day 4 and day 7 respectively. The tumor size and body weight of all the tumor-bearing mice were monitored. The tumor size was measured externally using calipers during the experimental period and was approximated by using the equation vol. = $(a \times b^2)/2$, where vol is volume, a is the length of the major axis, and b is the length of the minor axis. The C-26 mouse colon carcinoma model was established in a similar manner. But only 10,000 C-26 cells were subcutaneously injected per mice. All other treatment procedures except the administered samples were consistent with HAK-1B study. All animal studies were performed in accordance to protocols approved by the Singapore Biological Resource Centre's Institutional Animal Care and Use Committee (IACUC).

2.2.10. Statistical analysis

Data were expressed as mean ± s.d. Student's t-test was used for all statistical analysis between two groups. ANOVA testing (OriginLab Corporation, MA, USA) of sample means was performed with $p < 0.05$ (denoted by *) being accepted to be statistically significant.

2.3. Results and discussion

2.3.1. Preparation and characterizations of Dox-loaded PEG-EGCG micelles

PEG-EGCG conjugates were synthesized by aldehyde-mediated reaction between A-ring of EGCG and aldehyde-terminated PEG, as described in a previous report [25]. In this study, we prepared Dox-loaded PEG-EGCG micelles using the dialysis method in which a mixture of Dox and PEG-EGCG conjugates in organic solvent was dialyzed against water. Driven by the interactions between EGCG moieties and Dox, we hypothesize that PEG-EGCG conjugates and Dox would self-assemble spontaneously to form Dox-encapsulated PEG-EGCG micelles (Figure 2-1).

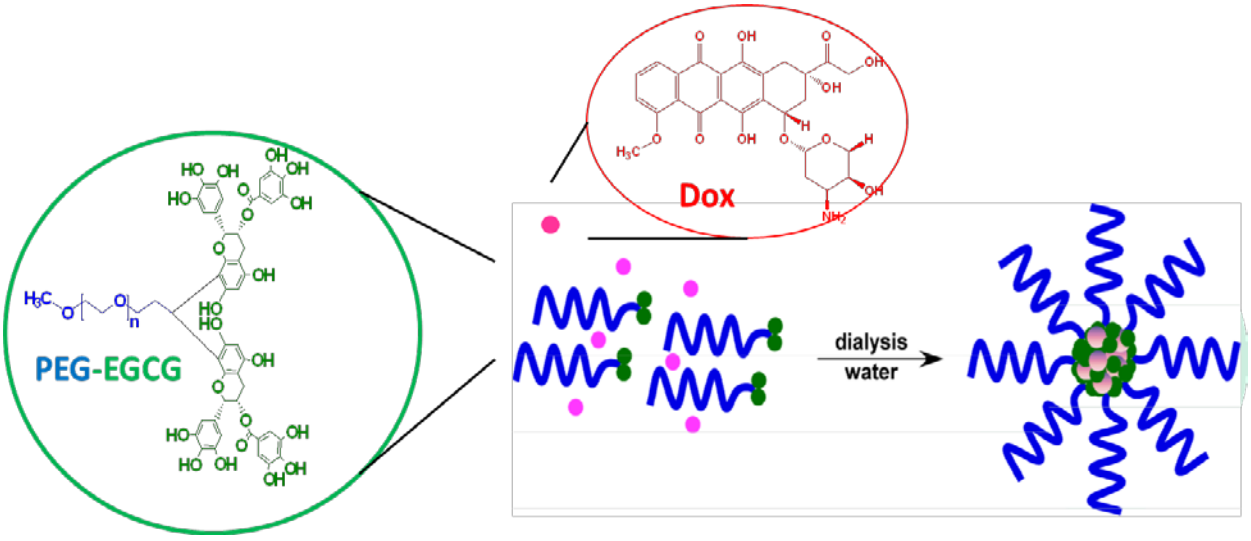

Figure 2-1. Formation of Dox-encapsulated PEG-EGCG micelles by the self-assembly of Dox and PEG-EGCG conjugates in aqueous solution.

We attempted to prepare micelles by varying the feed weight ratio of PEG-EGCG conjugates to Dox. The feed Dox concentration was fixed at 12 mg/ml. Six different feed PEG-EGCG (Mw 5,000) to Dox weight ratios in the range of 0.04 - 2 were used. A control with PEG-EGCG (0 mg/ml) was also set up. Figure 2-2 illustrates the appearance of the test solutions after dialysis. Distinct red Dox precipitate was observed for samples prepared using PEG-EGCG to

Dox feed weight ratios below 0.08 (Figure 2-2 a). In contrast, samples with PEG-EGCG to Dox feed weight ratios above 0.25 yielded clear homogeneous solutions without any precipitate (Figure 2-2 b). It is clear from the results that the solubility of Dox dramatically increased with higher PEG-EGCG concentration.

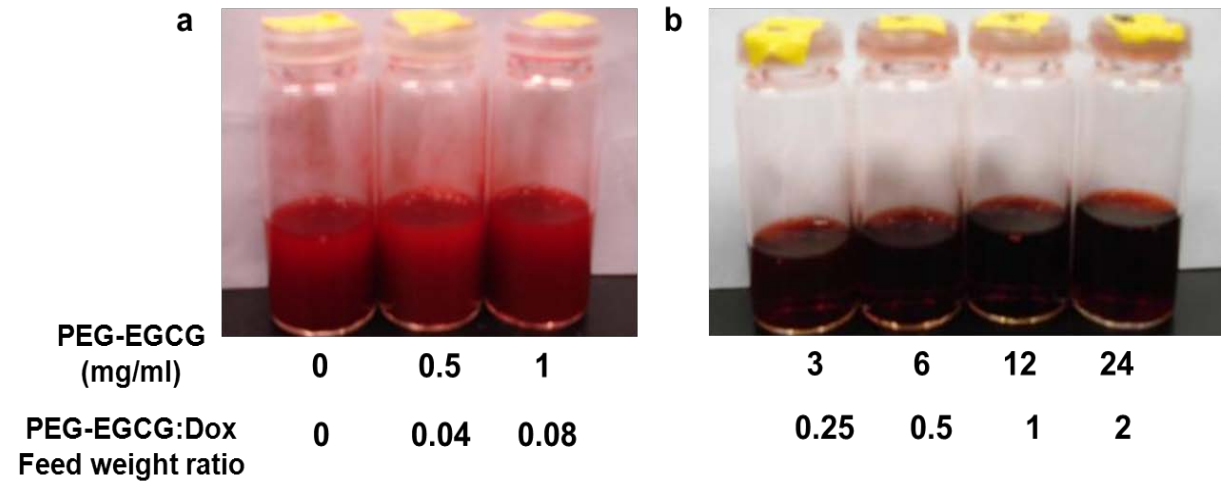

Figure 2-2. Preparation of PEG-EGCG and Dox micelles using dialysis method. (a) Formation of free Dox precipitates in PEG-EGCG (Mw 5,000) to Dox feed weight ratio < 0.08. (b) Clear homogenous solutions were obtained at PEG-EGCG to Dox feed weight ratios > 0.25.

In accordance with previous report [27], in absence of PEG-EGCG, the hydrophobic Dox molecules interacted with one another to form Dox-Dox self-aggregates, leading to precipitation in aqueous environment. The formation of Dox self-aggregates was corroborated by the observation of self-quenching of Dox fluorescence with increasing Dox concentrations (Figure 2-3 a). Besides Dox-Dox associations, Dox molecules could also interact with EGCG molecules through hydrophobic and π-π stacking interactions, resulting in concentration-dependent quenching of Dox fluorescence as shown in Figure 2-3 b. Therefore the solubility data suggests that the interactions between Dox and EGCG moieties on PEG-EGCG contributed to the complete dissolution of Dox within PEG-EGCG micelles.

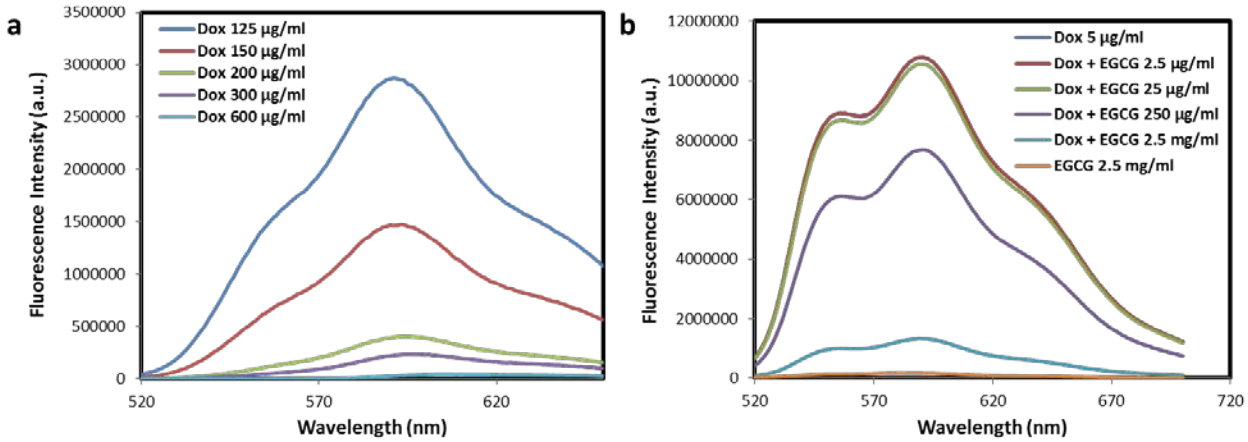

Figure 2-3. (a) Self-quenching of Dox fluorescence with increasing Dox concentrations. (b) EGCG induced quenching of Dox fluorescence with fixed Dox concentration of 5 µg/ml.

To verify that the interactions between EGCG and Dox led to micelle formation, ^{1}H NMR analysis was performed on the sample with PEG-EGCG to Dox feed weight feed ratio of 0.25 which yielded a clear solution. The sample was freeze-dried and resuspended in two solvents - DMSO-d_6 and D_2O (Figure 2-4). In DMSO-d_6, prominent peaks (4.0 - 8.5 ppm) of Dox were observed along with the ethylene proton peak of PEG at ~3.6 ppm, indicating that the sample contained both PEG and Dox. In contrast, only the peak corresponding to ethylene repeating unit of PEG was visible in D_2O but not Dox peaks. A possible explanation is that in DMSO-d_6, both the PEG-EGCG and Dox were fully dissolved in mixture form, thereby contributing to ^{1}H NMR signal. However in D_2O, they adopted a core-shell conformation in which Dox was encapsulated within the core and thus insufficiently solvated to produce a signal. Therefore these results indicate the successful encapsulation of Dox by PEG-EGCG conjugates to form micelles, which is consistent with other reports of micelle formation based on ^{1}H NMR analysis [28, 29].

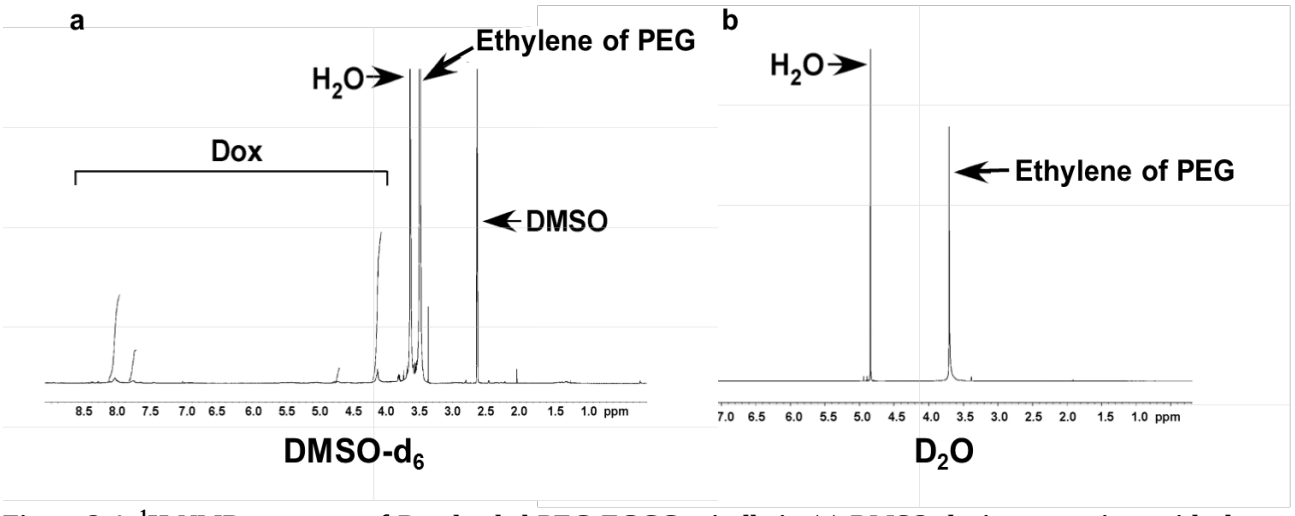

Figure 2-4. ^{1}H NMR spectrum of Dox-loaded PEG-EGCG micelle in (a) DMSO-d_6, in comparison with the spectrum observed in (b) D_2O.

2.3.2. Characterizations of Dox-loaded PEG-EGCG micelles

After confirming micelle formation from the characterization above, we investigated the physicochemical properties of the micelles. Table 2-1 summarizes the results. The micelles prepared with PEG-EGCG (Mw 5,000) to Dox feed weight ratios of 0.25, 0.5, 1 and 2 were denoted as 5kPE-0.25, 5kPE-0.5, 5kPE-1 and 5kPE-2 respectively. First, drug loading efficiency (DLE) improved with increasing PEG-EGCG to Dox feed weight ratio, since increasing PEG-EGCG probably resulted in more efficient Dox entrapment. This was supported by finding that the solubility of Dox was enhanced with higher PEG-EGCG concentrations. Second, drug loading content (DLC) increased with decreasing PEG-EGCG to Dox feed weight ratio. We noted that a very low PEG-EGCG to Dox feed weight ratios of 0.25 was sufficient to achieve effective Dox encapsulation, which led to an exceptionally high DLC of 5kPE-0.25 micelles at 86 %. This is significantly higher than the average Dox loading content of 5 - 20 % obtained from using other block copolymer micelles [8]. This is probably because existing block copolymer micelles tend to incorporate high molecular weight hydrophobic blocks to interact with Dox, thus decreasing the weight percentage of the drug in the carrier system considerably.

For instance, PEG-poly(b-benzyl-l-aspartate) (PEG-PBLA) micelles that attained a DLC of 20 % were formed using block copolymer with molecular weight of ~ 18,000 Da [30]. In contrast, as PEG-EGCG conjugate had a much smaller molecular weight of ~ 6,000 Da, the weight percentage of Dox in PEG-EGCG micelles was increased significantly. It is worth mentioning that a DLC of 86 % indicated that the molar ratio of Dox to EGCG ratio was ~ 30 to 1. To achieve this high level of Dox loading, we hypothesize that during dialysis in aqueous environment, hydrophobic Dox molecules with interact with each other as well as with EGCG moieties. The interaction between Dox and EGCG would drive the self-assembly of core-shell nanostructures in the form of micelles. In the process of micelle formation, many Dox molecules, including Dox-Dox self-aggregates, were packed into the concentrated hydrophobic core, thereby yielding clear solutions (Figure 2-2). While in the absence of PEG-EGCG, Dox-Dox self-aggregates precipitated readily. As a result of the effective encapsulation of Dox and Dox-Dox self-aggregates, an exceptionally high drug loading content was obtained.

Finally, the particle sizes of all the micelles were determined. As PEG-EGCG to Dox feed weight ratio increased from 0.25 to 2, the particle sizes decreased from 93 nm to 21.4 nm. The reduction in size as a function of increasing PEG-EGCG to Dox feed weight ratio correlates well with DLC. This implies that particle size could be directly influenced by the amount of Dox encapsulated within the core of micelle.

We also prepared another batch of highly concentrated Dox-loaded PEG-EGCG micelles using PEG-EGCG (Mw 10,000). A modification was introduced in the preparation protocol for this batch - The feed Dox and PEG-EGCG concentrations were lowered to 1 mg/ml.

The characteristics of this batch of micelles (10kPE) are listed in Table 2-1. The DLEs were higher than the 5kPE counterparts while the DLCs were found to be similar to 5kPE

micelles. Interestingly, we observed that particle size was considerably larger (124 - 152 nm) compared to 5kPE micelles, possibly due to increase in the PEG chain lengths. 10kPE-1 micelles were further concentrated by ultrafiltration to increase Dox concentration of the micelle (10kPE-1U) for *in vitro* and *in vivo* studies.

Table 2-1. Characterization of Dox-loaded PEG-EGCG micelle with various PEG-EGCG to Dox feed weight ratios and PEG-EGCG molecular weights.

Samples	Feed weight ratio of PEG-EGCG to Dox	Initial PEG-EGCG concentration	DLE (w/w %)	DLC (w/w %)	Size (nm)
5kPE-0.25	0.25	3	57 ± 3.8	86 ± 1.8	96 ± 15
5kPE-0.5	0.5	6	65 ± 5.6	68 ± 3.7	33 ± 5.1
5kPE-1	1	12	75 ± 4.0	49 ± 2.2	29 ± 2.6
5kPE-2	2	24	78 ± 5.9	34 ± 2.2	31 ± 11
10kPE-0.25	0.25	0.5	77 ± 0.8	88 ± 3.4	152 ± 4.7
10kPE-0.5	0.5	1	79 ± 4.2	69 ± 2.4	135 ± 4.8
10kPE-1	1	2	82 ± 4.8	49 ± 1.5	124 ± 5.5
10kPE-2	2	4	88 ± 4.4	34 ± 1.1	136 ± 8.9

2.3.3. Quenching of Dox fluorescence in PEG-EGCG micelles

It has been reported that the π-π stacking of Dox molecules led to the quenching of Dox fluorescence encapsulated within polymeric micelles [31, 32]. To investigate the interactions of Dox within PEG-EGCG micelles, we examined the fluorescence of Dox in the micelle configuration. It could be clearly seen that while the absorbance of Dox at equal concentrations was similar in both the free form and the micelle encapsulated form, Dox fluorescence was significantly decreased when encapsulated in the 10kPE micelles (Figure 2-5). The quenching of Dox fluorescence confirmed the π-π stacking of Dox molecules within the hydrophobic core of

PEG-EGCG micelles, which could be attributed to interactions between Dox itself as well as Dox and the aromatic EGCG moieties.

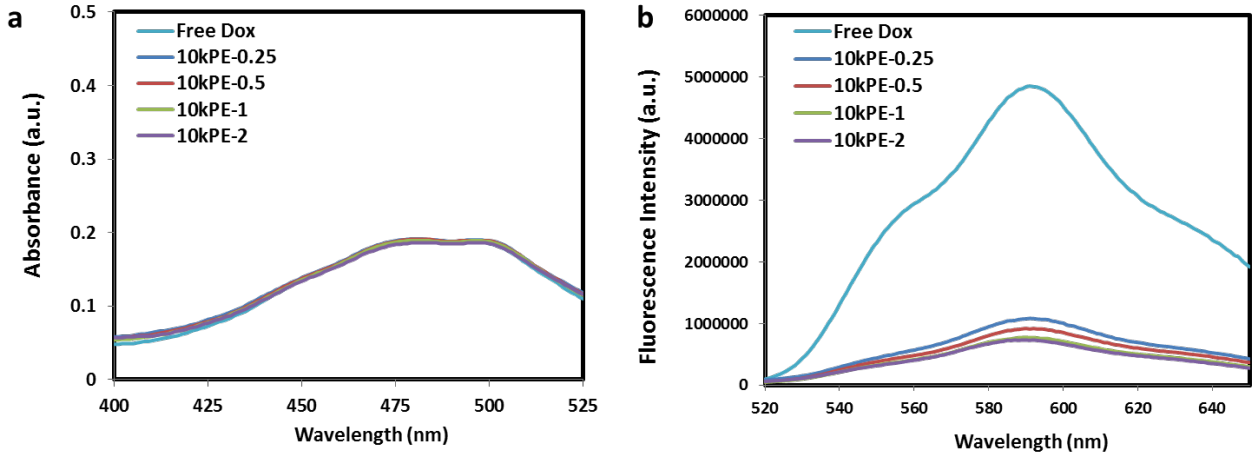

Figure 2-5. (a) Absorbance of free Dox and Dox-loaded 10kPE micelles and (b) fluorescence intensities of free Dox and Dox loaded 10kPE micelles at equivalent concentrations.

2.3.4. Stability of Dox-loaded PEG-EGCG micelles

2.3.4.1. Thermodynamic stability

Micelle stability is an important consideration for drug delivery application *in vivo*. The two components of stability - thermodynamic and kinetic parameters of Dox-loaded PEG-EGCG micelles were assessed. Thermodynamic stability is governed by the critical micelle concentration (CMC) of the polymer, which is defined as the concentration below which the disassembly of micelle occurs [16]. In other words, a lower CMC value means that micelles are more stable. In general, drug-loaded micelles are subjected to severe dilution upon intravenous injection. Micelles with high CMCs are more easily destabilized, leading to drug leakage and unspecific toxicity. Here the CMC of Dox-loaded PEG-EGCG micelles (10kPE-1U) was determined to be 0.15 mg/l (Figure 2-6), which was about 2 orders of magnitude lower than most other block copolymer micelles [33, 34]. For instance, PEG-poly(caprolactone) (PCL) micelles

and PEG-polycarbonate micelles were reported to have CMCs of 12 - 20 mg/l [28] and 15 - 63 mg/l [35] respectively.

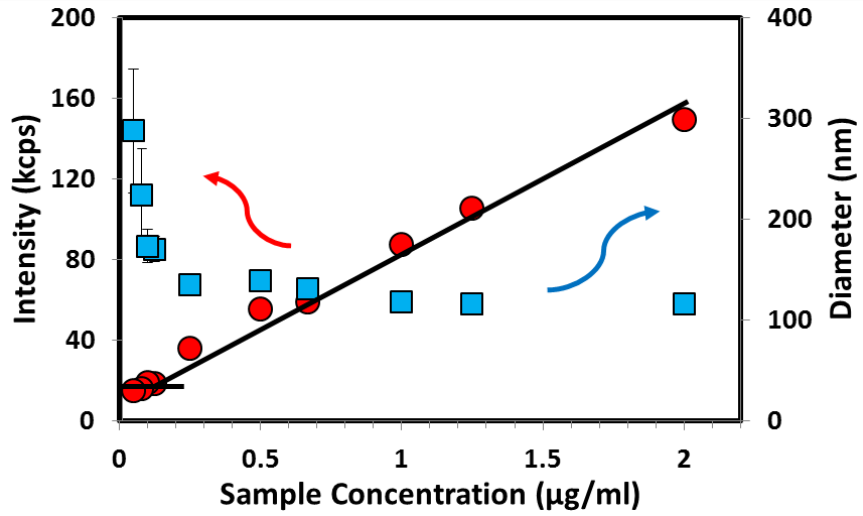

Figure 2-6. Evaluation of critical micelle concentration (CMC) of Dox-loaded PEG-EGCG micelles using DLS technique.

2.3.4.2. Kinetic stability

Apart from dilution effect, another concern for micellar carriers is plasma protein destabilization. Plasma proteins can partition into core compartment of micelles to trigger disassembly [14]. Moreover, adsorption of opsonin proteins on the surface of nanoparticles also leads to aggregation and clearance by the reticulo-endothelial system (RES) in the liver and spleen [36]. To study the kinetic stability of micelles, the particle size of the 10kPE-1U was monitored as a function of time in a simulated physiological environment, i.e. PBS (pH 7.3) containing 10 % FBS at 37 $^{\circ}$C. We found no significant change in size observed over a period of 4 weeks (Figure 2-7 a). This strongly suggests that the 10kPE-1U was highly stable in the presence of serum and was effective in preventing protein adsorption and aggregation.

The kinetic stability of micelles was also probed by DLS in the presence of the surfactant sodium dodecyl sulfate (SDS), which acted as a destabilizing agent as described by others [37,

38]. Figure 2-7 b shows the time dependence in scattered light intensity of 10kPE-1U. SDS-treated micelles exhibited a small decrease in scattered light intensity to about 90 % in 1 h. The signal then increased to 96 % and was maintained at > 92 % for 48 h, suggesting that there was little dissociation of 10kPE-1U. In fact, the scattered light intensity was preserved at > 90 % at even after 4 weeks at room temperature. The ability to withstand SDS challenge even after 4 weeks again confirms the high kinetic stability of micelles. Overall, Dox-loaded PEG-EGCG micelles demonstrated excellent thermodynamic and kinetic stability. This could probably be attributed to the strong interactions between EGCG and Dox in the micellar core, thus enabling the micellar structure to be maintained effectively. The highly stable micelles hold great promise for *in vivo* applications.

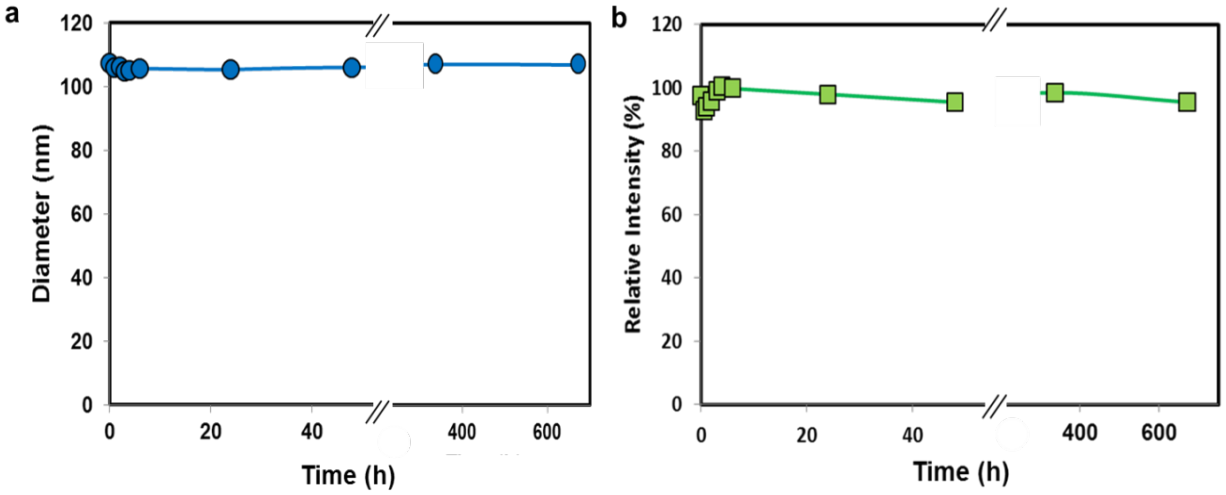

Figure 2-7. Kinetic stability of Dox-loaded PEG-EGCG micelles. (a) The effect of serum on particle size as a function of time. (b) The effect of SDS on DLS light intensity as a function of time.

2.3.5. *In vitro* release profile of Dox-loaded PEG-EGCG micelles

Drug release is an important parameter in carrier design for both reducing systemic drug leakage and achieving therapeutic efficacy. *In vitro* Dox release from PEG-EGCG micelles was investigated. For PEG-EGCG (Mw 5,000) micelles, we found that micelles prepared from all the various PEG-EGCG to Dox feed weight ratios released Dox slowly, reaching a cumulative

release of 8 - 9 % in 14 days (Figure 2-8 a). For the concentrated Dox-loaded PEG-EGCG micelle (10kPE-1U), we observed an initial stage of rapid Dox release to reach ~ 30 % over the first 48 h (Figure 2-8 b). Subsequently, Dox release slowed down and no further increment was observed up to 120 h. The low cumulative release and gradual retardation of Dox release is in line with the high stability of micelles and is probably a direct result of the strong binding between Dox and EGCG within the micelle core. This finding suggests that Dox leakage from PEG-EGCG micelles in the blood stream could be minimized.

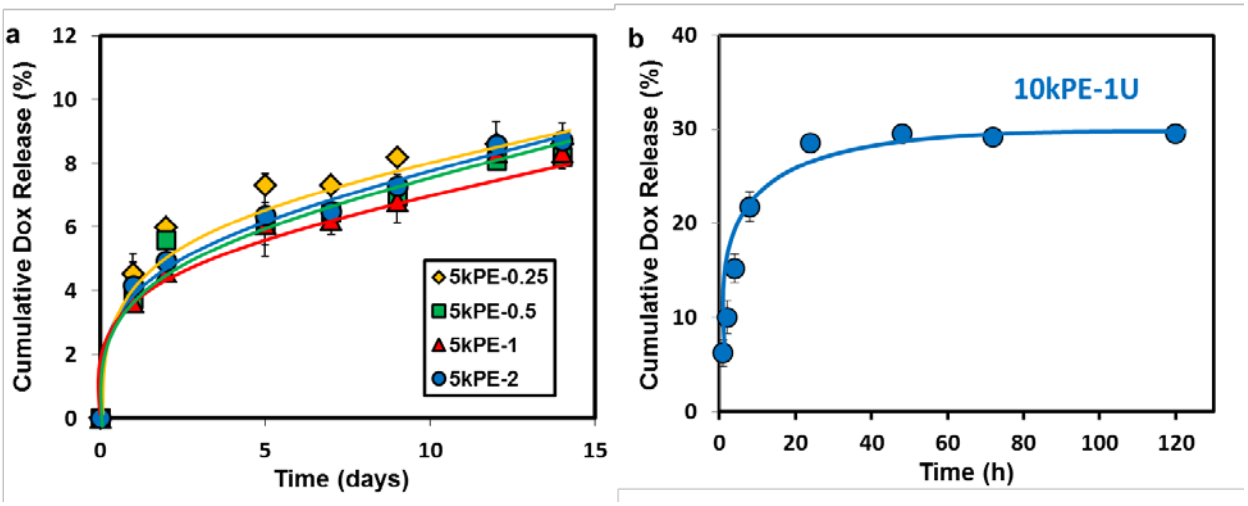

Figure 2-8. *In vitro* release profile of Dox from PEG-EGCG micelles. (a) PEG-EGCG (Mw 5,000) micelles of various PEG-EGCG to Dox feed weight ratios; (b) 10kPE-1U.

2.3.6. Cytotoxicity of Dox-loaded PEG-EGCG micelles against HAK-1B cells *in vitro*

Upon reaching the tumor site, it is imperative the Dox-loaded PEG-EGCG micelles could exert toxicity against cancer cells. Hence the cytotoxicity of Dox-loaded PEG-EGCG micelles was evaluated against C-26 colon carcinoma and HAK-1B liver carcinoma cells *in vitro*. Free Dox was used as comparison. The results in Figure 2-9 a clearly illustrates that the viability of C-26 cells decreased as a function of increasing Dox equivalent concentrations of Dox-loaded PEG-EGCG (Mw 5,000) micelles. We also found that increasing PEG-EGCG to Dox feed weight ratio of micelles led to an increase in cytotoxicity (5kPE-2 > 5kPE-1 > 5kPE-0.5 > 5kPE-

0.25). In comparison, free Dox displayed much higher cell-killing efficacy than all the micelle compositions. The concentrated Dox-loaded PEG-EGCG micelle - 10kPE-1U also demonstrated concentration dependent toxicity against HAK-1B cells (Figure 2-9 b). Although its toxicity was much lower than free Dox, the micelle (10kPE-1U) showed a significant enhancement in toxicity over time; from an IC_{50} of ~ 2 µg/ml at 48 h to ~ 0.25 µg/ml at 72 h. This extended toxicity towards HAK-1B cells could be attributed to the gradual release of Dox encapsulated in the micelles.

To assess the cellular uptake and distribution, confocal microscopy was used to compare the intracellular trafficking of free Dox and 10kPE-1U in HAK-1B cells. The representative images are presented in Figure 2-10. Strong Dox fluorescence was observed in cell nuclei after 4 h of cell incubation with free Dox. Longer incubation period of 24 h led to more intense Dox fluorescence in the nuclei. In contrast, we detected weak Dox fluorescence in 10kPE-1U treated cells at 4 h and majority of Dox fluorescence was observed in the cytoplasm rather than the cell nuclei. When cells were incubated with 10kPE-1U for 24 h, Dox fluorescence in cytoplasm was increased significantly and some nuclear localization of Dox was observed. The rate of Dox accumulation in cells was observed to be much faster for free Dox as compared to Dox-loaded micelle probably because free Dox could enter the cell rapidly by passive diffusion while micelles were reported to gain access through the slower endocytosis pathway [28, 39]. While it is possible that the slower uptake may also be ascribed to the delayed release of Dox from the micelles, the difference in distribution pattern of Dox intracellularly suggests otherwise. Unlike the intense nuclear localization visible with free Dox treatment, strong fluorescence was located mainly in the cytoplasm (possibly within the endosomal or lysosomal compartments) of cells treated with micelles. This indicates that intact Dox-loaded micelles, rather than the released free

Dox, were internalized. It is expected that free Dox was then slowly released from the micelles after cellular uptake via endocytosis. This is supported by our previous finding of enhancement in micelle cytotoxicity over time.

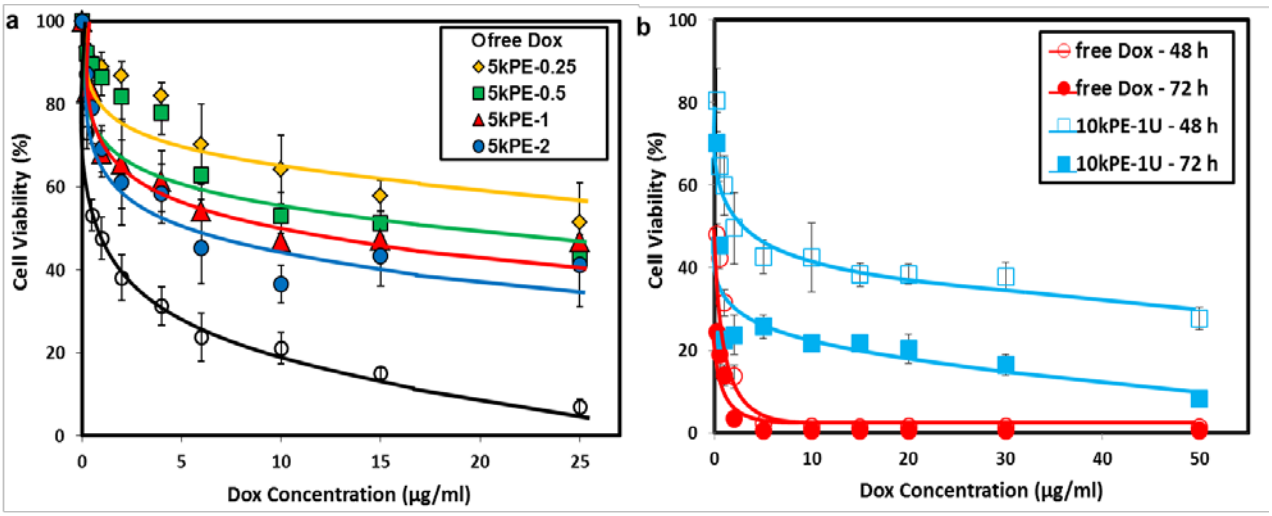

Figure 2-9. *In vitro* cytotoxicity of Dox-loaded PEG-EGCG micelles and free Dox on (a) C-26 murine colon cancer cells after incubation for 48 h and (b) HAK-1B human liver carcinoma cells after incubation for 48 h and 72 h respectively (n = 5).

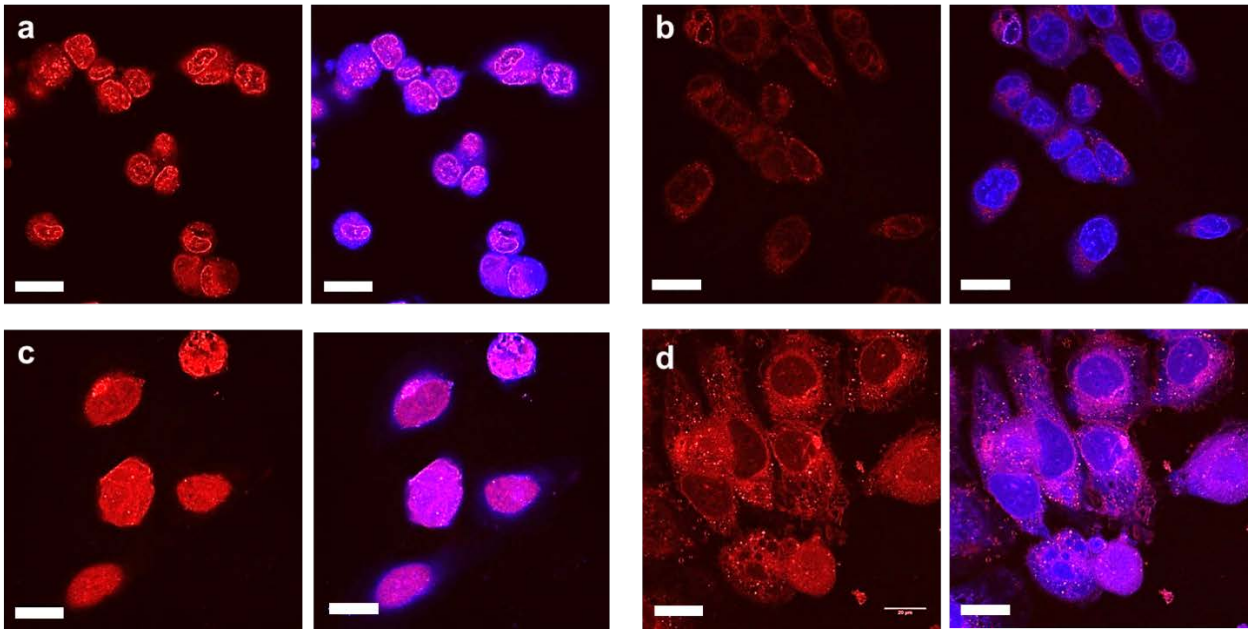

Figure 2-10. Confocal microscopy images of HAK-1B cells incubated with free Dox for (a) 4 h and (c) 24 h; and with Dox-loaded PEG-EGCG micelles for (b) 4 h and (d) 24 h. For each panel, left image shows the cells with Dox fluorescence, and the right image shows the overlay of Dox fluorescence with nuclear staining by Hoechst 33342. Scale bar = 20 μm.

2.3.7. Antitumor efficacy of Dox-loaded PEG-EGCG micelles *in vivo*

2.3.7.1. Antitumor efficacy on C-26 tumor model

The antitumor efficacy of micelles was evaluated firstly on the C-26 murine colon carcinoma model, with free Dox as control. The formulations were injected intravenously 3 times on days 0, 4 and 7 in nude mice bearing C-26 tumors. A survey of the literature showed that 10 mg/kg was the maximum dosage for free Dox in C-26 *in vivo* tumor study as toxicity was significant above this dose [40, 41]. Hence we included 10 mg/kg free Dox for comparison. We observed that free Dox at 10 mg/kg demonstrated significant tumor regression compared to PBS group (Figure 2-11 a). In contrast, all the Dox-loaded PEG-EGCG micelles did not show significant tumor growth inhibition at 10 mg/kg Dox equivalent concentration compared to PBS control. We also failed to observe any tumor growth inhibition at an even higher micelle dosage of 20 mg/kg. The tumor regression of free Dox treatment was accompanied by severe toxicity. Mice treated with free Dox experienced a steady decline in body weight that led to their toxic death in 10 days. On the other hand, the Dox-loaded PEG-EGCG micelles did not show any adverse effects on body weights of mice even at 20 mg/kg (Figure 2-11 b). These results suggest that Dox-loaded PEG-EGCG micelles were less toxic than free Dox against both tumor and other healthy organs. The lack of antitumor efficacy prompted us to escalate micelle dosages even further to 30 mg/kg and 40 mg/kg. The micelle treatments at these higher dosages were well-tolerated in mice with little effect on body weight but still no tumor growth inhibition effect was observed (Figure 2-11 c, d). It is worth mentioning that the mice had to be euthanized at a relatively early stage (10 days) into the study because of rapid tumor proliferation, leading to excessive tumor burden. It is possible that the high stability and slow drug release property of the micelles may have resulted in delayed antitumor effect, leading to lack of therapeutic efficacy in

this period of observation. Meanwhile, we also prepared Dox-loaded PEG-EGCG micelles with PEG-EGCG of other molecular weights beside 5,000 (5kPE), including 10,000 (10kPE), 20,000 (20kPE) and 30,000 (30kPE) using the exact same method as the 5kPE micelles. PEG has been widely used as a hydrophilic surface coating for nanoparticle drug carriers to evade body's immune cells and increase circulation time [42]. As such, many studies have reported that PEG molecular weight may have an influence on many important parameters such as stability, biodistribution, pharmacokinetics of nanoparticles [36, 43, 44]. Thus we evaluated the effect of PEG molecular weight on antitumor efficacy of these micelles *in vivo* using the C-26 tumor model. We observed that the Dox-loaded PEG-EGCG (Mw 10,000) micelles, in particular 10kPE-1, showed the most promise in suppressing tumor proliferation (Figure 2-11 e). Moreover, all the micelle treatments did not have an adverse effect on body weights of mice (Figure 2-11 f). Therefore, we chose the PEG-EGCG (Mw 10,000) micelle 10kPE-1 for further investigation.

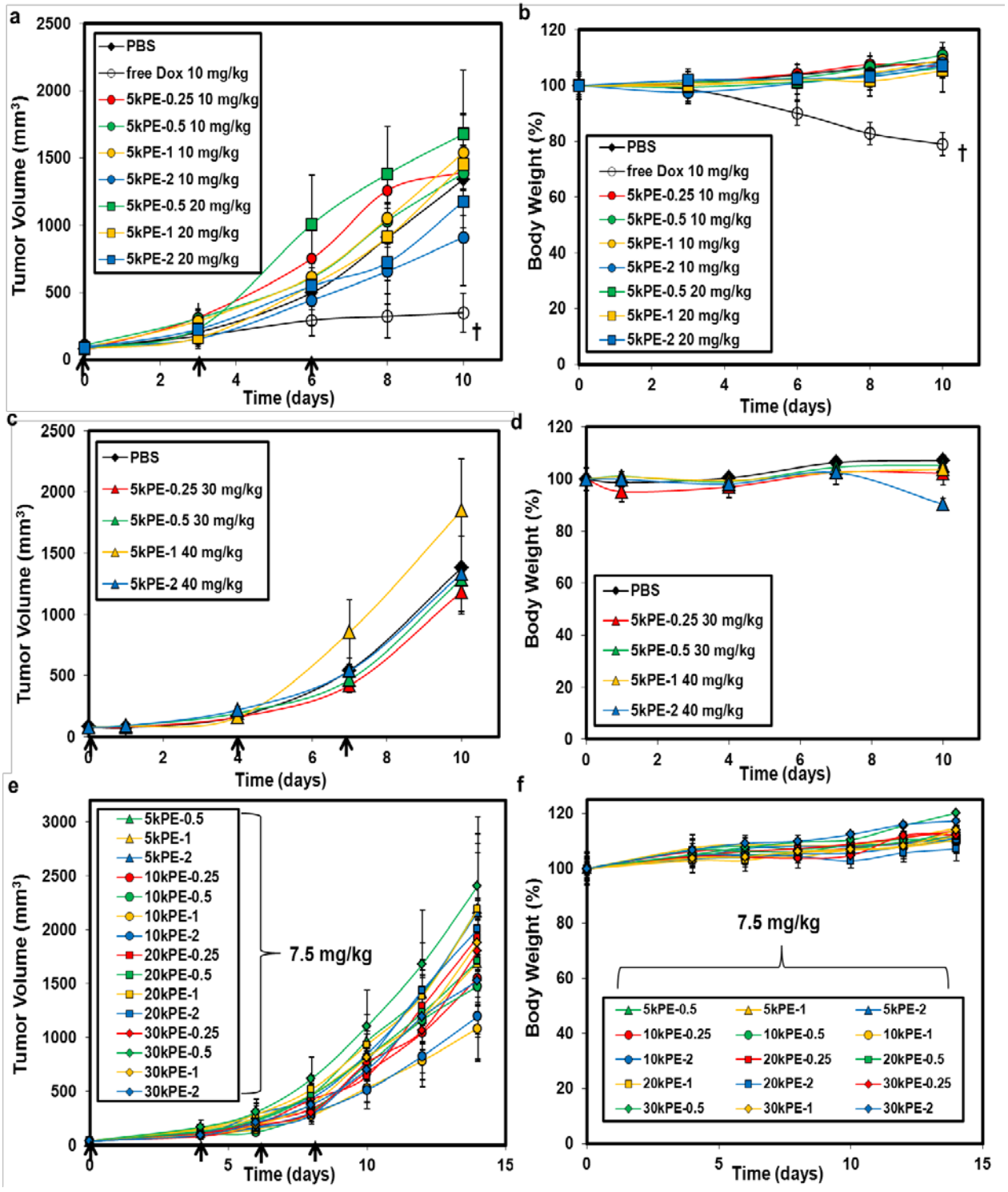

Figure 2-11. Effect of increasing dosage of Dox-loaded PEG-EGCG (Mw 5,000) micelles on (a, c) tumor growth and (b, d) body weight of mice bearing C-26 subcutaneous tumors (n = 5). Free Dox 10 mg/kg was used as comparison. Effect of PEG-EGCG molecular weight on (e) tumor volume and (f) body weight of C-26 tumor-bearing mice treated with Dox-loaded PEG-EGCG micelles using a fixed dosage of 7.5 mg/kg (n = 3). For all three set of experiments, i.v. injections were given on the days indicated by the arrows. † toxic deaths.

2.3.7.2. Antitumor efficacy on HAK-1B tumor model

To address the limitation of the previous *in vivo* tumor model, we performed a new set of *in vivo* experiments using another tumor model - HAK-1B. HAK-1B human liver carcinoma cells were selected instead of C-26 murine colon carcinoma cells for some reasons. First, the HAK-1B cancer cell line is derived from human patient [45], thus making it more clinically relevant than the C-26 colon carcinoma, which originates from mouse. Second, HAK-1B tumor was reported to develop at slower rate than C-26 tumor [46]. Previously, we noted that rapid growing C-26 tumor did not respond well to PEG-EGCG micelle treatment. As the micelles had high stability and released Dox slowly over a sustained period, we hypothesize that the therapeutic effect of micelle may be prolonged and more apparent on slow-growing tumors such as HAK-1B. Third, slow tumor growth also mirrors the clinical situation. In such cases, more organized and less permeable vasculatures are given time to develop, making the tumors difficult to treat using conventional nanocarriers *via* EPR targeting [47, 48]. Henceforth, the antitumor efficacy of the optimized Dox-loaded PEG-EGCG (Mw 10,000) micelles (10kPE-1U) was evaluated using HAK-1B tumor model.

Apart from 10kPE-1U, two other Dox formulations – stand-alone Dox and DOXIL were also used for comparison in the *in vivo* study. DOXIL, which is one of the most successful drug carriers to date, is a PEGylated liposomal formulation of Dox clinically approved for the treatment of Karposi's sarcoma and epithelial ovarian cancer [7]. From the C-26 *in vivo* study (Figure 2-11), we observed that dosage of 10 mg/kg free Dox was effective in retarding tumor growth but also lethal in mice while dosages of up to 40 mg/kg of Dox-loaded PEG-EGCG micelles were non-toxic overall. This suggests that Dox-loaded PEG-EGCG micelles probably have a much higher effective dose. In order to establish a fair comparison of Dox-loaded PEG-

EGCG micelles with the other Dox formulations, the therapeutic efficacy should be evaluated at their respective effective doses. A search on DOXIL revealed that its maximum tolerated dose is similar to free Dox [49].Therefore we set the maximum dosage of both free Dox and DOXIL at 10 mg/kg and chose 3 dosages below that – 1, 2 and 5 mg/kg to approximate the effective dose. In contrast, since Dox-loaded PEG-EGCG micelles were projected to have a much higher effective dose, we tested 2 markedly higher dosages - 25 mg/kg and 50 mg/kg. All three formulations were administered *via* tail vein injections on days 0, 4 and 7 into BALB/c nude mice bearing subcutaneous HAK-1B tumors. Figure 2-10 illustrates the results of the tumor growth inhibition study. As expected, we observed greater tumor growth inhibition effect for free Dox as the dosage was raised (Figure 2-12 a). However, the mice also suffered from greater toxicity as reflected by the decrease in mean body weight (Figure 2-12 b). Dosage of 10 mg/kg resulted in severe toxicity as evident from the dramatic decline in body weights leading to eventual deaths of animals. Similar results on tumor volume (Figure 2-12 c) and body weight (Figure 2-12 d) were obtained for DOXIL treatment group. In addition, at 5 mg/kg for both free Dox and DOXIL, no significant tumor suppression compared to PBS group was observed ($p > 0.05$). We observed that increasing the dosage of 10kPE-1U also enhanced tumor growth inhibition (Figure 2-12 e). In contrast to the toxicity profile of free Dox and DOXIL, at noticeably higher dosages of 25 and 50 mg/kg, micelle treatment induced little toxicity in mice, based on the small variation in mean body weight (Figure 2-12 f). The attenuation in systemic toxicity could be a direct result of the high stability and little Dox leakage of PEG-EGCG micelles during circulation, contributing to reduced unspecific distribution of Dox to non-target sites. More importantly, we noted that 10kPE-1U at 50 mg/kg dosage demonstrated significant tumor growth inhibition compared to PBS group ($p < 0.05$), possibly due to passive targeting of

micellar nanoparticles by EPR effect. It is worth to highlight that 10kPE-1U demonstrated superior anticancer efficacy than the optimal dosages of both clinically used Dox formulations in this experiment setting. This could probably be attributed to the higher dosage of micelles administered, contributing to increased Dox tumor localization compared to free Dox and DOXIL. Overall as a result of enhanced stability and reduced toxicity, Dox-loaded PEG-EGCG micelle offered a considerably higher maximum tolerated dose over free Dox and DOXIL.

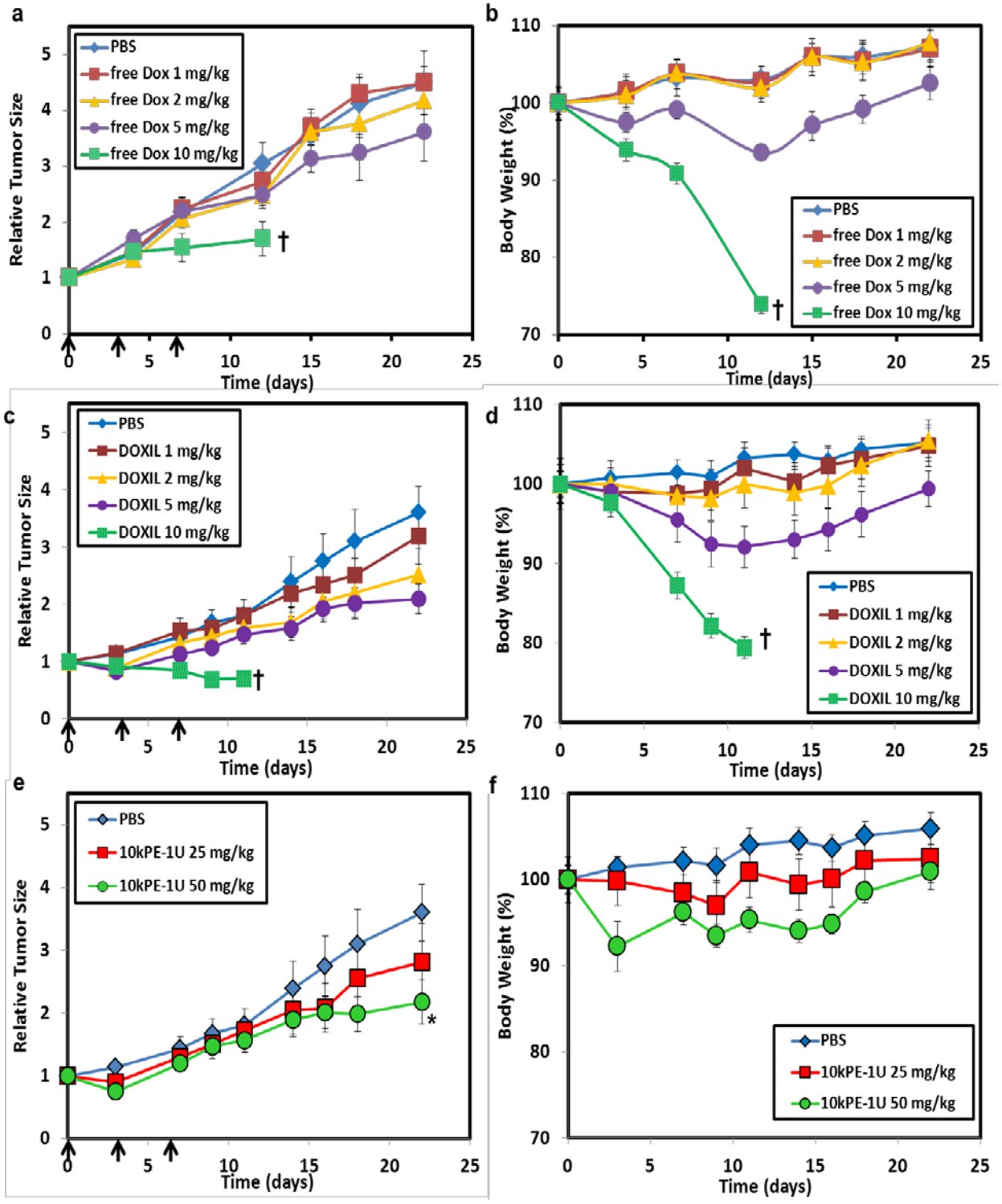

Figure 2-12. ***In vivo*** **antitumor efficacy of various Dox formulations in the HAK-1B tumor-bearing mouse model. Three i.v. injections of various Dox equivalent doses of free Dox, DOXIL and Dox-loaded PEG-EGCG micelle were administered on the days indicated by arrows. Effect of free Dox 1 – 10 mg/kg on (a) relative tumor size and (b) body weight; Effect of DOXIL 1 – 10 mg/kg on (c) relative tumor size and (d) body weight; Effect of 10kPE-1U 25 mg/kg and 50 mg/kg on (e) relative tumor size and (f) body weight (n = 8 - 10). Data is reported as mean ± SEM for the tumor volume and body weight. * p < 0.05 versus PBS group, † toxic deaths.**

2.4. Conclusion

Dox-encapsulated PEG-EGCG micelles were formed by the self-assembly of PEG-EGCG conjugates and Dox in aqueous solution, triggered by the interactions between EGCG moieties and Dox molecules. As a result of strong interactions between Dox and EGCG, these Dox-loaded PEG-EGCG micelles were observed to have a remarkably high drug loading content of up to 86 %, high stability and slow release rate. As a result of high stability and minimal drug leakage in circulation, Dox-loaded PEG-EGCG micelle demonstrated reduced toxicity *in vivo* and a much elevated maximum tolerated dose free compared to two clinically relevant Dox formulations - Dox and DOXIL. Most notably, Dox-loaded PEG-EGCG micelle at 50 mg/kg achieved more significant tumor growth inhibition effect against HAK-1B subcutaneous tumors compared to optimal dosages of both Dox and DOXIL. Taken together, this work demonstrated that PEG-EGCG micelle can provide for an effective and safe carrier to deliver Dox for cancer therapy.

References

1. Thurston, D.E., *Chemistry and pharmacology of anticancer drugs*. 2006: CRC press.
2. Gewirtz, D., *A critical evaluation of the mechanisms of action proposed for the antitumor effects of the anthracycline antibiotics adriamycin and daunorubicin.* Biochemical Pharmacology, 1999. **57**(7): p. 727-741.
3. Singal, P.K. and N. Iliskovic, *Doxorubicin-induced cardiomyopathy.* New England Journal of Medicine, 1998. **339**(13): p. 900-905.
4. Peer, D., et al., *Nanocarriers as an emerging platform for cancer therapy.* Nat Nano, 2007. **2**(12): p. 751-760.
5. Zhang, L., et al., *Nanoparticles in medicine: therapeutic applications and developments.* Clinical Pharmacology & Therapeutics, 2008. **83**(5): p. 761-769.
6. Torchilin, V., *Tumor delivery of macromolecular drugs based on the EPR effect.* Advanced Drug Delivery Reviews, 2011. **63**(3): p. 131-135.
7. Barenholz, Y., *Doxil® — The first FDA-approved nano-drug: Lessons learned.* Journal of Controlled Release, 2012. **160**(2): p. 117-134.
8. Aliabadi, H.M. and A. Lavasanifar, *Polymeric micelles for drug delivery.* Expert Opinion on Drug Delivery, 2006. **3**(1): p. 139-162.
9. Mahmud, A., et al., *Polymeric micelles for drug targeting.* Journal of Drug Targeting, 2007. **15**(9): p. 553-584.
10. Maeda, H., et al., *Tumor vascular permeability and the EPR effect in macromolecular therapeutics: a review.* Journal of Controlled Release, 2000. **65**(1): p. 271-284.
11. Matsumura, Y. and K. Kataoka, *Preclinical and clinical studies of anticancer agent-incorporating polymer micelles.* Cancer Science, 2009. **100**(4): p. 572-579.
12. Gong, J., et al., *Polymeric micelles drug delivery system in oncology.* Journal of Controlled Release, 2012. **159**(3): p. 312-323.
13. Bae, Y. and K. Kataoka, *Intelligent polymeric micelles from functional poly(ethylene glycol)-poly(amino acid) block copolymers.* Advanced Drug Delivery Reviews, 2009. **61**(10): p. 768-784.
14. Kim, S., et al., *Overcoming the barriers in micellar drug delivery: loading efficiency, in vivo stability, and micelle–cell interaction.* Expert Opinion on Drug Delivery, 2010. **7**(1): p. 49-62.
15. Mikhail, A.S. and C. Allen, *Block copolymer micelles for delivery of cancer therapy: Transport at the whole body, tissue and cellular levels.* Journal of Controlled Release, 2009. **138**(3): p. 214-223.
16. Allen, C., D. Maysinger, and A. Eisenberg, *Nano-engineering block copolymer aggregates for drug delivery.* Colloids and Surfaces B: Biointerfaces, 1999. **16**(1): p. 3-27.
17. Chen, H., et al., *Fast release of lipophilic agents from circulating PEG-PDLLA micelles revealed by in vivo forster resonance energy transfer imaging.* Langmuir, 2008. **24**(10): p. 5213-5217.
18. Miller, T., et al., *Premature drug release of polymeric micelles and its effects on tumor targeting.* International Journal of Pharmaceutics, 2013. **445**(1–2): p. 117-124.
19. Kwon, I.K., et al., *Analysis on the current status of targeted drug delivery to tumors.* Journal of Controlled Release, 2012. **164**(2): p. 108-114.
20. Azam, S., et al., *Prooxidant property of green tea polyphenols epicatechin and epigallocatechin-3-gallate: implications for anticancer properties.* Toxicology in vitro, 2004. **18**(5): p. 555-561.
21. Jung, Y.D. and L.M. Ellis, *Inhibition of tumour invasion and angiogenesis by epigallocatechin gallate (EGCG), a major component of green tea.* International journal of experimental pathology, 2001. **82**(6): p. 309-316.
22. Boulikas, T., *Introduction to Anticancer Therapeutics*, in *Anticancer Therapeutics*. 2008, John Wiley & Sons, Ltd. p. 47-54.

23. Hudson, S.A., et al., *(−)-Epigallocatechin-3-gallate (EGCG) maintains κ-casein in its pre-fibrillar state without redirecting its aggregation pathway.* Journal of molecular biology, 2009. **392**(3): p. 689-700.
24. Ghosh, K.S., B.K. Sahoo, and S. Dasgupta, *Spectrophotometric studies on the interaction between (−)-epigallocatechin gallate and lysozyme.* Chemical Physics Letters, 2008. **452**(1): p. 193-197.
25. Chung, J.E., et al., *Self-assembled micellar nanocomplexes comprising green tea catechin derivatives and protein drugs for cancer therapy.* Nat Nano, 2014. **9**(11): p. 907-912.
26. Topel, Ö., et al., *Determination of critical micelle concentration of polybutadiene-block-poly(ethyleneoxide) diblock copolymer by fluorescence spectroscopy and dynamic light scattering.* Journal of Molecular Liquids, 2013. **177**(0): p. 40-43.
27. Kohori, F., et al., *Process design for efficient and controlled drug incorporation into polymeric micelle carrier systems.* Journal of Controlled Release, 2002. **78**(1): p. 155-163.
28. Shuai, X., et al., *Micellar carriers based on block copolymers of poly(epsilon-caprolactone) and poly(ethylene glycol) for doxorubicin delivery.* Journal of controlled release : official journal of the Controlled Release Society, 2004. **98**(3): p. 415-26.
29. Kim, S.Y. and Y.M. Lee, *Taxol-loaded block copolymer nanospheres composed of methoxy poly(ethylene glycol) and poly(ε-caprolactone) as novel anticancer drug carriers.* Biomaterials, 2001. **22**(13): p. 1697-1704.
30. Kataoka, K., et al., *Doxorubicin-loaded poly(ethylene glycol)–poly(β-benzyl-l-aspartate) copolymer micelles: their pharmaceutical characteristics and biological significance.* Journal of Controlled Release, 2000. **64**(1–3): p. 143-153.
31. Lai, Y., et al., *A novel micelle of coumarin derivative monoend-functionalized PEG for anti-tumor drug delivery: in vitro and in vivo study.* Journal of drug targeting, 2012. **20**(3): p. 246-254.
32. Lai, Y., et al., *Polymeric micelles with π–π conjugated cinnamic acid as lipophilic moieties for doxorubicin delivery.* Journal of Materials Chemistry B, 2013. **1**(34): p. 4289-4296.
33. Qiu, L. and Y. Bae, *Polymer Architecture and Drug Delivery.* Pharmaceutical Research, 2006. **23**(1): p. 1-30.
34. Wiradharma, N., et al., *Self-assembled polymer nanostructures for delivery of anticancer therapeutics.* Nano Today, 2009. **4**(4): p. 302-317.
35. Ebrahim Attia, A.B., et al., *The effect of kinetic stability on biodistribution and anti-tumor efficacy of drug-loaded biodegradable polymeric micelles.* Biomaterials, 2013. **34**(12): p. 3132-3140.
36. Owens Iii, D.E. and N.A. Peppas, *Opsonization, biodistribution, and pharmacokinetics of polymeric nanoparticles.* International Journal of Pharmaceutics, 2006. **307**(1): p. 93-102.
37. Kim, S.H., et al., *Hydrogen bonding-enhanced micelle assemblies for drug delivery.* Biomaterials, 2010. **31**(31): p. 8063-8071.
38. Zhao, X., et al., *Enhanced Stability of Polymeric Micelles Based on Postfunctionalized Poly(ethylene glycol)-b-poly(γ-propargyl l-glutamate): The Substituent Effect.* Biomacromolecules, 2012. **13**(5): p. 1315-1322.
39. Dai, X., et al., *Fluorescence intensity and lifetime imaging of free and micellar-encapsulated doxorubicin in living cells.* Nanomedicine: Nanotechnology, Biology and Medicine, 2008. **4**(1): p. 49-56.
40. Yokoyama, M., et al., *Characterization of physical entrapment and chemical conjugation of adriamycin in polymeric micelles and their design for in vivo delivery to a solid tumor.* Journal of Controlled Release, 1998. **50**(1–3): p. 79-92.
41. Huang, S.K., et al., *Pharmacokinetics and therapeutics of sterically stabilized liposomes in mice bearing C-26 colon carcinoma.* Cancer Research, 1992. **52**(24): p. 6774-6781.
42. Veronese, F.M. and G. Pasut, *PEGylation, successful approach to drug delivery.* Drug discovery today, 2005. **10**(21): p. 1451-1458.

43. Yamaoka, T., Y. Tabata, and Y. Ikada, *Distribution and tissue uptake of poly (ethylene glycol) with different molecular weights after intravenous administration to mice*. Journal of Pharmaceutical Sciences, 1994. **83**(4): p. 601-606.
44. Photos, P.J., et al., *Polymer vesicles in vivo: correlations with PEG molecular weight.* Journal of Controlled Release, 2003. **90**(3): p. 323-334.
45. Yano, H., et al., *Establishment of two distinct human hepatocellular carcinoma cell lines from a single nodule showing clonal dedifferentiation of cancer cells.* Hepatology, 1993. **18**(2): p. 320-327.
46. Xu, K., et al., *Injectable hyaluronic acid-tyramine hydrogels incorporating interferon-α2a for liver cancer therapy*. Journal of Controlled Release, 2013. **166**(3): p. 203-210.
47. Nichols, J.W. and Y.H. Bae, *EPR: Evidence and fallacy*. Journal of Controlled Release, 2014.
48. Taurin, S., H. Nehoff, and K. Greish, *Anticancer nanomedicine and tumor vascular permeability; Where is the missing link?* Journal of Controlled Release, 2012. **164**(3): p. 265-275.
49. Solomon, R. and A.A. Gabizon, *Clinical pharmacology of liposomal anthracyclines: focus on pegylated liposomal Doxorubicin.* Clinical Lymphoma and Myeloma, 2008. **8**(1): p. 21-32.

Chapter 3: Targeted intracellular protein delivery based on hyaluronic acid-green tea catechin nanogel complexes

3.1. Introduction

Despite recent progress in protein carrier design, the delivery of functional proteins intracellularly still remains a challenge. In order to deliver proteins into the cytosol, several obstacles have to be overcome, including penetration of the cell membrane, resistance to degradation by lysosomal enzymes as well as release from the endosomal compartments [1]. More recently, intracellular delivery of cytotoxic proteins has generated potential interest for cancer therapy. More specifically, delivery of cytotoxic protein cargoes such as RNase A and caspase-3 have been explored for this purpose [2-4]. However, there remains a considerable gap between cancer cells recognition and cargo delivery. To this end, a liposomal nanocarrier with anisamide decorated surface has been designed to deliver cytochrome C (Cyt C) intracellularly to target lung tumors [5].

Among all the polymeric nanocarrier formulations, nanogels have received increasing interest as efficient carriers for various proteins. Their advantages include reversible binding to proteins without the need for chemical modification, protection from degradation by proteases, controllable release profile and high stability [6]. For instance, Akiyoshi *et al*. developed self-assembling cholesterol-grafted pullulan (CHP)-based nanogels to successfully encapsulate, stabilize and deliver interleukin-12 (IL-12) *in vivo* [7]. Ethylenediamine group functionalized pullulan nanogels have also achieved delivery of bovine serum albumin (BSA) and β-galactosidase into Hela cells [8]. Additionally, Park *et al*. have shown that heparin-pluronic nanogels could be used for the intracellular delivery of RNase A [4]; and paclitaxel and DNase simultaneously [9] to achieve significant anticancer effects.

In particular, hyaluronic acid (HA) is often chosen as a component of the nanogel formulations because of its ability to target HA receptor - CD44, overexpressed in many cancer

cells including cancer stem cells [10, 11]. Lee *et al*. synthesized HA/siRNA nanogels to selectively target CD44 overexpressing HCT-116 colon cancer cells *in vitro* [12], while Wei *et al*. developed cholesterol modified HA nanogels to physically encapsulate and deliver small molecule drugs etoposide and salinomycin to kill cancer stem cells [11]. Thus, it is predicted that the incorporation of HA would not only enable targeted delivery of payload into cancer cells.

Here, we introduce the design of a novel polymeric carrier comprising HA-EGCG conjugate for the targeted intracellular delivery of proteins into cancer cells. The HA backbone affords the active targeting motif for CD44 that is overexpressed in many types of cancer cell. On the other hand, EGCG, the main component of green tea catechins, is well known for its anti-oxidative and anti-carcinogenic properties [13, 14]. Since EGCG has an ability to bind protein [15, 16], we expect that the conjugation of EGCG to the HA backbone allows for the complexation of the HA-EGCG carrier with the protein of interest.

The protein we chose is Granzyme B (GzmB). It is a serine protease secreted by the cytotoxic T-cells and natural killer cells in response to foreign cells invasion. When it is present in the cell cytosol, it initiates a caspase activation cascade, leading to apoptosis. The entry of GzmB into target cells is normally mediated by a membrane destabilizing protein – perforin [17]. Some studies also found that even though GzmB could be internalized by cells, it is unable to cause apoptosis unless perforin is added simultaneously [18, 19]. Our objective is to make use of HA-EGCG conjugate to chaperon GzmB into cytosol of cancer cells. To this end, we prepared nanogel complexes comprising HA-EGCG, GzmB and linear polyethyleneimine (PEI). Physical interactions between HA-EGCG and GzmB and PEI provide the driving force for self-assembly (Figure 3-1 a). HA-EGCG coating on nanogel surface allows for the targeted delivery of nanogel complexes into cancer cells via CD44-mediated endocytosis. PEI is used to facilitate the release

of GzmB in the cytosol. The presence of multiple cationic amine groups on PEI is widely known to have high buffering capacity in the acidic environment of the endosomal compartments of cells [20], which subsequently results in the endosome disruption. Finally, GzmB would be released into cytoplasm to achieve cancer cell apoptosis (Figure 3-1 b).

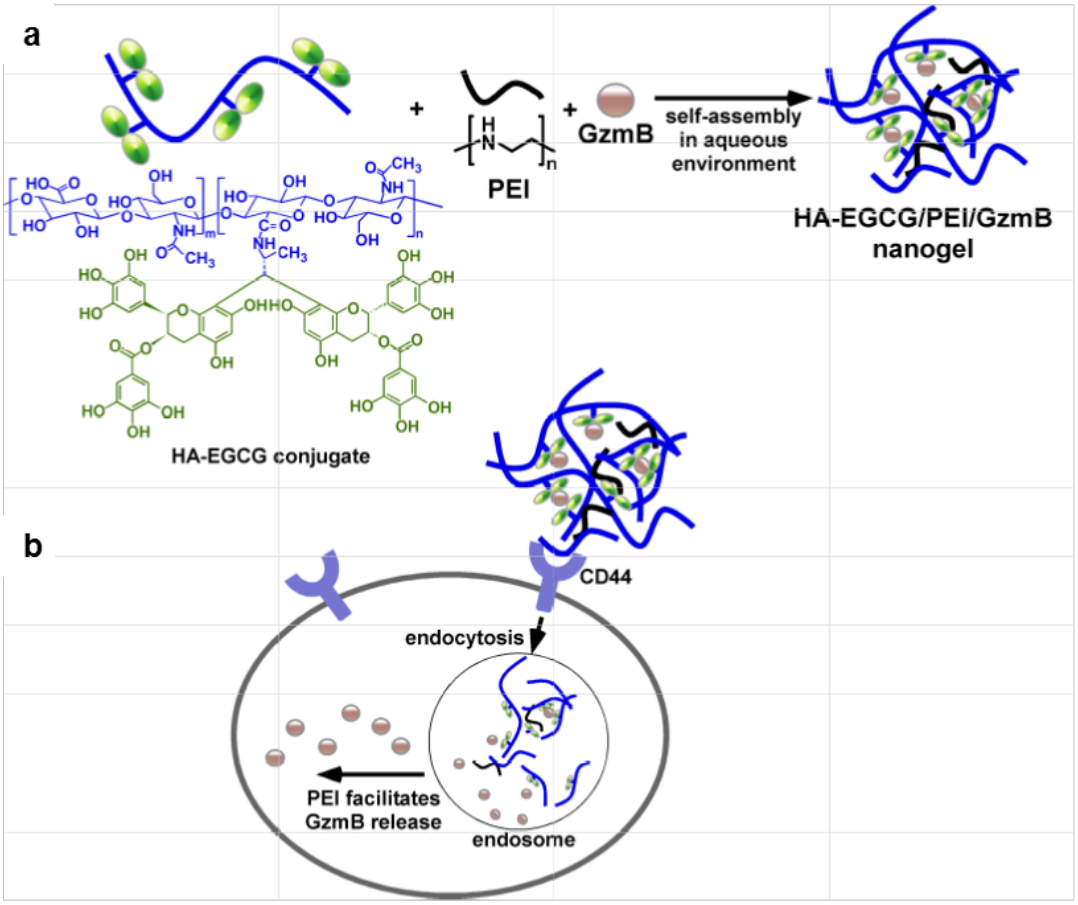

Figure 3-1. (a) Formation of self-assembled nanogel complexes comprising HA-EGCG, PEI and GzmB; (b) CD44-mediated uptake of nanogel and the facilitation of GzmB release by PEI from endosome, which triggers apoptosis in cancer cells.

3.2. Materials and Methods

3.2.1. Materials

Hyaluronic acid (HA, 90 KDa) was kindly donated by JNC Corporation (Tokyo, Japan). Fmoc-Ala-aldehyde was purchased from Bachem (Switzerland). EGCG (TEAVIGO) was purchased from DMS Nutritional Products Ltd (Switzerland). Tetrahydrofuran (THF), methanesulfonic acid (MSA), *N*-hydroxysuccinimide (NHS), 1-ethyl-3-(3-dimethylaminopropyl)-carbodiimide hydrochloride (EDC·HCl), dimethylformamide (DMF), triethylamine (TEA), lysozyme from chicken egg white, lysozyme substrate *Micrococcus lysodeikticus*, mouse Granzyme B (GzmB) and chloroquine diphosphate were all purchased from Sigma-Aldrich. Exgen 500 transfection reagent (Linear PEI 22 kDa) was obtained from Fermentas INC. AlamarBlue® was purchased from Invitrogen. CD44 antibody (156-3C11) was purchased from Novus Biologicals. BioPORTER® was acquired from Gelantis. Phosphate buffer saline (PBS, 150 mM, pH 7.3) was supplied by the media preparation facility in Biopolis, Singapore.

3.2.2. Synthesis of HA-EGCG conjugates

HA-EGCG conjugates were synthesized in a 3-step process. The first step was synthesizing Fmoc-Ala-bridged EGCG dimer, which was synthesized in a similar fashion to a protocol developed in our laboratory [21] with minor modifications (Scheme 3-1). EGCG (15.5 g, 33.8 mmol) was dissolved in 50 ml of anhydrous THF by stirring at room temperature. Then, Fmoc-Ala-aldehyde (1 g, 3.4 mmol) was added, followed by 162 μl of MSA. The mixture was incubated at room temperature for 24 h. Next day, the product was precipitated out by adding 450 ml of H_2O to the mixture while stirring vigorously. The precipitate was collected by centrifugation at 10000 rpm for 5 min. The product was re-dissolved in 10 ml of THF and then

precipitated again with 100 ml of H_2O. The precipitation cycle was repeated till all monomeric EGCG was removed from the product as determined by LC/MS (Acquity UPLC equipped with SQD single quadrupole detector (Waters, Milford, MA). Gradient elution was done using Acquity UPLC BEH C18 Column (1.7 µm, 2.1 x 100 mm) starting from water:acetonitrile (95:5, v/v) to (20:80 v/v) in 8 min at a flow rate of 0.5 ml/min). After that, the product was dried overnight under vacuum at room temperature. Yield: (3.3 g, 82 %).

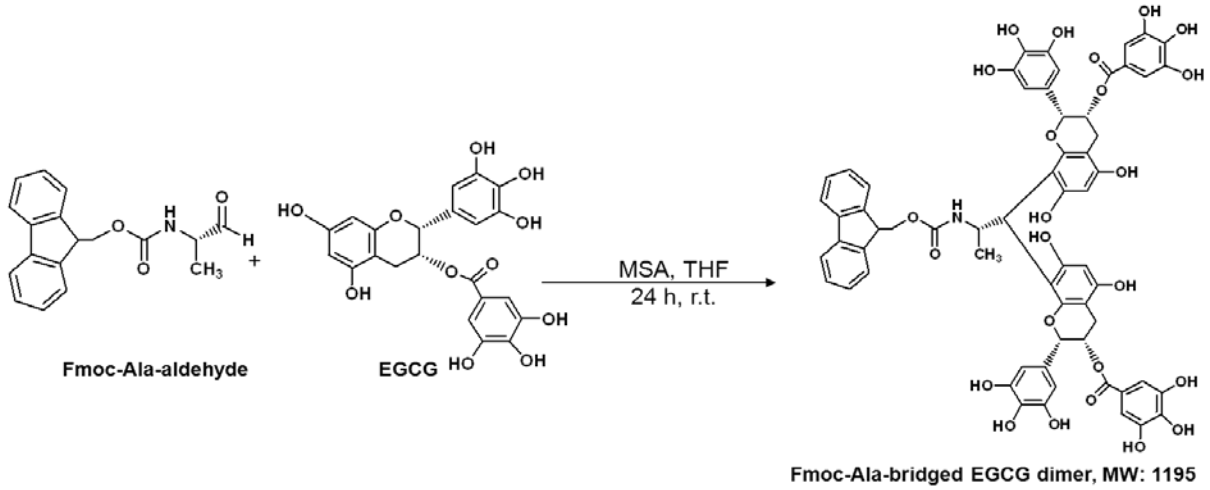

Scheme 3-1. Synthesis of Fmoc-Ala-bridged EGCG dimer.

The second step consisted of the deprotection of Fmoc-Ala-bridged EGCG dimer. It was performed with 50 % TEA in DMF (Scheme 3-2). Fmoc-Ala-bridged EGCG dimer (3.3 g, 2.76 mmol) was first dissolved in 12.4 ml of DMF. Then, 12.4 ml of TEA was added dropwise into the mixture while stirring vigorously. The mixture was incubated for 8 h to ensure complete de-protection. After which the mixture was centrifuged and the clear supernatant collected. One hundred and fifty ml of dichloromethane was added to the supernatant, and the resultant precipitate was collected by filtration. The product was washed twice with 30 ml of dichloromethane and then dried overnight under vacuum at room temperature. Yield: (3.2 g, 97 %)

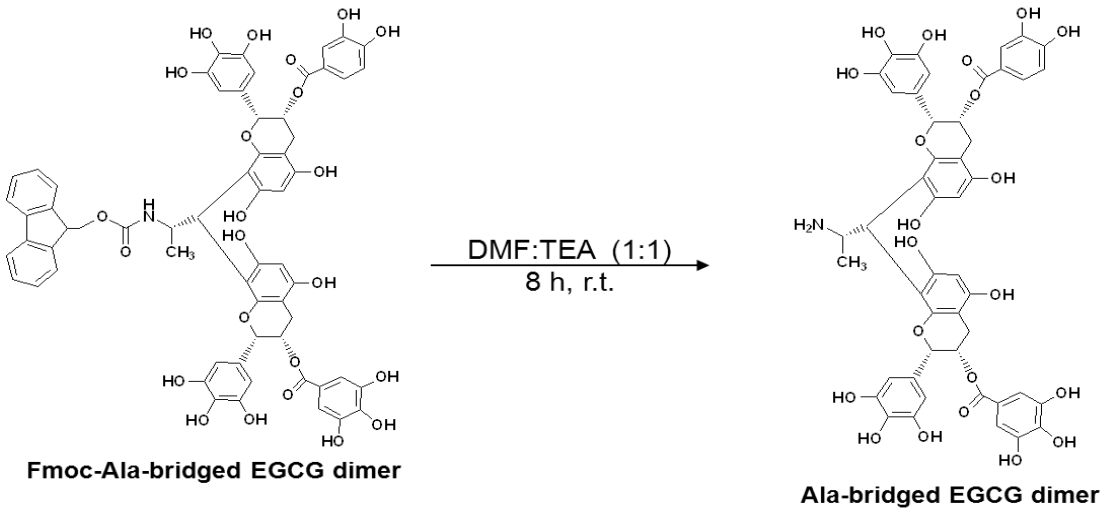

Scheme 3-2. Deprotection of Fmoc-Ala-bridged EGCG dimer.

The final step involved conjugating the Ala-bridged EGCG dimer onto HA, by a conventional carbodiimide reaction (Scheme 3-3). HA (700 mg, 1.83 mmol) was dissolved in 60 ml of MilliQ water by stirring. The carboxylic acid of HA was activated by adding NHS (420 mg, 3.66 mmol) and EDC·HCl (700 mg, 3.66 mmol). The pH of the mixture was maintained at 4.7 for 5 h. Next, Ala-bridged EGCG dimer (1.8 g, 1.83 mmol) dissolved in 20 ml of DMF:HCl mixture (19:1) was added dropwise to the mixture and the pH was adjusted to 4.7. To prevent the oxidation of EGCG, oxygen was removed from the mixture by three cycles of degassing (vacuum/sonication) and refilling with N_2. The mixture was incubated overnight at room temperature. The purification of HA-EGCG conjugates was done by precipitation according to previously established protocol [22]. Briefly, the pH of the mixture was lowered to 3, and then 368 ml of MilliQ water and 49 ml of 5 M NaCl were added. Then, the HA-EGCG conjugate was precipitated by addition of 912 ml of EtOH. The precipitate was collected by centrifugation. The precipitation cycle was repeated twice (2^{nd} cycle: MilliQ water (795 ml), 5 M NaCl (88 ml) and EtOH (1.8 L); 3^{rd} cycle: MilliQ water (1.6 L), 5 M NaCl (176 ml) and EtOH (3.65 L)) to remove

unconjugated Ala-bridged EGCG dimer. Finally, the HA-EGCG conjugate was dissolved in 450 ml of MilliQ water and dialyzed against MilliQ water using a dialysis membrane (Mw cut-off: 3500 Da) at pH 3.5 overnight under N_2 atm. The product was freeze-dried. Yield: 320 mg. To determine the degree of substitution (number of Ala-EGCG dimers conjugated for every 100 disaccharide units), the conjugates were dissolved at 0.1 mg/ml in water and UV-Vis spectrum was recorded with a Hitachi U-2810 spectrometer (Figure 3-2). The amount of EGCG contained in the conjugate was determined by comparing the absorbance at 274 nm with a set of EGCG standards. The degree of substitution was found to be 2.3.

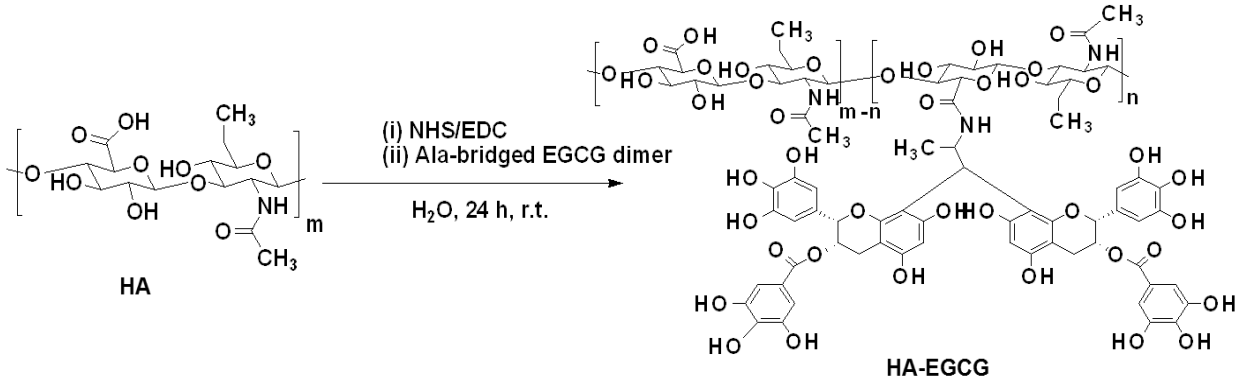

Scheme 3-3. Synthesis of HA-EGCG conjugate.

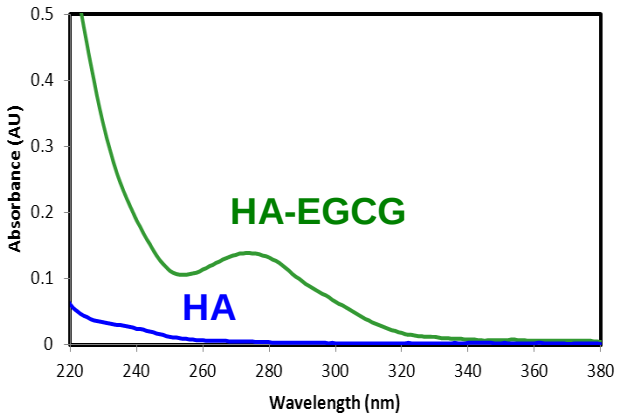

Figure 3-2. UV-VIS spectrum of HA-EGCG and HA in water. The concentrations of both HA-EGCG and HA were 100 µg/ml.

3.2.3. Particle size and zeta potential measurements

Stock solutions of HA-EGCG, HA, linear PEI and lysozyme were prepared in MilliQ water. One hundred µl of PEI (100 µg/ml) was added to 100 µl of lysozyme (200 µg/ml) at room temperature. After 5 min, 200 µl of HA-EGCG (1 mg/ml) and 600 µl of MilliQ water were added to the mixture. HA was also utilized as a comparison. The mixture solution was then incubated for 1 h at room temperature to form nanogel complexes before the measurement of dynamic light scattering (ZetaPALS, Brookhaven Instrument Corp., Holtsville, NY, USA). The measurements were done in quintuplicates. For the measurement of zeta potential (Zetasizer, Malvern Instrument Ltd., Worchestershire, UK), 100 µl of PEI (10 µg/ml) was added to 100 µl of lysozyme (20 µg/ml) at room temperature. After 5 min, HA-EGCG of different concentrations and MilliQ water were added to the mixture. The total volume of the final mixture was 1 ml. Measurements were performed in triplicates after 1 h incubation at room temperature. All data are expressed as the mean ± standard deviation.

3.2.4. Binding studies by fluorescence measurement

Quenching of intrinsic lysozyme fluorescence was used to monitor the binding interactions between HA-EGCG and lysozyme. Stock solutions of HA-EGCG, HA or EGCG at 1 mg/ml were prepared in MilliQ water. These solutions were diluted to various concentrations using PBS and mixed with lysozyme fixed at a concentration of 100 µg/ml. After incubation at room temperature for 1 h, fluorometric measurements were performed using a Hitachi spectrofluorometer model F-2500 using an excitation wavelength of 295 nm. Emission spectra were recorded from 305 to 400 nm. The emission intensities at 339 nm, which were found to be the emission peaks, were compared among the different samples. All measurements were done in triplicates. For EGCG and HA-EGCG, the fluorescence intensity was corrected using a known

formula [23] since the emission peak of lysozyme at 339 nm overlapped with EGCG absorption. The equation to obtain the actual fluorescence intensity F is given below:

$$F = F_u \times 10^{Q\,(S_{\lambda ex} + S_{\lambda em})}$$

where F_u is the measured, uncorrected emission intensity. $S_{\lambda ex}$ and $S_{\lambda em}$ are slopes of absorbance versus concentration linear plots of EGCG and HA-EGCG standards at the excitation (295 nm) and emission wavelengths (339 nm) respectively. Q refers to the concentration of EGCG or HA-EGCG. Subsequently the fluorescence intensity ratio was calculated using the following equation:

$$\text{Fluorescence Intensity Ratio } (F/F_0) = \frac{\text{Fluorescence intensity of sample}}{\text{Fluorescence intensity of lyosozyme alone}}$$

where F is the corrected fluorescence intensity and F_0 is the intrinsic fluorescence intensity of lysozyme alone.

3.2.5. Lysozyme activity assay

Nanogel complexes comprising HA-EGCG, lysozyme and PEI were prepared in the eppendolf tubes in a similar manner as described above. Lysozyme and PEI concentrations were fixed at 20 and 2 μg/ml respectively but HA-EGCG of different concentrations was used. All the samples were then incubated for 30 min for complexation to occur. To determine the activities of lysozyme, they were transferred to the wells of a 96-well UV microplate followed by 100 μl of *Micrococcus lysodeikticus* (0.15 w/v % in PBS). The plate was then shaken for 15 s orbitally before absorbance at 450 nm was measured using the microplate reader. The absorbance decay plot was fitted to a linear equation, and the slopes were used to determine lysozyme activities of

the samples. The lysozyme activities were calculated as a percentage of the activity of lyoszyme alone using the following equation:

$$\text{Lysozyme Activity}\,(\%) = \frac{\text{Slope of absorbance decay plot with sample}}{\text{Slope of absorbance decay plot without sample}} \times 100$$

To determine the restoration of lysozyme activity, Triton-x 100 solutions of different concentrations were prepared in PBS and were added to the nanogel complexes and incubated for 5 min. Then the mixtures were added to the wells of the 96-well plate and activities of lysozyme were determined by the aforementioned method.

3.2.6. Cell viability assay

HCT-116 human colorectal carcinoma cells were seeded at 20,000 cells per well in BD Falcon 96-well microplates with complete growth medium (McCoy's 5A, 10 % (v/v) FBS, 1 % (v/v) penicillin/streptomycin) and left to attach for 48 h. Nanogel complexes comprising HA-EGCG, GzmB and PEI were prepared by firstly adding PEI to GzmB and letting the mixture sit for 20 min at room temperature. Following that, HA-EGCG was added and the resultant complexes were incubated for another 30 min. The concentrations of HA-EGCG were varied but GzmB and PEI concentrations were kept at 2 and 1 μg/ml respectively. The mixture solution of GzmB and chloroquine (CQ) (100 μM) was also prepared as a positive control. In addition, complexes of GzmB (2 μg/ml) with Bioporter® were also prepared according to the protocol provided by Genlantis, USA. In a separate experiment, another set of nanogel complexes was prepared in a similar manner as described above, using various combinations of PEI, GzmB and HA or HA-EGCG. The final concentrations of PEI, GzmB and HA/HA-EGCG were fixed at 1, 2 and 10 μg/ml respectively. In all the experiments, cell viability was analyzed using AlamarBlue®

after 48 h treatment. Briefly, the culture medium was aspirated and the cells were gently washed with PBS once before fresh medium with AlamarBlue® 10 % (v/v) was added to each well. The cells were incubated for 2 h and the fluorescence measurement was performed using a Tecan Infinite Microplate Reader. Excitation and emission wavelengths were set at 545 and 590 nm, respectively. The results were expressed as percentage of viability compared with untreated cells. All results are expressed as the mean ± standard deviation of quadruplicates. The same procedure was repeated for HepG2 human liver carcinoma cells cultured with Dulbecco's modified Eagle's medium (DMEM).

3.2.7. Conjugation of FITC to lysozyme

Briefly, 2 mg of Fluorescein-5-isothiocyanate, (FITC) (Invitrogen) and 200 mg of lysozyme were dissolved in 0.1 M borate buffer (pH 9.0). After incubation for 60 min at room temperature, pH was adjusted to 7.5 with 0.1 M boric acid. The solution was dialyzed for 72 h at 4 ^{o}C while refreshing distilled water twice daily. Subsequently, the final product was obtained by lyophilization. The isolated FITC-lysozyme was then characterized by UV-VIS absorption spectroscopy, and the labeling efficiency was found to be 3.5 moles FITC per mole of protein.

3.2.8. Flow cytometry studies

The cells (HCT-116 or HepG2) were first harvested from culture flasks by trypsin treatment. The cells were then incubated with primary CD44 antibody for 30 min. In addition, the cells were also treated with PBS and isotype control in parallel to confirm that the signal was a result of the CD44 antibody binding only. After that, the samples were centrifuged and washed with PBS three times to remove the background fluorescence. Following that, FITC-labeled

secondary antibody was added and left to attach for 30 min. After another three cycles of washing and centrifugation, cells were resuspended with 200 µL of PBS. The extent of cells which was stained positive for CD44 was evaluated by FACSCalibur flow cytometer (BD Biosciences, USA).

3.2.9. Intracellular caspase imaging

Fluorescence imaging of caspases was performed with the Image-iT ™ LIVE Red Caspase-3 and -7 Detection Kit (Invitrogen). HCT-116 cells were seeded in 8-well chamber slides at density of 20,000 cells/well with complete growth medium (McCoy's 5A with 10 % FBS) and allowed to attach for 48 h. After that, they were treated with nanogel complexes with and without PEI and incubated for 5 h. The staining procedure was then performed in accordance with the staining protocol provided by Invitrogen. The cells were then viewed immediately under a confocal laser scanning microscope (Zeiss LSM 510 META).

3.2.10. Intracellular trafficking studies

HCT-116 cells were seeded in 8-well chamber slides (Lab-Tek®) at density of 20,000 cells/well with complete growth medium (McCoy's 5A with 10 % FBS) and left to attach for 24 h. Nanogels were similarly prepared as the cell viability study, but FITC-labeled lysozyme was used instead of GzmB. The FITC-lysozyme concentration was fixed at 20 µg/ml. The cells were then incubated with the nanogel complexes for 16 h in the dark. Subsequently, the cells were washed twice with ice-cold PBS and fixed with fresh 4 % paraformaldehyde for 15 min at room temperature. The cell nuclei were then stained with 4, 6-diamidino-2-phenylindole (DAPI) and visualized using confocal microscopy.

3.3. Results and Discussion

3.3.1. Synthesis and characterization of HA-EGCG conjugate

In this study, HA-EGCG was synthesized by a condensation reaction between Ala-bridged EGCG dimer and carboxyl group of HA. Fmoc-Ala-bridged EGCG dimer was synthesized by the aldehyde-mediated reaction between Fmoc-Ala-aldehyde and A-ring of EGCG. Subsequently, the Fmoc group was deprotected. In the final step, Ala-bridged EGCG dimer was conjugated to HA by conventional carbodiimide reaction.

The Fmoc-Ala-bridged EGCG dimer intermediate was characterized by various Mass Spectroscopy techniques. It was firstly characterized by Liquid Chromatography Mass Spectroscopy (LCMS) (Figure 3-3 a). The UV-absorbance peaks indicated the presence of EGCG containing products and the four peaks that were observed could possibly be attributed to the isomers of Fmoc-Ala-bridged EGCG dimer. This is because the conjugation site between the EGCG and Fmoc-Ala-aldehyde could be at either the 6' or 8' position of A-ring of EGCG, giving rise to four isomeric configurations - 6-6, 6-8, 8-6 and 8-8. We presumed that the peak at m/z 1194.50 observed in the representative mass spectrum corresponded to the product Fmoc-Ala-bridged EGCG dimer (Mw 1193 Da). To confirm the identity of the signal, mass analysis was performed using two more methods – Fast-Atom Bombardment Mass Spectroscopy (FABMS) (Figure 3-3 b) and high resolution Electron Spray Ionization-Mass Spectroscopy (ESI-MS negative ionization) (Figure 3-3 c). Both the FABMS and high resolution ESI-MS yielded a prominent peak at m/z ratio 1192, which was consistent with the mass of the Fmoc-Ala-bridged EGCG dimer intermediate. Taken together, the characterizations indicated that the synthesis of Fmoc-Ala-bridged EGCG dimer was successful. Subsequently, we continued with the following

steps of HA-EGCG synthesis. The EGCG content in the final product HA-EGCG was measured by comparing the UV absorbance of HA-EGCG against a standard curve for EGCG with wavelength peak of 274 nm. The degree of substitution was 2.3.

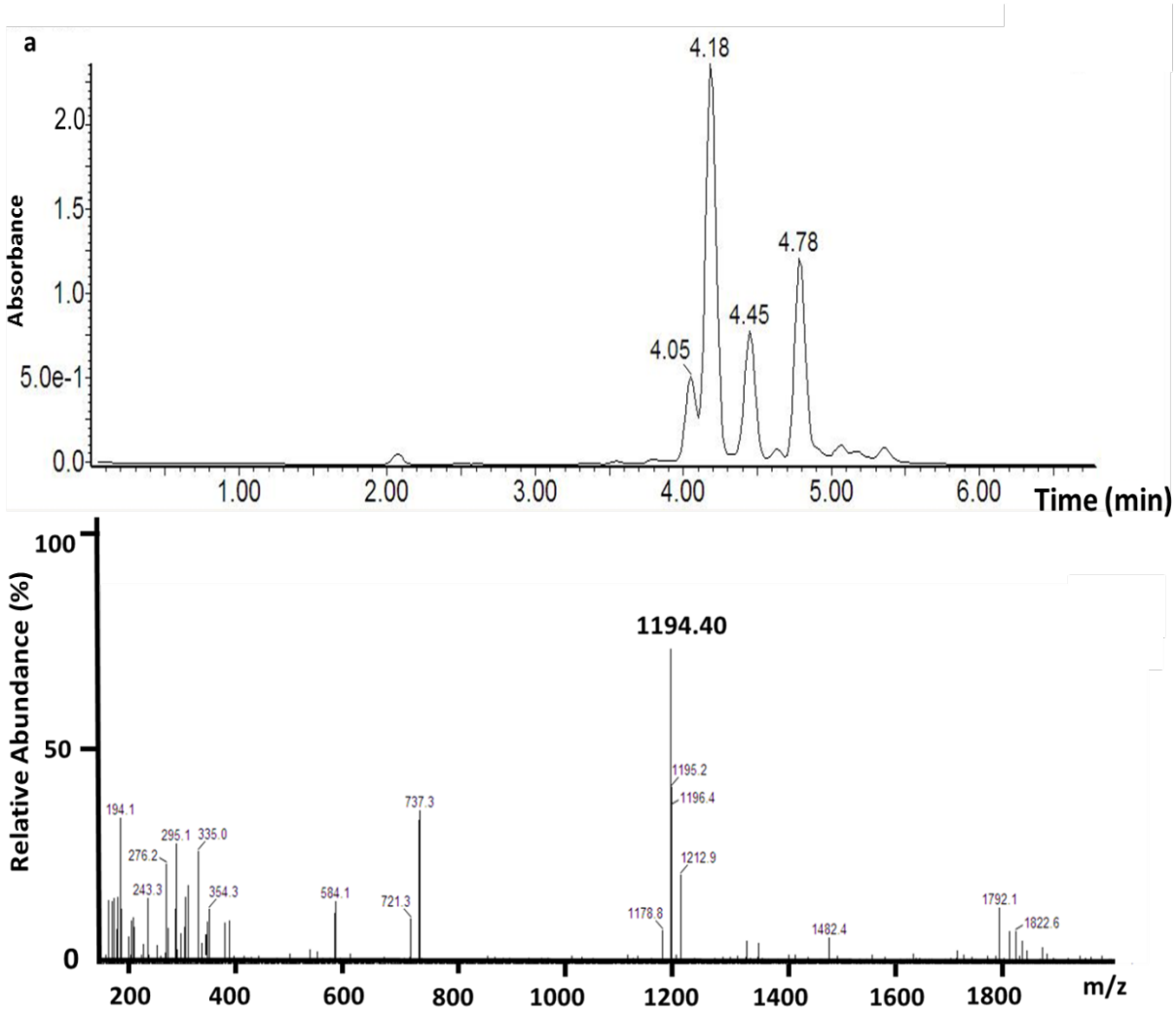

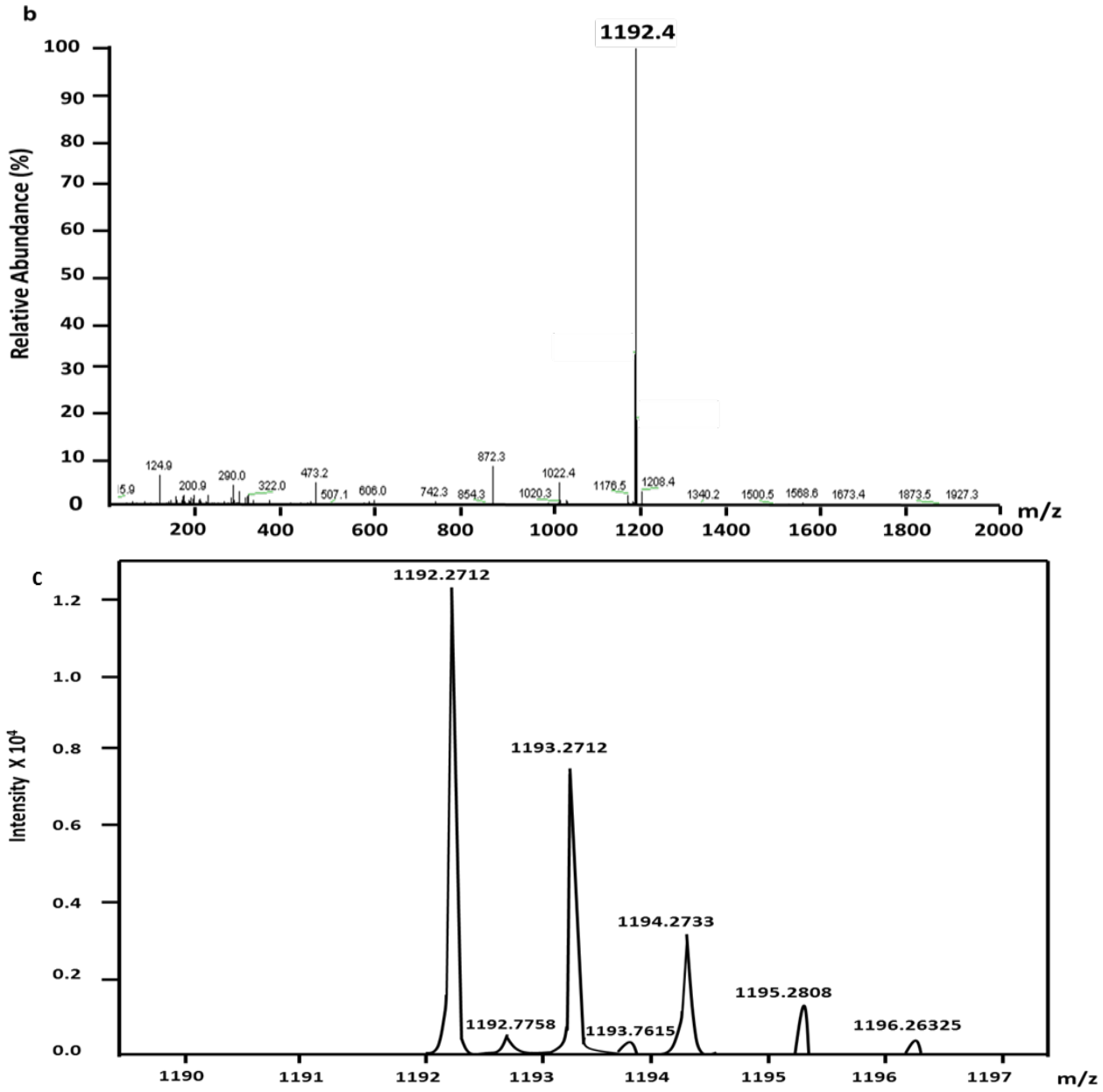

Figure 3-3. Characterizations of Fmoc-Ala-bridged EGCG dimer (a) Liquid Chromatography Mass Spectroscopy (LCMS), (b) Fast-Atom Bombardment Mass Spectroscopy (FABMS) and (c) Electron Spray Ionization-Mass Spectroscopy (ESI-MS negative ionization) at high resolution.

3.3.2. Characterizations of HA-EGCG nanogel

3.3.2.1. Size and zeta potential of HA-EGCG nanogels

We used a model protein, lysozyme, to study the complexation behavior between HA-EGCG and GzmB. Lysozyme (Mw 14.3 kDa, pI 9.20) was chosen because it has relatively similar molecular weight and isoelectric point as GzmB (Mw 30 kDa, pI ~10). First we studied the particle size of the nanogel by dynamic light scattering. The ternary nanogel complex comprising of HA-EGCG/lysozyme/PEI was found to have a size of around 160 nm (Figure 3-4 a). In contrast, the HA/lysozyme/PEI complex control had a size of 222 nm (Figure 3-4 b). Furthermore, the HA-EGCG nanogel was observed to have much lower polydispersity with a single size distribution whereas HA nanogel had two disparate distributions. The hydrophobic and π-π stacking interactions between EGCG moiety and amino acid residues in lysozyme possibly led to stronger binding, resulting in smaller nanogel particulates. In contrast, HA/lysozyme/PEI particles was probably held together weakly by ionic interactions between the carboxylate anion of HA chain and positively charged amino acid residues lysozyme.

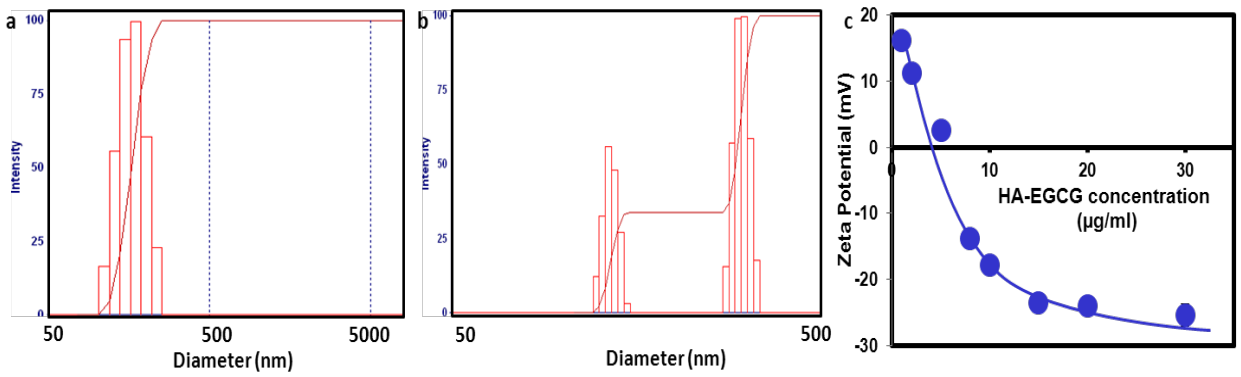

Figure 3-4. (a) Dynamic light scattering data of HA-EGCG/Lysozyme/PEI nanogel complex and (b) HA/Lysozyme/PEI complex, at concentrations of 200 µg/ml, 20 µg/ml and 10 µg/ml respectively; (c) Zeta potential measurements of nanogel complexes with increasing HA-EGCG concentration.

The baseline index of HA-EGCG/lysozyme/PEI nanogel complexes was also consistently higher than that of HA/lysozyme/PEI complexes (Table 3-1). Baseline index is an indication of sample quality, which refers to the difference between the measured baseline and calculated

baseline of the autocorrelation function. In practical terms, a low sample quality signaled the presence of large particles or aggregates. All in all, these results indicated that HA-EGCG/lysozyme/PEI nanogel complexes were more stable and homogeneous than HA/lysozyme/PEI mixture.

Table 3-1. Dynamic light scattering results of HA-EGCG nanogels and HA control.

Samples	Size (nm)	Polydipersity	Baseline Index
HA/lysozyme/PEI	222.8 ± 4.9	0.155 ± 0.017	7.0 ± 1.7
HA-EGCG/lysozyme/PEI	159.8 ± 3.2	0.101 ± 0.019	9.1 ± 0.8

Next we examined the effect of HA-EGCG concentration on the surface charge of the nanogel complexes with fixed concentrations of lysozyme (2 μg/ml) and PEI (1 μg/ml). As shown in Figure 3-4 c, the zeta potential of the HA-EGCG nanogel complexes decreased with increasing HA-EGCG concentrations due to the negatively charged carboxylate anions on HA. In particular, zeta potential became negative when HA-EGCG concentrations exceeded 5 μg/ml. Since zeta potential is an indication of the charge at the surface of nanoparticles, this observation suggested that the HA-EGCG conjugate was able to cover the surface of the nanogel complexes at concentrations > 5 μg/ml.

3.3.2.2. Binding of HA-EGCG to lysozyme

To estimate the strength of binding interactions between HA-EGCG and proteins in the formation of nanogel, we measured the extent of quenching of intrinsic tryptophan fluorescence in the proteins, based on a previously reported method [24]. The ability of HA-EGCG to quench lysozyme fluorescence was analyzed by comparing with both HA and EGCG at equivalent concentrations. The fluorescence intensities of samples were then expressed as a ratio of the

intrinsic fluorescence of lysozyme alone. HA alone did not quench lysozyme fluorescence, indicating that there was no binding (Figure 3-5 a). In contrast, HA-EGCG decreased lysozyme fluorescence in a concentration dependent manner and interestingly to a much greater extent than EGCG alone (Figure 3-5 b). For instance, HA-EGCG quenched fluorescence by 78 % at EGCG concentrations of 25 µg/ml whereas EGCG at 30 µg/ml only managed 30 % fluorescence reduction. This suggested that the conjugation of EGCG to HA enhanced the binding interaction between EGCG moiety and lysozyme, possibly because the HA backbone increased the local concentration of EGCG moieties around a lysozyme molecule.

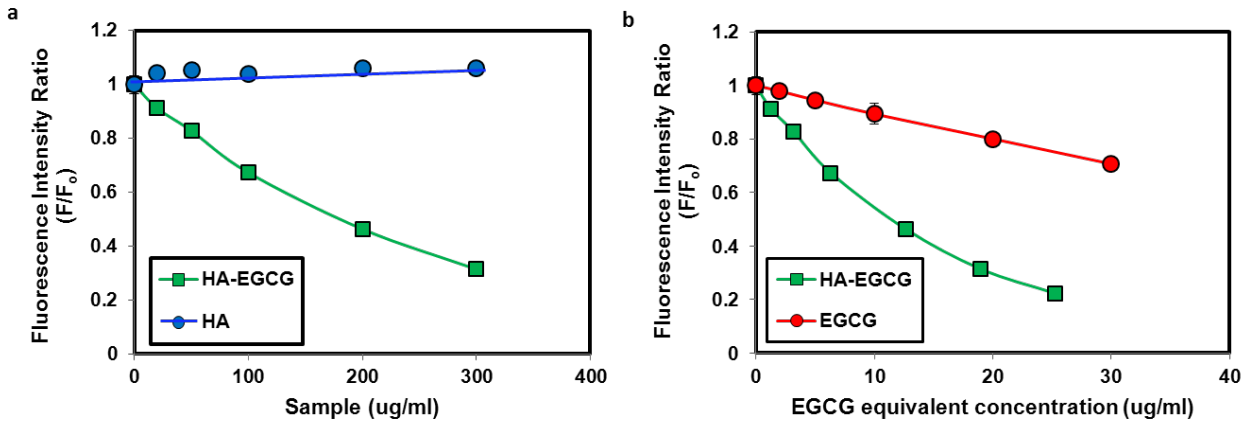

Figure 3-5. Comparison of fluorescence quenching abilities of various samples - (a) HA and HA-EGCG and (b) EGCG and HA-EGCG at equivalent concentrations.

3.3.2.3. Complexation-dissociation behavior of HA-EGCG with lysozyme

The complexation of HA-EGCG conjugates with lysozyme was further verified by lysozyme activity assay using *M. lysodeikticus* as the lysozyme substrate [25]. Binding of lysozyme to HA-EGCG would hinder enzyme-substrate reaction and that would be reflected by a decrease in enzymatic activity level. Indeed, we found that HA-EGCG decreased lysozyme activity in a concentration-dependent manner, whereas HA did not (Figure 3-6 a). Since complexation with HA-EGCG would hinder protein activity, dissociation of the complex to

release the functional protein is necessary once the nanogel complex is internalized within the cell, so that the protein can achieve its intended function. To investigate the ability of the complexes to release proteins, we destabilized the pre-prepared HA/lysozyme/PEI and HA-EGCG/lysozyme/PEI nanogel complexes (100 µg/ml) with Triton-X, which was expected to disrupt the hydrophobic interactions within the complex [26]. From the results on Figure 3-6 b, we demonstrated that addition of 0.1 w/v % of Triton-X to the HA-EGCG nanogel complexes led to the successful restoration of lysozyme activity from 85 % to 99 % while no effect was observed for the HA counterpart.

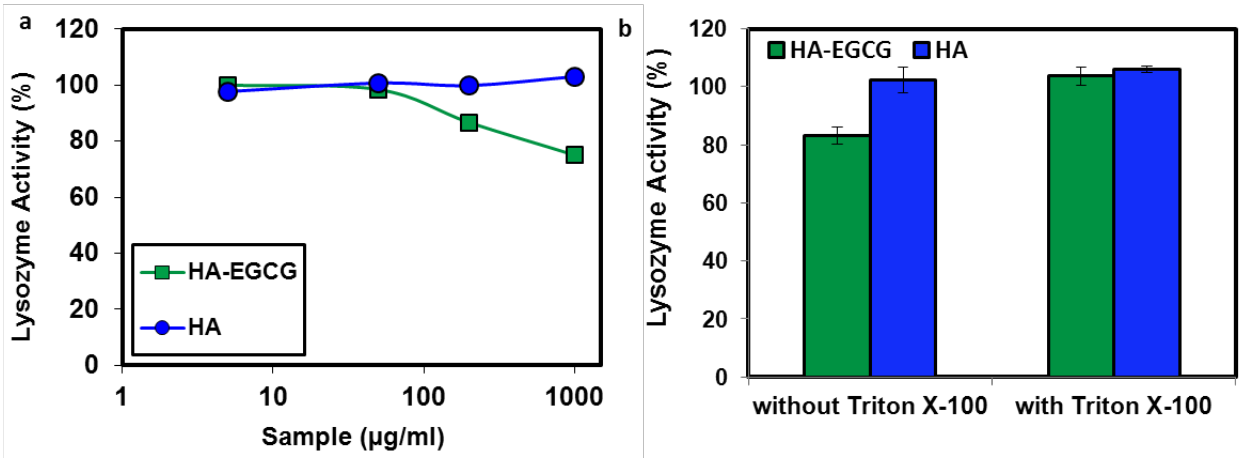

Figure 3-6. (a) Lysozyme activities of HA/lysozyme/PEI complex and HA-EGCG/lysozyme/PEI nanogel complex. (b) Addition of Triton-x successfully restored the lysozyme activity in the HA-EGCG/lysozyme/PEI nanogel complex.

3.3.3. Inhibition of HCT-116 cell proliferation by HA-EGCG/GzmB/PEI nanogels

The confirmation of the complexation-dissociation behavior of HA-EGCG with lysozyme and PEI motivated us to investigate the potential of GzmB as the cargo for delivery. As mentioned above, GzmB is a cytotoxic protein that is known to initiate apoptosis intracellularly. By taking advantage of the HA receptor targeting, we aimed to achieve specific eradication of cancer cells by using HA-EGCG nanogels to deliver GzmB into cytosol of those cells. HCT-116 colon cancer cells overexpressing CD44 were used for the *in vitro* assessment.

First we verified that GzmB alone did not affect cell viability (Figure 3-7 a). This agreed well with previous studies that showed cell death mediated by GzmB could only be observed when its release into cytoplasm was facilitated by perforin [18, 19]. A positive control comprising chloroquine (CQ), a common lysosomotropic agent, was also set up. GzmB/CQ treatment was observed to induce > 70 % cell death. Even though CQ was successful in enabling GzmB-mediated cell death, its usage is undesirable as it is toxic [27]. Next we investigated the optimal HA-EGCG/GzmB/PEI nanogel formulation for cell inhibition. When we increased HA-EGCG concentration of the nanogel complexes, we observed a drop in cell viability from 2 – 10 µg/ml where it reached a minimum of around 48 % at an optimal HA-EGCG/GzmB/PEI concentration ratio of 10 µg/ml /2 µg/ml /1 µg/ml respectively (Figure 3-7 a). The effect was reversed when HA-EGCG increased from 10 µg /ml to 20 µg/ml. The initial increase in cytotoxicity could be attributed to greater stability of nanogel complex as a result of stronger binding interactions between HA-EGCG and GzmB. However, further enhancement of HA-EGCG GzmB interactions probably retarded the release of GzmB from the complex thus resulting in a drop in GzmB-mediated toxicity. In contrast to HA-EGCG nanogel complexes, HA complexes with different HA concentrations had little effect on cell viability throughout. This suggested that HA-EGCG had the ability to form efficient complexes with GzmB whereas HA failed to do so.

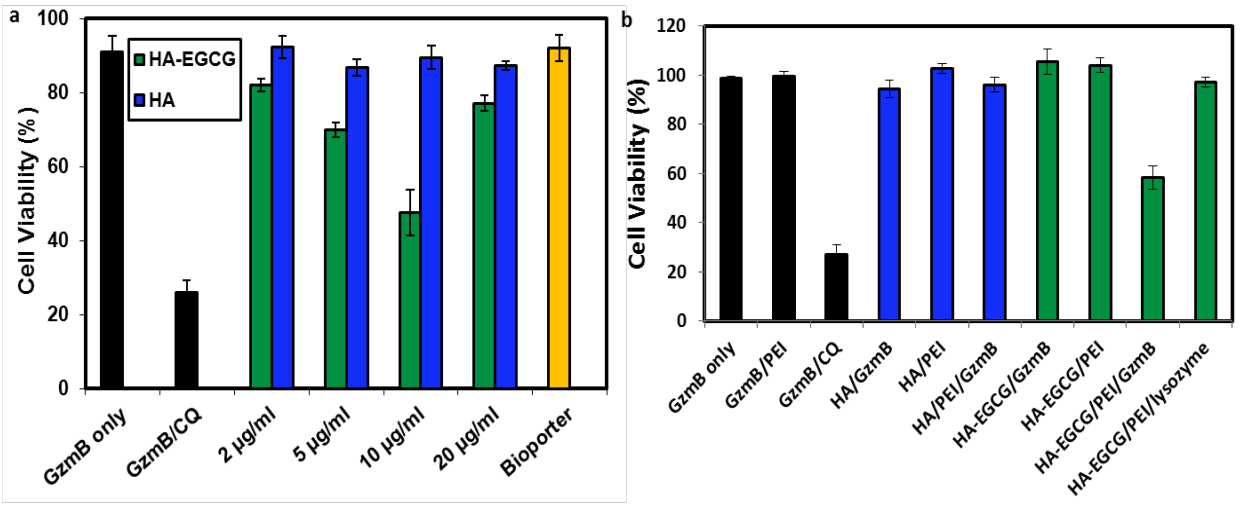

Figure 3-7. (a) Cell viability of HCT-116 cells after treatment with HA-EGCG/GzmB/PEI nanogels complexes with increasing concentrations of HA and HA-EGCG, while GzmB and PEI concentrations were fixed at 2 µg/ml and 1 µg/ml respectively (n = 4). CQ was used as positive control. GzmB alone and Bioporter/GzmB treatment were used as comparison. (b) Cell viability of HCT-116 cells treated with various combinations of optimized HA-EGCG, HA and GzmB concentrations (n = 4).

It is also worth mentioning here that so far there has been no successful delivery of positively charged proteins such as GzmB in a targeted manner similar to what was shown here because most of the carriers were designed carry positive charge to exploit the electrostatic interactions with the negatively charged cell membrane. One of the few carriers that has been reported to deliver GzmB intracellularly is Bioporter® [28], a commercial liposomal carrier. Thus we included Bioporter® for comparison. However we observed that Bioporter®/GzmB complex failed to induce significant toxicity in HCT-116 cells (Figure 3-7 a). This discrepancy could possibly be attributed to the difference in cell line, which may influence the efficiency of Bioporter® facilitated GzmB delivery.

Subsequently various combinations of HA, HA-EGCG, GzmB and PEI complexes at the optimized concentrations were prepared to assess their effects on cell viability (Figure 3-7 b). The result showed that all other treatments besides CQ/GzmB and HA-EGCG/GzmB/PEI nanogel complex had no effects on cell viability, indicating that the other components were not

responsible for cytotoxicity. We also observed no toxicity from nanogel complexes prepared using the model protein lysozyme. This suggests that the toxicity induced by HA-EGCG/GzmB/PEI nanogel complexes was the result of GzmB mediated cell killing. In addition, the fact that HA-EGCG/GzmB complexes alone were not able to induce cytotoxicity in the cells confirmed the role of PEI in facilitating intracellular GzmB delivery (Figure 3-7 b). The presence of PEI in the complex could be critical for the dissociation and release of GzmB in the cytosol.

3.3.4. Induction of apoptosis by HA-EGCG/GzmB/PEI nanogels

Successful intracellular delivery of GzmB in cytosol by nanogels would result in apoptosis, leading to cell death. One feature of the early stages of apoptosis is the activation of caspase enzymes, especially caspases-3 and 7 [29]. To assess the extent of apoptosis in cells treated with various complexes, we proceeded to detect intracellular caspase-3 and caspase-7 by a fluorescently labeled substrate using confocal microscopy. HCT-116 cells treated with complexes formed with HA/GzmB/PEI and GzmB/PEI mixture showed little fluorescence throughout (Figures 3-8 a, b). In contrast, ubiquitous fluorescence was detected in cells treated with HA-EGCG/GzmB/PEI, suggesting that caspase level was enhanced in those cells and cellular toxicity was indeed due to apoptosis (Figure 3-8 c). Presence of some activated caspase in these cells was possibly due to apoptosis caused by the growth of cells in serum-free condition.

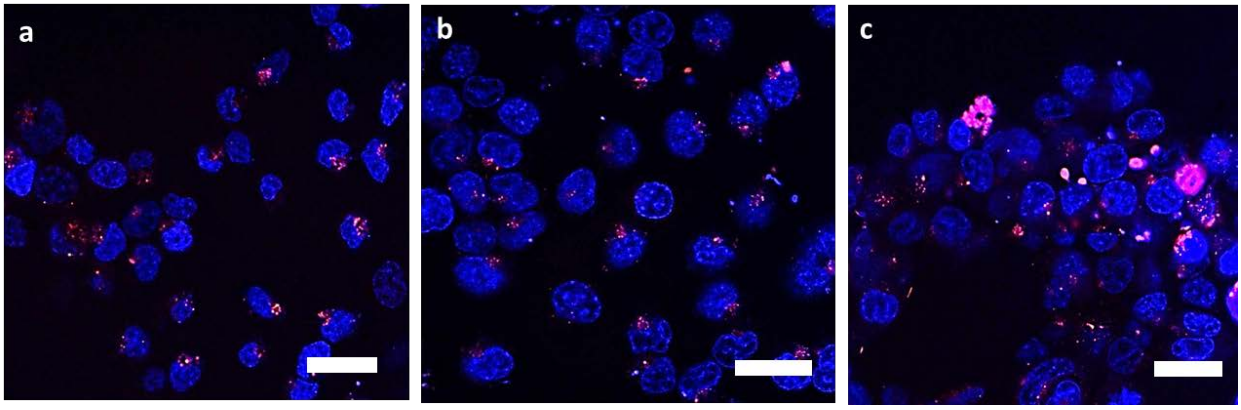

Figure 3-8. HCT-116 cells treated with (a) GzmB/PEI, (b) HA/GzmB/PEI (c) HA-EGCG/GzmB/PEI for 4 h followed by staining with fluorescently labeled caspase substrates. Scale bar = 20 µm.

3.3.5. Effect of HA-EGCG/GzmB/PEI nanogels on low CD44-expressing cells

To verify the CD44 targeting capability of the HA-EGCG/GzmB/PEI nanogel complexes, we investigated the effect of complexes on another cell line - HepG2, a cell line that was reported to have low CD44 expression [30]. CD44 expression levels were evaluated by Fluorescence Activated Cell Sorting (FACS) (Figure 3-9) following antibody staining in both HCT-116 and HepG2 cells. The results confirmed that HCT-116 cells had much higher affinity for CD44 antibody than HepG2 cells in which 99.1 % of HCT-116 cells displayed fluorescent signal as compared to 0 % in HepG2. When we investigated the effects of various combinations of complexes at optimized concentrations on HepG2 cell viability, we found that except for the CQ/GzmB treatment which induced about 60 % cell death, various combinations of HA or HA-EGCG complexes had no effect on the cell viability (Figure 3-10). The ineffectiveness of HA-EGCG/GzmB/PEI nanogel complexes against CD44 low-expressing cell line suggested that the nanogel complexes were able to achieve targeted killing of CD44 overexpressing cells only.

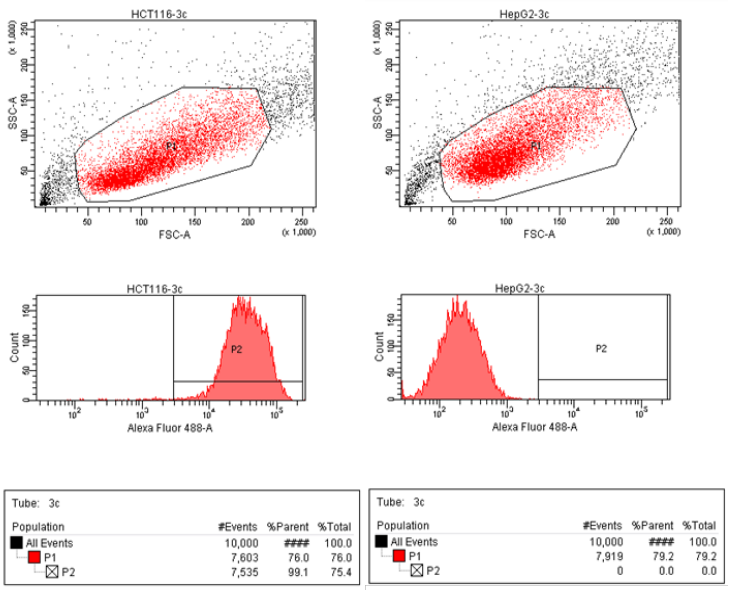

Figure 3-9. Fluorescent-activated cell sorting results of CD44 antibody binding to HCT-116 and HepG2 cells.

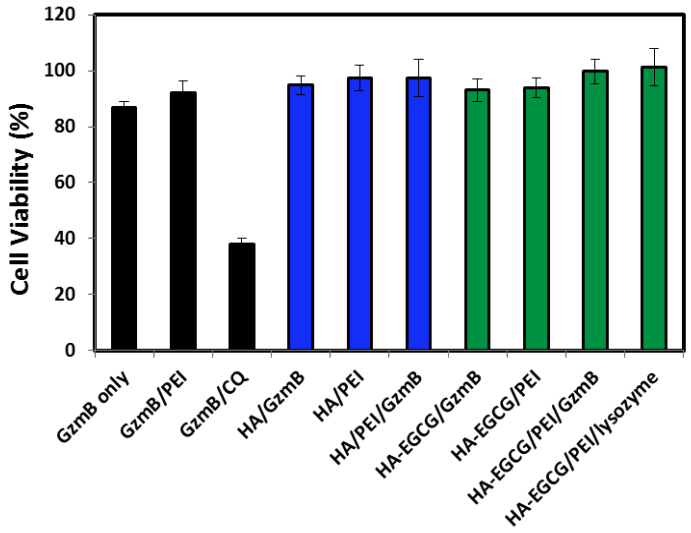

Figure 3-10. Cell viability of HepG2 cells treated with various combinations of optimized HA-EGCG, HA and GzmB concentrations (n = 4). CQ was used as positive control.

3.3.6. Intracellular trafficking of HA-EGCG/FITC-lysozyme/PEI nanogels

To further understand this difference in toxicity of nanogel complexes on the two cell lines, cellular uptake was elucidated by intracellular trafficking of a fluorescently labeled FITC-lysozyme. When HCT-116 cell or HepG2 cells were incubated with HA-EGCG/FITC-lysozyme

complexes for 16 h, we observed much more robust uptake of FITC-lysozyme in HCT-116 cells as compared to HepG2 cells (Figure 3-11). Higher uptake in HCT-116 was expected as a result of the efficient internalization of HA-EGCG nanogel complexes by abundant HA receptors on HCT-116 cell surface, and that is supported by the significantly greater toxicity of the HA-EGCG/GzmB/PEI nanogel complexes toward HCT-116 cells compared to HepG2 cells. Moreover, inclusion of PEI in the HA-EGCG/FITC-lysozyme complexes clearly triggered the release of FITC-lysozyme in HCT-116 cells, resulting in the FITC-lysozyme being evenly distributed throughout the cell cytosol. This agreed well with the previous observation that PEI played an important role in facilitating the escape of FITC-lysozyme from endosomal compartments within the cells.

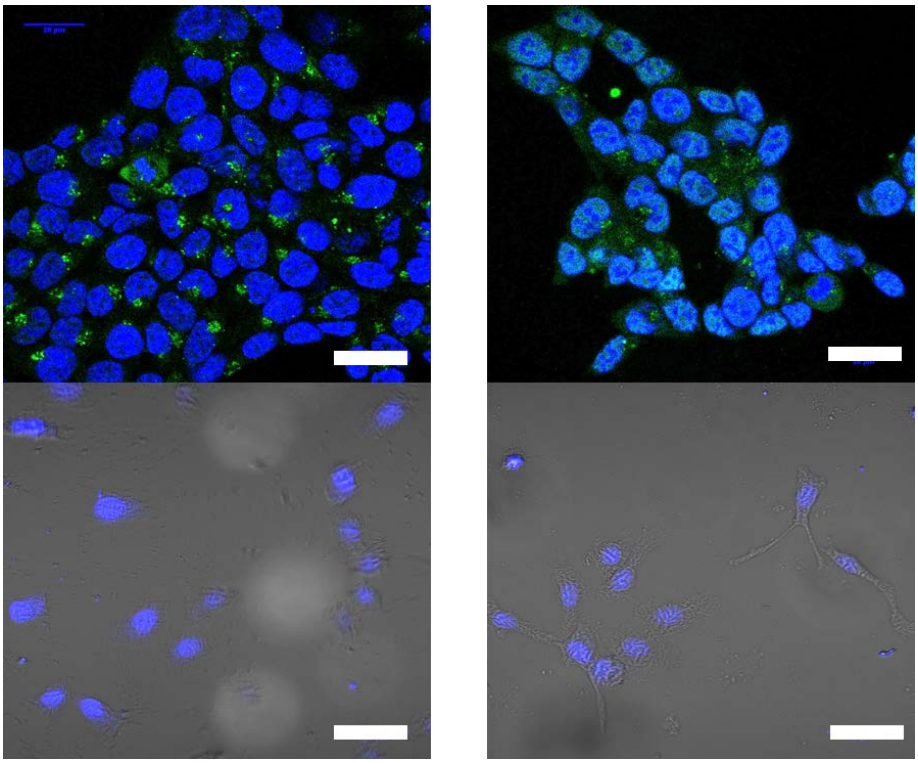

Figure 3-11. (a) Intracellular uptake of HA-EGCG/FITC-lysozyme nanogel complexes into HCT-116 cells without PEI; and (b) release of FITC-lysozyme in cytosol facilitated by PEI. Limited uptake of FITC-lysozyme was observed with HepG2 cells in both nanogel complexes with (c) and without (d) PEI. Scale bar = 20 µm.

3.4. Conclusion

This study has shown an efficient way of targeted cancer cell eradication by intracellular delivery of GzmB using HA-EGCG conjugates. Self-assembled HA-EGCG/GzmB/PEI nanogel complexes were prepared by simple mixing and they demonstrated targeted toxicity against CD44 overexpressing HCT-116 cells but not CD44 negative cells. The toxicity was attributed to GzmB mediated apoptosis, indicating the successful intracellular delivery of GzmB by HA-EGCG conjugates. As a result of EGCG's ability to interact with many bioactive molecules, it is expected that our approach can be extended to delivery of other cytotoxic agents, making HA-EGCG nanogel complex a novel and versatile platform for targeted cancer therapy.

.

References

1. Torchilin, V., *Intracellular delivery of protein and peptide therapeutics.* Drug Discovery Today: Technologies, 2008. **5**(2–3): p. e95-e103.
2. Bale, S.S., et al., *Nanoparticle-Mediated Cytoplasmic Delivery of Proteins To Target Cellular Machinery.* ACS Nano, 2010. **4**(3): p. 1493-1500.
3. Biswas, A., et al., *Endoprotease-Mediated Intracellular Protein Delivery Using Nanocapsules.* ACS Nano, 2011. **5**(2): p. 1385-1394.
4. Choi, J.H., et al., *Intracellular delivery and anti-cancer effect of self-assembled heparin-Pluronic nanogels with RNase A.* Journal of Controlled Release, 2010. **147**(3): p. 420-427.
5. Kim, S.K., M.B. Foote, and L. Huang, *The targeted intracellular delivery of cytochrome C protein to tumors using lipid-apolipoprotein nanoparticles.* Biomaterials, 2012. **33**(15): p. 3959-3966.
6. Chacko, R.T., et al., *Polymer nanogels: A versatile nanoscopic drug delivery platform.* Advanced Drug Delivery Reviews, 2012. **64**(9): p. 836-851.
7. Shimizu, T., et al., *Nanogel DDS enables sustained release of IL-12 for tumor immunotherapy.* Biochem Biophys Res Commun, 2008. **367**(2): p. 330-5.
8. Ayame, H., N. Morimoto, and K. Akiyoshi, *Self-Assembled Cationic Nanogels for Intracellular Protein Delivery.* Bioconjugate Chemistry, 2008. **19**(4): p. 882-890.
9. Joung, Y.K., et al., *Heparin-Conjugated Pluronic Nanogels as Multi-Drug Nanocarriers for Combination Chemotherapy.* Molecular Pharmaceutics, 2012. **10**(2): p. 685-693.
10. Lee, H., et al., *Target-specific intracellular delivery of siRNA using degradable hyaluronic acid nanogels.* Journal of controlled release : official journal of the Controlled Release Society, 2007. **119**(2): p. 245-52.
11. Wei, X., et al., *Hyaluronic Acid-Based Nanogel–Drug Conjugates with Enhanced Anticancer Activity Designed for the Targeting of CD44-Positive and Drug-Resistant Tumors.* Bioconjugate Chemistry, 2013. **24**(4): p. 658-668.
12. Lee, H., et al., *Target-specific intracellular delivery of siRNA using degradable hyaluronic acid nanogels.* J Control Release, 2007. **119**(2): p. 245-52.
13. Tachibana, H., et al., *A receptor for green tea polyphenol EGCG.* Nat Struct Mol Biol, 2004. **11**(4): p. 380-381.
14. Yang, C., J. Lambert, and S. Sang, *Antioxidative and anti-carcinogenic activities of tea polyphenols.* Archives of Toxicology, 2009. **83**(1): p. 11-21.
15. Maiti, T.K., K.S. Ghosh, and S. Dasgupta, *Interaction of (-)-epigallocatechin-3-gallate with human serum albumin: fluorescence, fourier transform infrared, circular dichroism, and docking studies.* Proteins, 2006. **64**(2): p. 355-62.
16. Abe, I., K. Kashiwagi, and H. Noguchi, *Antioxidative galloyl esters as enzyme inhibitors of p-hydroxybenzoate hydroxylase.* FEBS Lett, 2000. **483**(2-3): p. 131-4.
17. Trapani, J.A. and M.J. Smyth, *Functional significance of the perforin/granzyme cell death pathway.* Nature Reviews Immunology, 2002. **2**(10): p. 735-747.
18. Keefe, D., et al., *Perforin triggers a plasma membrane-repair response that facilitates CTL induction of apoptosis.* Immunity, 2005. **23**(3): p. 249-262.
19. Thiery, J., et al., *Perforin activates clathrin-and dynamin-dependent endocytosis, which is required for plasma membrane repair and delivery of granzyme B for granzyme-mediated apoptosis.* Blood, 2010. **115**(8): p. 1582-1593.

20. Boussif, O., et al., *A versatile vector for gene and oligonucleotide transfer into cells in culture and in vivo: polyethylenimine.* Proceedings of the National Academy of Sciences, 1995. **92**(16): p. 7297-7301.
21. Lee, F., et al., *Synthesis and bioactivity of conjugate composed of green tea catechin and hyaluronic acid; In preparation.*
22. Homma, A., et al., *Novel hyaluronic acid-methotrexate conjugates for osteoarthritis treatment.* Bioorg Med Chem, 2009. **17**(13): p. 4647-56.
23. Shpigelman, A., G. Israeli, and Y.D. Livney, *Thermally-induced protein–polyphenol co-assemblies: beta lactoglobulin-based nanocomplexes as protective nanovehicles for EGCG.* Food Hydrocolloids, 2010. **24**(8): p. 735-743.
24. Ghosh, K.S., B.K. Sahoo, and S. Dasgupta, *Spectrophotometric studies on the interaction between (−)-epigallocatechin gallate and lysozyme.* Chemical Physics Letters, 2008. **452**(1): p. 193-197.
25. Lee, F., J.E. Chung, and M. Kurisawa, *An injectable hyaluronic acid–tyramine hydrogel system for protein delivery.* Journal of Controlled Release, 2009. **134**(3): p. 186-193.
26. Zordan-Nudo, T., et al., *Effects of nonionic detergents on P-glycoprotein drug binding and reversal of multidrug resistance.* Cancer Res, 1993. **53**(24): p. 5994-6000.
27. Adebayo, R.A., et al., *Chloroquine-induced pruritus in malaria fever: contribution of malaria parasitaemia and the effects of prednisolone, niacin, and their combination, compared with antihistamine.* British Journal of Clinical Pharmacology, 1997. **44**(2): p. 157-161.
28. Zelphati, O., et al., *Intracellular Delivery of Proteins with a New Lipid-mediated Delivery System.* J. Biol. Chem., 2001. **276**(37): p. 35103-35110.
29. Lakhani, S.A., et al., *Caspases 3 and 7: key mediators of mitochondrial events of apoptosis.* Science, 2006. **311**(5762): p. 847-851.
30. Coradini, D., et al., *Inhibition of Hepatocellular Carcinomas in vitro and Hepatic Metastases in vivo in Mice by the Histone Deacetylase Inhibitor HA-But.* Clinical Cancer Research, 2004. **10**(14): p. 4822-4830.

Chapter 4: Targeted gene delivery based on hyaluronic acid-green tea catechin nanogel complexes

4.1. Introduction

Gene therapy is a promising treatment for many diseases, including cancer; for example, the tumor suppressor gene *p*53 has been used for the treatment of ovarian carcinoma [1, 2]. Hence, many gene delivery vehicles have been developed for cancer gene therapy. Non-viral vectors have been garnering increasing interest in recent years due to their non-immunogenicity, ease of modification and scalability [3-5]. Among them, polyethyleneimine (PEI) is one of the most widely used because of its high transfection efficiency [6, 7]. However, there are several limitations to the usage of PEI - 1) significant toxicity as its high positive charge density disrupt cell membranes [8, 9]. 2) non-specific interactions with blood components such as serum proteins due to the surface charge of PEI/DNA complex [10]. 3) aggregation of PEI/DNA complexes under physiological conditions [11, 12]. Therefore, numerous approaches were explored to modify PEI [13-15] to reduce toxicity, decrease non-specific interactions with proteins and minimize aggregation. To target a specific disease such as cancer, recognition motifs have also been incorporated to achieve selective delivery of genetic materials into cancer cells [16].

Hyaluronic acid (HA) is a glycosaminoglycan composed of repeating disaccharide units of *N*-acetyl-*D*-glucosamine and *D*-glucuronic acid. It is a main component of the extracellular matrix (ECM) and is involved in many cellular functions including cell proliferation, differentiation and migration [17, 18]. Since HA possesses attractive properties such as biodegradability and biocompatibility, it has been integrated in designs of vectors for drug/gene delivery [19]. More importantly, HA has been chosen because of its ability to interact with CD44 that is overexpressed on many cancer cells [20, 21]. To exploit the HA-CD44 targeting property, many HA-based delivery systems have been developed to transport therapeutics such as proteins,

peptides and nucleotides [22, 23] into cancer cells specifically. In particular for gene delivery, HA has been shown to form a ternary complex with PEI/DNA because of the ionic interactions between carboxyl residues and amine groups of PEI. These HA-coated PEI/DNA ternary complexes were demonstrated to enhance gene transfer into specific cells by CD44 targeting [24, 25]; as well as reduce toxicity [26] and minimize aggregation by shielding of positive charges [27].

In this study, we describe the synthesis of novel HA-EGCG conjugates for the targeted delivery of DNA into cancer cells. EGCG is a major constituent of green tea catechins and it has been shown to interact with many macromolecules including DNA *via* hydrogen bonding, π-π stacking and hydrophobic interactions [28-30]. Thus we hypothesize that the conjugation of EGCG to the HA backbone would enable HA-EGCG conjugates to interact more favorably with DNA than HA alone. It is expected that the strong binding interactions between HA-EGCG and PEI/DNA complex would lead to the formation of stable HA-EGCG/PEI/DNA nanogel complexes (Figure 4-1 a). This allows the HA-EGCG nanogel complexes to be internalized efficiently into CD44 overexpressing cancer cells *via* receptor-mediated endocytosis, thereby achieving enhanced gene expression in cancer cells (Figure 4-1 b).

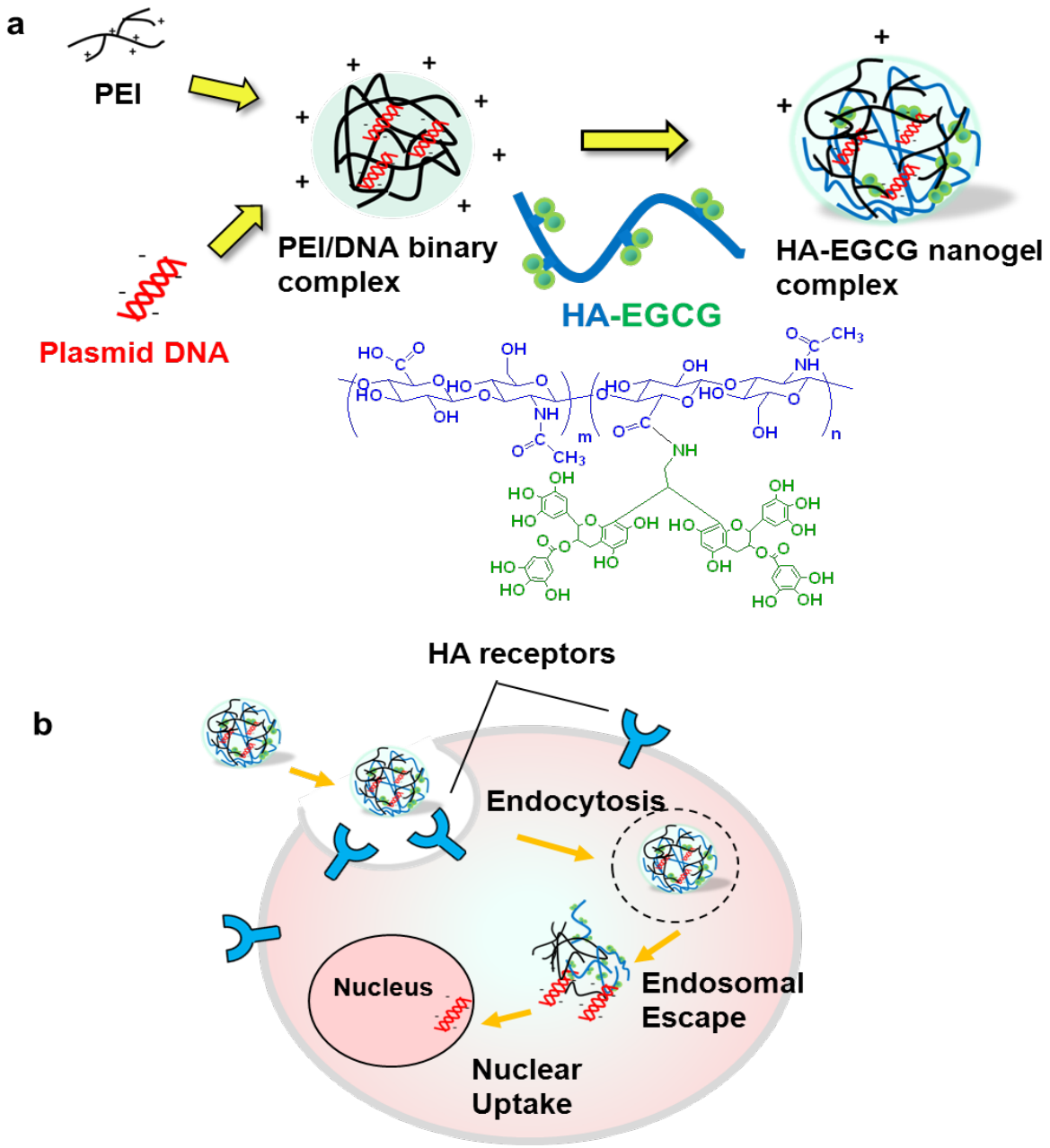

Figure 4-1. Schematic representation of HA-EGCG/PEI/DNA nanogel complex formation and application for targeted gene delivery. (a) Binary complex between PEI and DNA was first prepared, followed by addition of HA-EGCG conjugate. (b) Presentation of HA-EGCG on outer surface of complex facilitates uptake of nanogel complexes by CD44 overexpressing cancer cells *via* HA receptors.

4.2. Materials and Methods

4.2.1. Materials

Hyaluronic acid (HA, 90 kDa) was kindly donated by JNC Corporation (Tokyo, Japan). Tetrahydrofuran (THF), methanesulfonic acid (MSA), 2,2-diethoxyethylamine (DA), *N*-hydroxysuccinimide (NHS), 1-ethyl-3-(3-dimethylaminopropyl)-carbodiimide hydrochloride (EDC·HCl), branched polyethyleneimine (PEI) were all obtained from Sigma-Aldrich. EGCG (TEAVIGO) was purchased from DMS Nutritional Products Ltd (Switzerland). Phosphate buffer saline (PBS, 150 mM, pH 7.3) and all cell culture media were supplied by the media preparation facility in Biopolis, Singapore.

4.2.2. Synthesis of HA-EGCG Conjugate

The HA-EGCG conjugate was synthesized in a two-step process established previously in our laboratory [31].

1) Synthesis of ethylamine-bridged EGCG dimers. In a glass vial containing 1.2 ml of cold MSA:THF (1:5 (v/v)) mixture, 145 μl of DA (1 mmol) was added while stirring. The resulting mixture was transferred dropwise to EGCG (2.29 g, 5 mmol), which was dissolved in 3.8 ml of THF and 1.7 ml of MSA, and stirred overnight in the dark at room temperature. Next day, the solvent (THF) was removed by evaporation and further dried under vacuum overnight at room temperature. The dried products were dissolved in 10 ml of H_2O and the unreacted EGCG were removed by extraction with 10 ml of ethyl acetate using a separation funnel. Unreacted EGCG moved to the organic phase while the ethylamine-bridged EGCG dimers remained in the aqueous phase. The extraction procedure was repeated until no free EGCG was detected in the aqueous phase using a Waters Acuity UPLC-MS. The concentration of the purified ethylamine-

bridged EGCG dimer in the aqueous phase was determined by absorbance at 274 nm and was found to be 84 mg/ml (yield = 88 %). The dimers were stored at -80 °C.

2) Synthesis of HA-EGCG conjugates. Ethylamine-bridged EGCG dimers were conjugated to HA by a typical carbodiimide/active ester-mediated coupling reaction [32]. HA (250 mg, 0.62 mmol) was dissolved by stirring in 20.2 ml of 0.4 M MES buffer (pH 5.2) with 2.5 ml of DMF. Next, NHS (89 mg, 0.78 mmol) and ethylamine-bridged EGCG dimers (0.205 mmol in 2.33 ml of H_2O) were added to the reaction mixture. Then, EDC·HCl (150 mg, 0.78 mmol) was added and the pH of the reaction was adjusted to 4.7. The reaction mixture was purged vigorously with N_2 for 10 min and then incubated in the dark overnight under N_2 at room temperature. The HA-EGCG conjugates were purified by precipitation using a previously established method with some modifications [32, 33]. Briefly, 125 ml of H_2O and 16.7 ml of 5 M NaCl solution were added to the reaction mixture and the pH was lowered to 3 with 10 M HCl solution. Then, 310 ml of ethanol was added while stirring. Under these conditions the HA-EGCG conjugates formed slurry precipitates which were collected by centrifugation (6000 rcf, 5 min). After decanting the supernatant, the precipitates were re-dissolved in 250 ml of water. After adding 33 ml of 5 M NaCl solution and the pH adjusted to 3, 620 ml of ethanol was added. The precipitates were collected by centrifugation and re-dissolved in 500 ml of H_2O. After adding 67 ml of 5 M NaCl solution and lowering the pH to 3, 1.24 L of ethanol was added. The precipitates were again collected by centrifugation and re-dissolved in 300 ml of H_2O. The conjugates were then dialyzed (Mw cut-off: 3500 Da) against H_2O in N_2 atmosphere overnight. Finally, the purified HA-EGCG conjugates were lyophilized. The yield was 185 mg (74 %). To calculate the degree of substitution (number of EGCG dimers conjugated for every 100 disaccharide units), the conjugates were dissolved at 0.1 mg/ml in water and UV-Vis spectrum

was recorded with a Hitachi U-2810 spectrometer. The amount of EGCG contained in the conjugate was determined by comparing the absorbance at 274 nm to the EGCG standard curve.

4.2.3. Preparation of various complexes

DNA plasmid (pEGFP-C1, 4.7 kbp) encoding for GFP was obtained from Clontech Laboratories, Inc. (CA, USA). PEI/DNA binary complexes were formed at various molar ratios of the amine group of PEI to the phosphate group on DNA (N/P ratios) by adding appropriate volumes of PEI to DNA in water. The solution was mixed gently and allowed to stand at room temperature for 15 min. For the formation HA or HA-EGCG nanogel complexes, HA or HA-EGCG were then added to the solution at designated molar ratios of the carboxyl group of HA to the phosphate group on DNA (C/P ratios) ranging from 0.1 to 10 and incubated for a further 30 min.

4.2.4. Hydrodynamic size and zeta potential measurements

A Malvern Zetasizer Nano ZS (Worcestershire, UK) was used to measure the hydrodynamic size and zeta potential of all the complexes. For size measurements, complexes were prepared accordingly with 1 µg of DNA and diluted to 1 ml final volume with MilliQ water. To determine the zeta potentials, samples were dispersed in diluted 10 mM NaCl instead. All measurements were performed in triplicates and the results were reported as mean ± s.d.

4.2.5. Agarose gel electrophoresis

The ability of all the complexes to condense plasmid DNA was assessed through the elimination of electrophoretic mobility using agarose gel electrophoresis. PEI/DNA binary complex at N/P 30 and HA or HA-EGCG/PEI/DNA nanogel complexes of various C/P ratios

containing plasmid 1 μg DNA were prepare with a final volume of 10 μl. The samples were then loaded in a 1.2 % agarose gel containing the SYBR® Safe dye (Invitrogen). Subsequently, the gel was run in 1 × Tris-acetate-EDTA (TAE) buffer at a constant voltage (100 V) for 25 min. Images were then captured with a Versadoc 4000 MP instrument (Bio-Rad Laboratories, Singapore). To examine the stability of the complexes, heparin was added (final concentration 1 mg/ml) to the complexes and further incubated for 30 min prior to gel electrophoresis.

4.2.6. GFP expression assay

Human embryonic kidney (HEK293) and human colorectal carcinoma (HCT-116) cells were maintained in Dulbecco's modified Eagle's medium (DMEM) and McCoy's 5A medium respectively, completed with 10 % (v/v) fetal bovine serum (FBS) and 1 % (v/v) penicillin/streptomycin at 37 °C with 5 % CO_2. For both cell types, 100,000 cells were added into each well of 24-well plates to attach for 24 h. On the day of transfection, 100 μl of PEI/DNA binary at various N/P ratios were prepared as above and then added to each well. For HA or HA-EGCG nanogel complexes, N/P ratio was fixed at 30 and the HA or HA-EGCG amounts added were calculated based on designated C/P ratios ranging from 0.1 to 10. The transfection experiments were performed in the presence of 10 % FBS. The amount of DNA introduced into each well was fixed at 1.5 μg. On the designated day of transfection analysis (72 h after transfection for HCT-116 and 48 h for HEK293), the cells were harvested and suspended in PBS for flow cytometry analysis (LSR II, BD Bioscience, CA, USA). 10,000 cells were gated and the percentage of cells expressing GFP was reported as mean ± s.d. of triplicates at least. Cells were defined to be positive for GFP if they fell within the gating region pre-set to include < 2 % of untreated control cells. At the same time, quantitative GFP expression was also estimated by mean fluorescence intensity. Images of GFP-positive cells were taken with an inverted

fluorescence microscope (IX71, Olympus Corporation, Tokyo, Japan) fitted with a DP70 camera (Olympus) at 4 × magnification.

To assess the HA receptor mediated uptake in cancer cells; a competitive inhibition assay was used in which the cells were pretreated with HA to saturate the receptors. Dextran was used as a control. After 1 h pretreatment, the complexes were then added to the cells. Percentage of cells transfected was evaluated by flow cytometry.

4.2.7. *In vitro* cytotoxicity assay

For both HEK293 and HCT-116 cells, 15,000 cells were seeded in each well of a 96-well microplate and incubated for one day to allow for cell attachment. The next day, cells were subjected to similar treatments as aforementioned in the GFP transfection experiment, albeit with volumes scaled down proportionally to 20 µl per well. Final DNA amount introduced into each well was 0.3 µg. Cell viability was evaluated by the AlamarBlue® assay (Invitrogen) at designated time-points similar to the GFP transfection assay. Briefly, cells were gently washed with PBS once before fresh medium with AlamarBlue® (10 % (v/v)) was added. The cells were incubated for another 2 h and fluorescence was measured using a Tecan Infinite Microplate Reader (Ex/Em: 545/590 nm). Cell viability was expressed as a percentage of untreated control cells and data was reported as mean ± s.d. of quadruplicates.

4.2.8. CD44 evaluation by flow cytometry

One million cells of each type were harvested and split into two equal portions. One was incubated with CD44 antibody (2 mg/ml) and the other incubated with the isotype control for 15 min at room temperature. After that they were washed 3 times with cold PBS with 10 % (v/v) FBS before flow cytometry analysis (LSR II, BD Bioscience, CA, USA).

4.2.9. Intracellular trafficking and cellular uptake

DNA labelling was done following the protocol provided by DNA labelling kit (Cy 5 *Label* IT® Tracker™ Intracellular Nucleic Acid Localization Kit (Mirus, USA). For intracellular trafficking study, HCT-116 cells were seeded in 8-well chamber slides (Lab-Tek®) at the density of 20 000 per well and left to attach for 24 h. The complexes were prepared with Cy 5-labelled pDNA (0.5 μg DNA per well) and added to the cells. At the designated time-points, the medium was removed and cells were washed with PBS thrice and fixed with 4 % paraformaldehyde. After that, cell nuclei were labelled with 4, 6-diamidino-2-phenylindole (DAPI) and the cells were visualized under a confocal laser scanning microscope (Zeiss LSM 510 META).

To quantify cellular uptake, HCT-116 cells were seeded in 24-well plates and complexes containing Cy 5-labelled plasmid DNA were prepared in the same manner as the transfection experiment and added to the cells. At the designated time-points, the fluorescent DNA-containing cells were collected and and suspended in PBS and evaluated by flow cytometry (LSR II, BD Bioscience, CA, USA). Uptake levels of complexes in the cells were analyzed with a gated population of living 5,000 cells.

4.2.10. Statistical analysis

Statistical analysis was determined by analysis of variance tests (ANOVA) using Microsoft Excel. Data sets were compared using two-tailed, unpaired Student's t-tests. And a p value of < 0.05 was considered to be statistically significant.

4.3. Results and discussion

4.3.1. Synthesis of HA-EGCG conjugates

HA-EGCG conjugates were synthesized as described in our previous report [31]. First, ethylamine-bridged EGCG dimer was synthesized by the coupling reaction of 2,2-diethoxyethylamine onto A-ring of EGCG. Subsequently, ethylamine-bridged EGCG dimer was conjugated to HA by conventional carbodiimide reaction between amine group of ethylamine-bridged EGCG dimer and carboxyl residue of HA. By comparing the UV absorbance of HA-EGCG against a standard curve for EGCG with wavelength peak of 274 nm, the EGCG content could be determined and the degree of substitution (number of EGCG dimers conjugated for every 100 disaccharide units) was estimated to be 2.5.

4.3.2. Optimization of PEI/DNA N/P ratios for transfection

To determine the optimal condition for PEI/DNA binary complexes, the transfection efficiencies and toxicities of binary complexes at escalating N/P ratios were evaluated in two different cell lines – a human colorectal carcinoma cell line - HCT-116 and a normal human embryonic kidney cell line - HEK293. In general, increasing the N/P ratio led to an increase in the percentage of cells transfected as well as a decrease in cell viability in both cell lines. In HCT-116 cells, the maximum transfection efficiency of 15.6 % was detected at N/P ratio of 30 with a corresponding cell viability of 84.8 % (Figure 4-2 a). The N/P ratio of 40 resulted in lower transfection efficiency and higher toxicity. For HEK293 cells, we observed that PEI/DNA complex at N/P ratio of 30 transfected 73.8 % of cells while maintaining 80.2 % of cell viability (Figure 4-2 b). Significant cell death was observed at N/P ratio of 40. Therefore the optimal N/P ratio of 30 was chosen for subsequent formation of nanogel complexes.

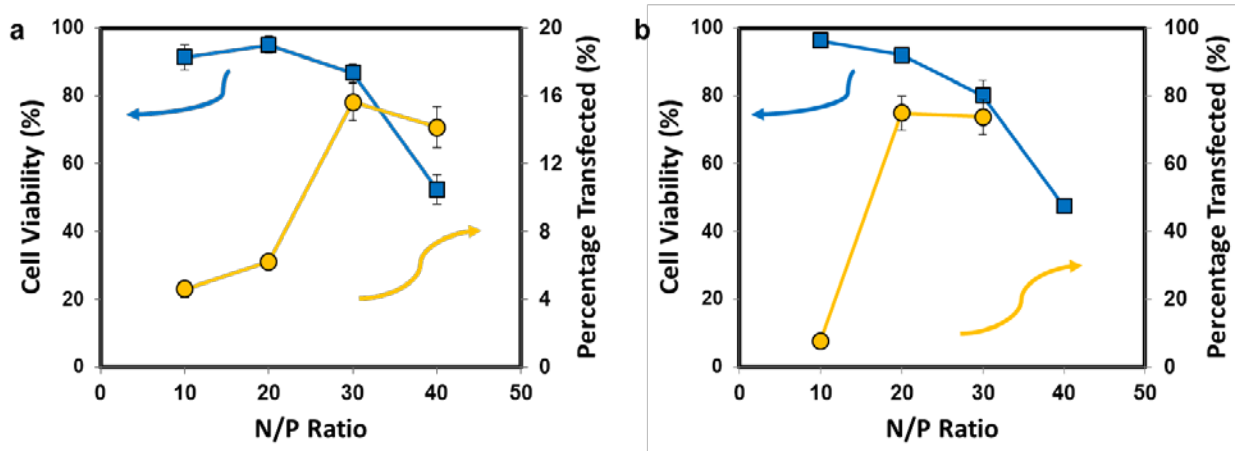

Figure 4-2. Optimization of PEI/DNA binary complexes for transfection. Percentage of cells transfected and cell viability of (a) HCT-116 cells and (b) HEK293 cells treated with PEI/DNA complex at various N/P ratios.

4.3.3. Characterizations of HA-EGCG nanogel complexes

We prepared HA-EGCG nanogel complexes by simply adding HA-EGCG conjugates to the pre-formed PEI/DNA binary complexes at N/P ratio of 30. HA complexes were similarly prepared as comparison. Various amounts of HA-EGCG or HA were added based on the carboxylate anion to DNA phosphate ratio (C/P ratio) within the range of 0.1 to 10. The size and zeta potential of the nanogel complexes were then measured. All of the complexes were found to be between 100-200 nm (Figure 4-3 a). The zeta potential, which is an indication of the surface charge of the complexes, decreased as a function of increasing HA-EGCG C/P ratios (Figure 4-3 b). This drop is due to the neutralization of the positive charges of PEI by the negatively charged carboxylate anions on HA. Interestingly, at the C/P ratio of 10, HA-EGCG nanogel complex had significantly lower surface charge than HA complexes (-7.5 mV vs. 1.2 mV). This indicates that HA-EGCG could probably provide a more stable anchorage onto the surface of the PEI/DNA binary complex than HA, contributing to the reduction in surface charge.

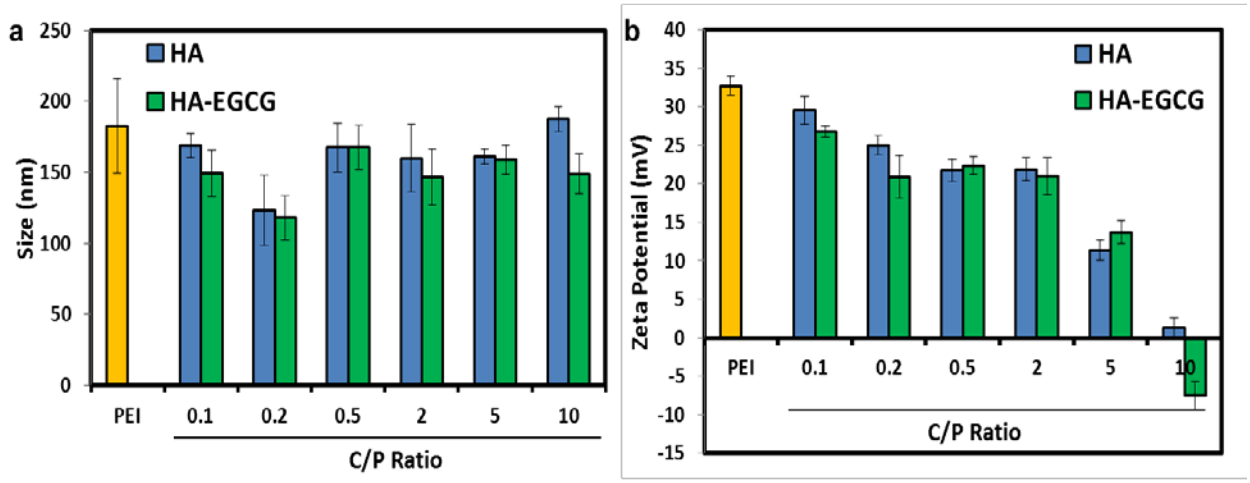

Figure 4-3. (a) Hydrodynamic sizes and (b) zeta potentials of HA-EGCG/PEI/DNA nanogel complexes of increasing C/P ratios.

4.3.4. Stability of HA-EGCG nanogel complexes

It has been well-documented that the presence of negatively-charged serum proteins would destabilize PEI/DNA complexes *via* adsorption and exchange reactions [34, 35]. To evaluate the stability of the complexes by assessment of DNA mobility *via* gel electrophoresis, all the complexes were challenged in the serum-simulated condition with the introduction of heparin. Figure 4-4 illustrates the results. In the absence of heparin, all the complexes showed strong DNA binding ability and total inhibition of DNA migration. Addition of heparin resulted in DNA liberation from all the HA/PEI/DNA complexes at various C/P ratios and PEI/DNA binary complexes. In contrast, complete DNA release was only observed in C/P ratios (0.1, 0.5 and 2) for HA-EGCG/PEI/DNA nanogel complexes. Partial release of DNA was seen in C/P ratio of 5 showing diminished DNA band intensity while DNA release was completely suppressed in C/P ratio of 10. This suggests that increasing HA-EGCG concentrations led to stronger interactions between HA-EGCG and PEI/DNA complex, contributing to enhanced

stability. As such, HA-EGCG nanogel complexes could possibly maintain their integrities more effectively in serum condition than the other complexes.

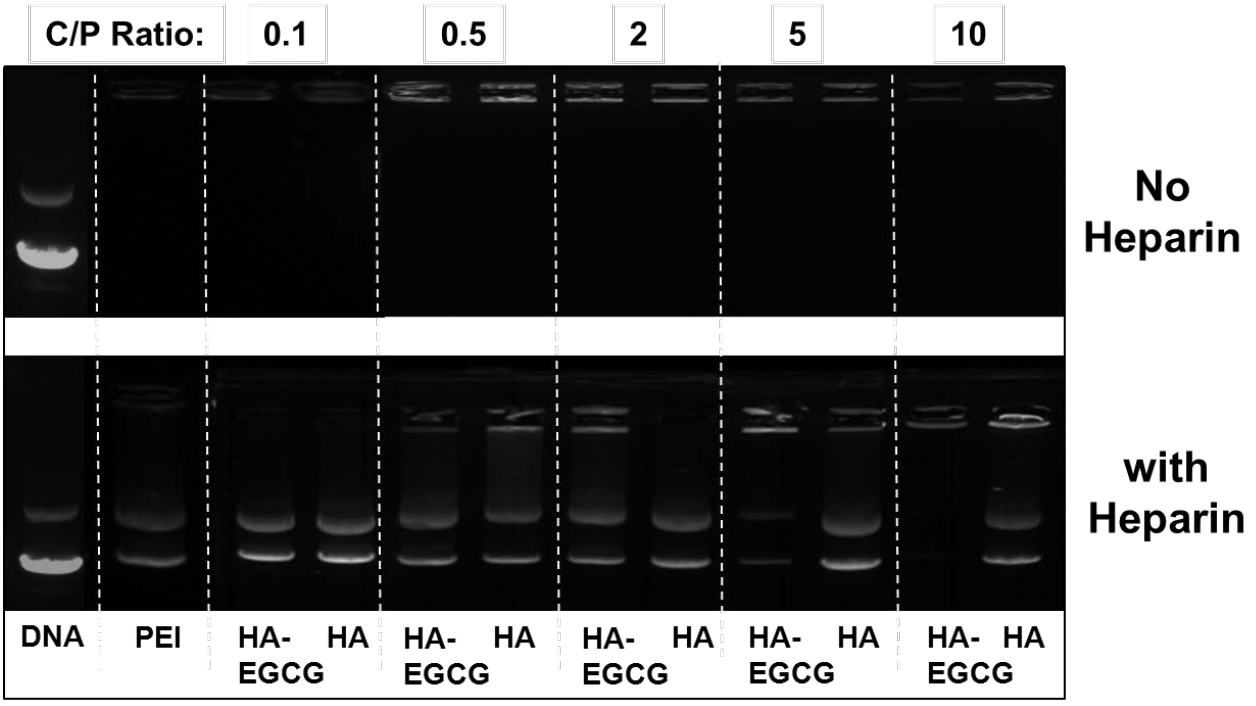

Figure 4-4. Agarose gel electrophoresis retardation assay of HA-EGCG/PEI/DNA nanogel complexes prepared at different C/P ratios. PEI/DNA binary complex at N/P ratio of 30 and HA/PEI/DNA complexes were used as comparison. Top panel shows complexes with no heparin treatment while bottom panel displays complexes treated with heparin (final concentration 1 mg/ml) for 30 min prior to gel electrophoresis.

4.3.5. Transfection efficiency and cytotoxicity of HA-EGCG nanogel complexes

Prior to investigating the *in vitro* transfection efficiency of HA-EGCG nanogel complexes, the two cell lines HCT-116 and HEK293 were assessed for CD44 expression. Similar to many cancer cells, a high proportion (99.4 %) of HCT-116 cells was found to express CD44 while only 3.2 % of normal HEK293 cells were found to be CD44 positive (Table 4-1).

Table 4-1. CD44 expression level in HCT-116 and HEK cells.

Cell line	Cell type	CD44 expression (%)
HCT-116	Human colorectal carcinoma	99.4
HEK293	Human embryonic kidney	3.2

Next we evaluated the transfection efficiency of HA-EGCG nanogel complexes in the CD44 overexpressing HCT-116 cells. The PEI/DNA binary complex at N/P ratio of 30 and HA/PEI/DNA complexes were used as comparison. A range of C/P ratios from 0.1 to 10 were examined. Figure 4-5 depicts the representative fluorescent microscopic images of GFP-expressing cells corresponding to the respective transfection conditions. The extent of GFP-positive cells transfected was quantified by flow cytometry (Figure 4-6). We observed that both HA and HA-EGCG nanogel complexes demonstrated significantly enhanced transfection efficiencies compared to PEI/DNA binary complexes at N/P ratio of 30 (Figure 4-6 a). In particular, HA-EGCG nanogel complex at C/P ratio of 0.5 and HA complex at C/P ratio of 5 successfully transfected 43.7 % and 37.2 % of HCT-116 cells respectively, which is about 2-fold increment over that of PEI/DNA binary complex at 19.0 %. The rise in transfection efficiency could probably be attributed to enhanced cellular uptake of complexes *via* CD44 mediated endocytosis. In addition, while the percentage of cells transfected increased as a function of increasing C/P ratios for both HA-EGCG nanogel complexes and HA complexes, we noted that this increase for HA complex was shifted toward much higher C/P ratios as compared to HA-EGCG nanogel complex. It is worth mentioning that the maximum transfection mediated by HA-EGCG nanogel complex at C/P ratio of 0.5 was superior to that mediated by HA complex at C/P ratio of 5 even though the amount of polymer used was 10 times lower. This could possibly be explained by the enhanced stability of the HA-EGCG nanogel complexes. Considering that all transfection experiments were performed in serum existing condition, the HA complexes were

more likely to be dissociated by the negatively charged serum proteins, resulting in lower gene delivery efficiency. Quantitative assessment of GFP expression by fluorescence intensity revealed similar trends as the percentage of cells transfected with GFP plasmid (Figure 4-6 b). Overall this *in vitro* transfection study clearly demonstrated that HA-EGCG nanogel complexes were more efficient than both PEI/DNA binary complex and HA complexes in transfecting CD44 overexpressing HCT-116 cells.

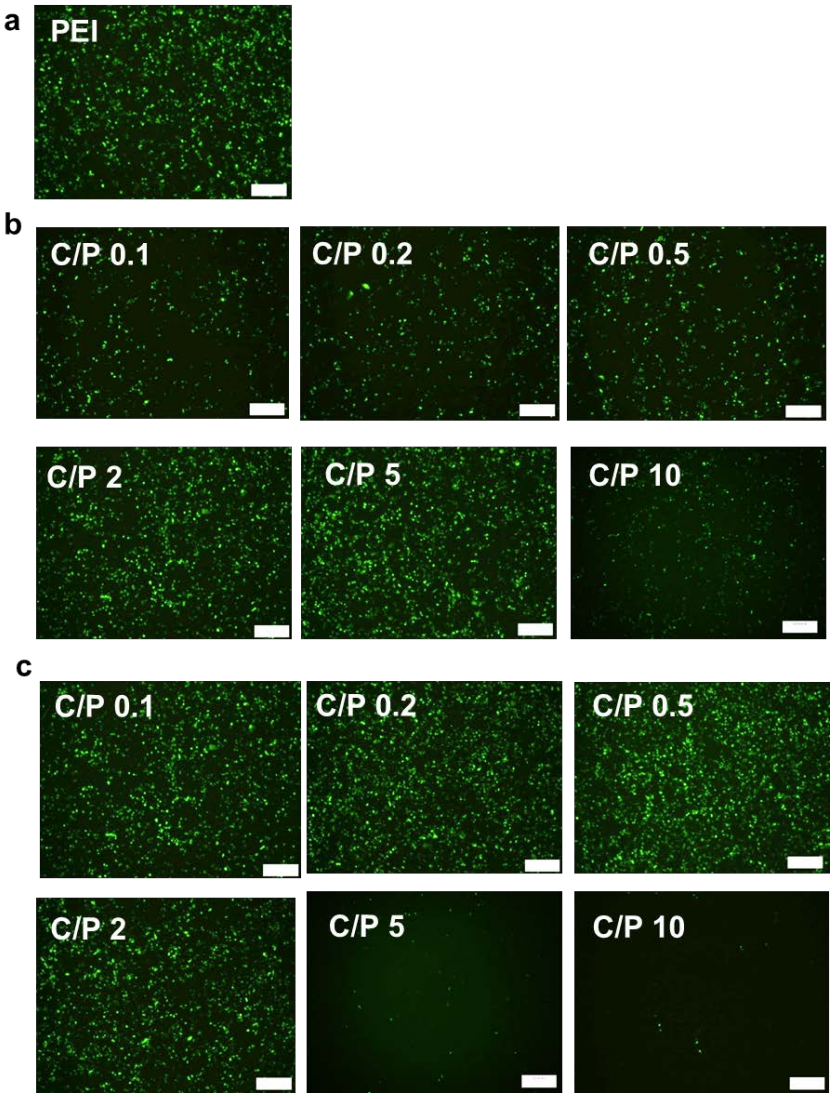

Figure 4-5. Representative images of distribution of GFP-positive cells after being transfected with various complex formulations; (a) PEI/DNA binary complex at N/P ratio of 30, (b) HA/PEI/DNA complexes and (c) HA-EGCG/PEI/DNA nanogel complexes at the indicated C/P ratios. Scale bar = 500 µm.

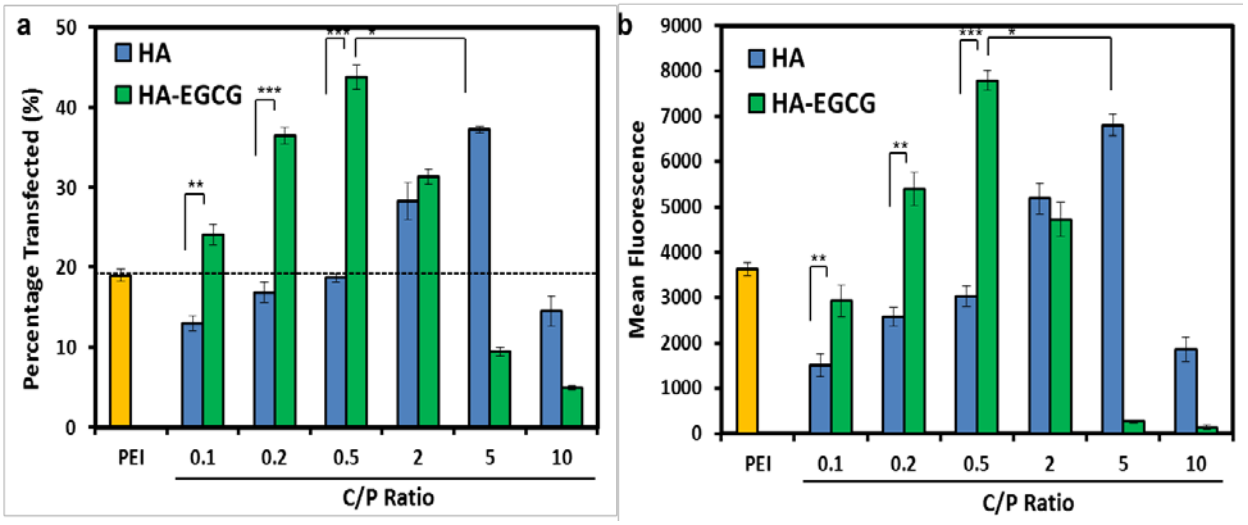

Figure 4-6. Transfection efficiency of HA-EGCG/PEI/DNA nanogel complexes in HCT-116 cells with PEI/DNA binary complex at N/P ratio of 30 and HA/PEI/DNA complexes as comparison. (a) Percentage of cells successfully transfected with GFP plasmid; (b) Mean fluorescence intensity of GFP expressed in the transfected cells. * $p < 0.005$; ** $p < 0.0005$; *** $p < 0.00005$.

To examine the mechanism of uptake of the HA-EGCG nanogel complexes, transfection experiment was performed following free HA pre-incubation to block the receptors. We observed that percentage of cells transfected decreased proportionately with increasing free HA concentration, from 43.7 % with 0 mg/ml HA to 4.1 % with 2 mg/ml HA pre-treatment (Figure 4-7). This suggests that HA-receptor mediated endocytosis facilitated intracellular delivery of HA-EGCG nanogel complexes into HCT-116 cells.

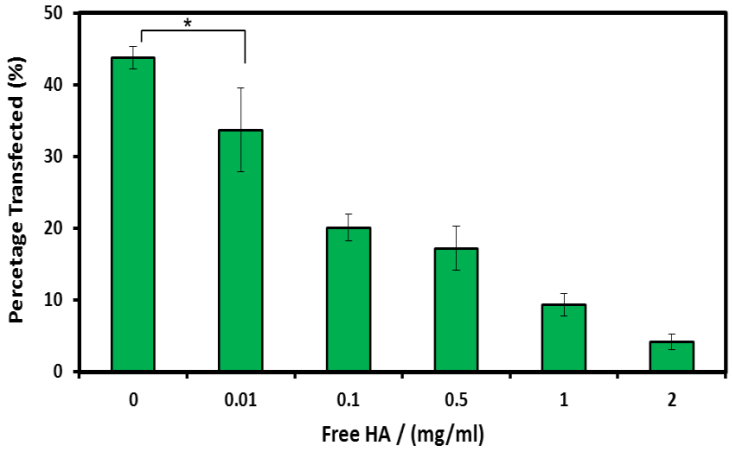

Figure 4-7. Transfection efficiency of HA-EGCG/PEI/DNA nanogel complex at C/P ratio of 0.5 in HCT-116 cells pre-incubated with free HA at increasing concentrations. * $p < 0.05$.

Given that the enhanced transfection observed in HCT-116 cells was mediated by CD44, HA-EGCG nanogel complexes could be exploited for cancer cell-specific transfection. To investigate the specificity of nanogel mediated gene delivery, transfection efficiencies of various complexes were then evaluated on low CD44 expressing normal HEK293 cells. From the results on Figure 4-8, it is evident that both the percentage of cells transfected and the fluorescence intensity were highest for PEI/DNA binary complex. Both HA and HA-EGCG nanogel complexes demonstrated lower transfection efficiencies at all the C/P ratios tested. It is generally accepted that the cationic charges on PEI facilitate cellular uptake through electrostatic interactions with the negatively charged cell membrane [9, 36]. Therefore in the absence of CD44, the lower surface charges of HA and HA-EGCG nanogel complexes probably resulted in retardation of complex internalization, leading to reduction in transfection efficiency. This finding clearly confirmed the specificity of HA-EGCG nanogel complexes to mediate superior gene delivery efficiency in high CD44 expressing cancer cells.

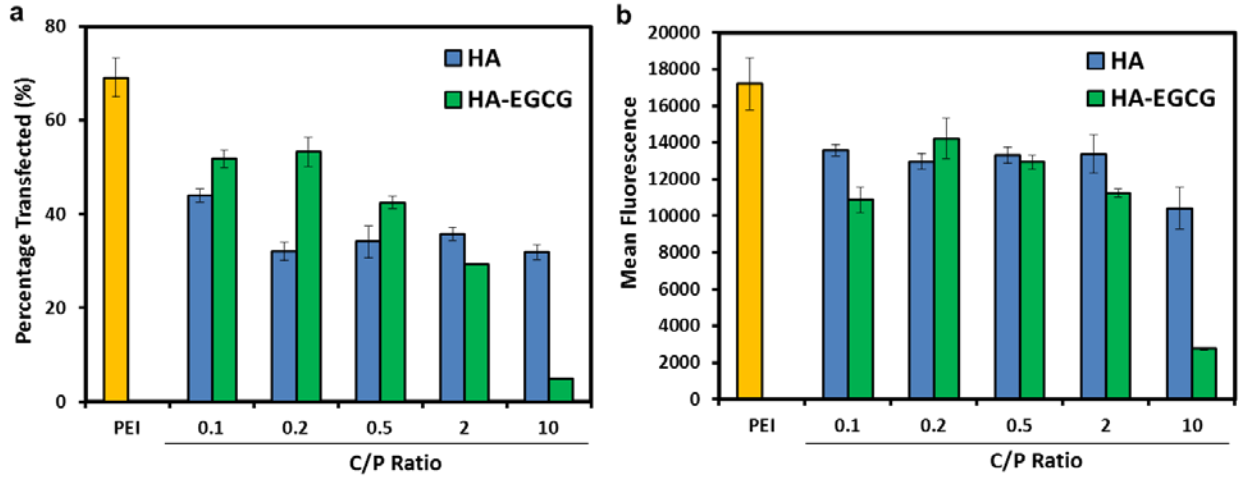

Figure 4-8. Transfection efficiency of HA-EGCG/PEI/DNA nanogel complexes in HEK293 cells with PEI/DNA binary complex at N/P ratio of 30 and HA/PEI/DNA complexes as comparison. (a) Percentage of cells successfully transfected with GFP plasmid; (b) Mean fluorescence intensity of GFP expressed in the transfected cells.

Next, the *in vitro* cytotoxicity of the complexes was assessed in both HCT-116 and HEK293 cells. We observed that HA-EGCG nanogel complexes did not result in significant

toxicity in both cell types at all the C/P ratios tested (Figure 4-9). In particular, at the optimal transfection C/P ratio of 0.5 for HA-EGCG nanogel complexes, the cell viabilities of both cell types were maintained above 80 %.

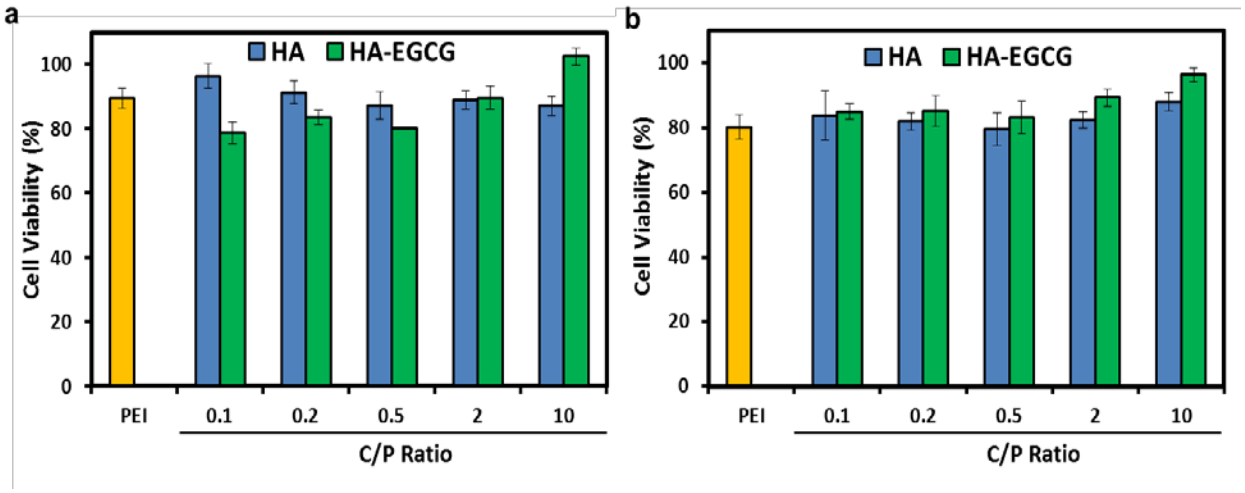

Figure 4-9. Effect of HA-EGCG/PEI/DNA nanogel complexes at the indicated C/P ratios on the cell viabilities of (a) HCT-116 and (b) HEK293 cells.

4.3.6. Cellular uptake of HA-EGCG nanogel complexes

To elucidate the effect of CD44 on cellular uptake, we incubated HCT-116 cells with various complexes containing plasmid DNA labelled with fluorescent dye - Cy 5 and observed the intracellular trafficking of complexes. Much stronger and more widespread fluorescence was observed in cells treated with HA-EGCG nanogel complex as compared to both PEI/DNA binary complex and HA complex after 1 and 4 h incubation (Figure 4-10). In addition, there was also a greater extent of nuclear (stained blue) co-localization of labelled DNA in HA-EGCG complex treated cells at 4 h. A quantitative analysis of DNA uptake by flow cytometry confirmed the visual findings (Figure 4-11 a). HA-EGCG nanogel complex demonstrated the highest mean fluorescence at both 1 and 4 h. In particular, at 4 h post-treatment the extent of uptake was 1.7 times of PEI/DNA complex and 1.3 times of HA complex. This indicates that CD44-mediated

endocytosis indeed led to increased uptake of the complexes, which in turn translated to improved transfection efficiency, as shown in (Figure 4-6 a).

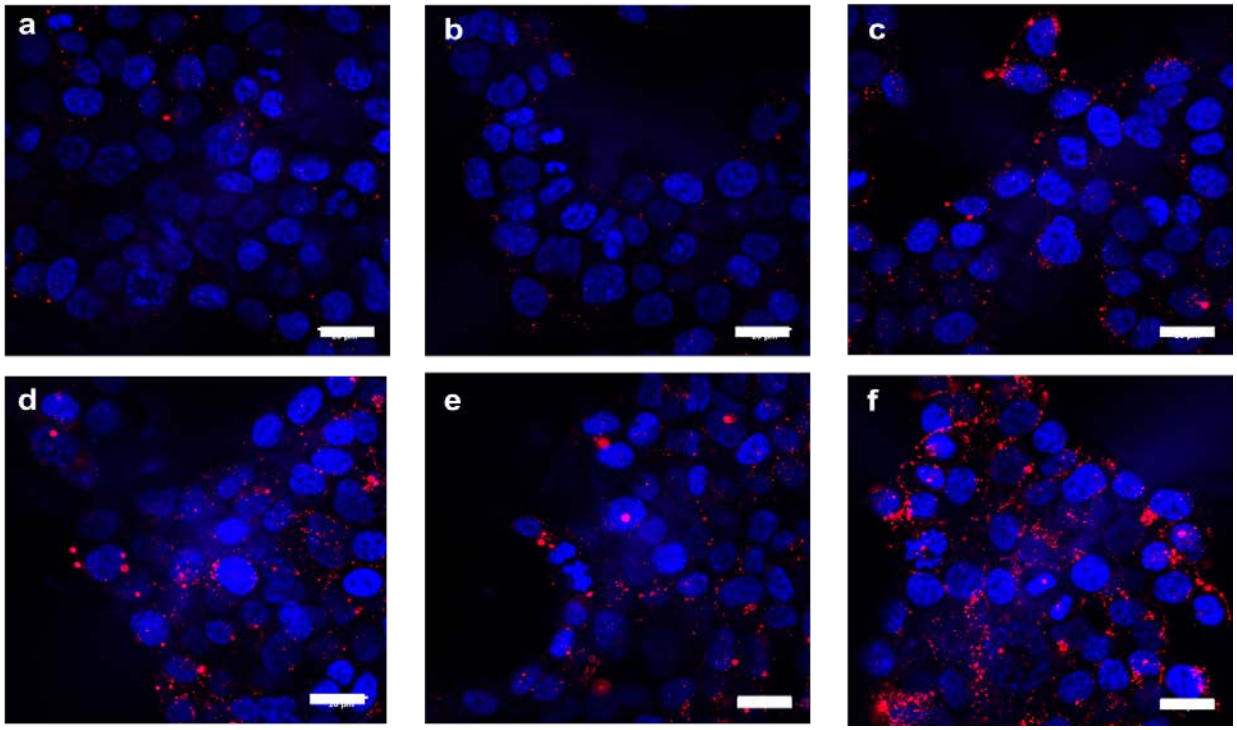

Figure 4-10. Intracellular distribution of Cy 5-labelled DNA in HCT-116 cells at 1 h (a, b, c) and 4 h (d, e, f). Images a, d represent cells treated with PEI/DNA binary complex at N/P ratio of 30; b, e represent cells treated with HA/PEI/DNA complex at C/P ratio 0.5 and c, f represent cells treated with HA-EGCG/PEI/DNA nanogel complex at C/P ratio of 0.5. Scale bar = 20 nm.

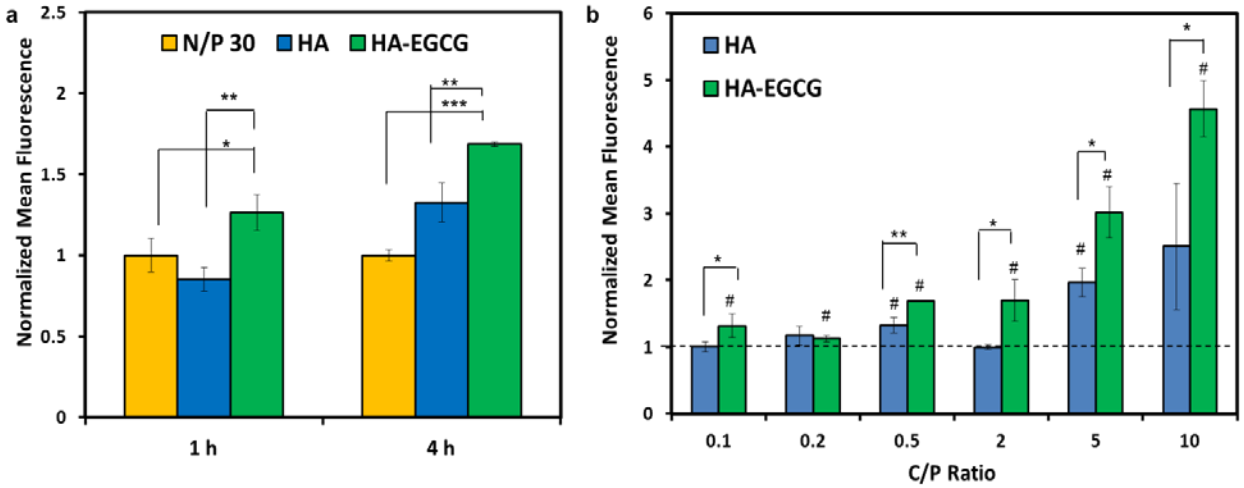

Figure 4-11. Mean fluorescence of cells treated with (a) PEI/DNA binary complex at N/P ratio of 30, HA/PEI/DNA complex and HA-EGCG/PEI/DNA nanogel complex both at C/P ratio of 0.5 at 1 and 4 h and (b) HA/PEI/DNA and HA-EGCG/PEI/DNA nanogel complexes at the indicated C/P ratios. Mean fluorescence of samples was normalized against mean fluorescence of PEI/DNA binary complex at N/P ratio of 30 at the particular time-point. # $p < 0.05$ versus PEI/DNA binary complex at N/P ratio of 30 at 4 h. * $p < 0.05$; ** $p < 0.001$, *** $p < 0.0005$.

To understand the effect of increasing HA/HA-EGCG on cellular uptake, HCT-116 cells were incubated with HA and HA-EGCG nanogel complexes containing Cy 5 labelled-DNA at different C/P ratios for 4 h and DNA internalization was subsequently evaluated by fluorescence measurements (Figure 4-11 b). We observed that internalization of HA-EGCG nanogel complexes at all C/P ratios were significantly higher than PEI/DNA binary complex at N/P ratio of 30. Furthermore, increasing HA-EGCG concentration also promoted internalization of the HA-EGCG complexes probably *via* HA receptor-mediated uptake. In particular, the uptake was enhanced by about 4-fold as C/P ratio escalated from 0.1 to 10. Interestingly, we noted that the increment in the extent of internalization of HA-EGCG nanogel complexes as a function of C/P ratio did not correlate well with the transfection results. Percentage of cells transfected reached a peak at C/P ratio 0.5 and declined drastically as C/P ratio increased to 10. This implies that another step apart from cellular uptake was impeding gene transfer. Besides efficient internalization, unpacking of DNA from complexes followed by DNA migration into nucleus are also recognized to be critical for gene delivery [37]. From the gel retardation results we noted that the HA-EGCG nanogel complexes were highly stable and resistant to heparin treatment. That is probably due to the strong interactions between HA-EGCG and PEI/DNA complex, in particular the non-covalent interactions between EGCG and DNA. Thus we hypothesize that high stability may have inhibited complex disassembly and DNA release upon internalization of the nanogel complexes, leading to decrease in transfection efficiency at higher C/P ratios. Nevertheless, we expect that the enhanced stability of HA-EGCG nanogel complexes may be beneficial for *in vivo* cancer therapy application by maintain the integrity of the complexes when they are challenged by numerous serum proteins present in the blood stream.

For HA complexes, we also observed a general increasing trend for cellular internalization as a function of increasing C/P ratios, although significant improvement over PEI/DNA binary complex NP at ratio of 30 was only observed at C/P ratios of 0.5 and 5. This suggests that the impact of CD44–mediated uptake in HA complexes was diminished compared to HA-EGCG. In addition, the cellular uptake of HA complexes was significantly lower than HA-EGCG nanogel complexes at all C/P ratios except 0.2. These observations could be attributed to the poor stability and serum compatibility of HA complexes, which may trigger complex disassembly even before encountering the HA receptors. Thus it can be concluded that in comparison to HA complexes, higher stability of HA-EGCG nanogel complexes facilitated more efficient uptake by CD44-mediated endocytosis, thereby contributing to enhancement in gene delivery efficiency.

4.4. Conclusion

We have demonstrated an efficient method to deliver DNA into CD44 overexpressing cancer cells specifically using HA-EGCG nanogel complex. Self-assembled HA-EGCG/PEI/DNA nanogel complexes were prepared by simple mixing. Strong interactions between HA-EGCG and PEI/DNA gave rise to increased stability of complexes. At the optimal HA-EGCG to PEI charge ratios, these nanogel complexes achieved significant enhancement in gene transfection than PEI/DNA binary complexes and HA/PEI/DNA complexes in CD44 overexpressing HCT-116 cancer cells. The improvement in transfection was attributed to increased cellular uptake imparted by CD44-mediated endocytosis. High stability of the nanogel complexes also facilitated efficient internalization and gene transfer in serum existing condition. Since the HA-EGCG nanogel complexes successfully mediated targeted delivery of DNA to CD44 overexpressing cancer cells, we expect that this carrier could also enable the delivery of suicide genes to eradicate these cells specifically. This makes HA-EGCG nanogel complex a promising candidate for targeted cancer therapy.

References

1. Mujoo, K., et al., *Adenoviral-mediated p53 tumor suppressor gene therapy of human ovarian carcinoma.* Oncogene, 1996. **12**(8): p. 1617-1623.
2. Nielsen, L.L. and D.C. Maneval, *P53 tumor suppressor gene therapy for cancer.* Cancer gene therapy, 1997. **5**(1): p. 52-63.
3. Liu, F. and L. Huang, *Development of non-viral vectors for systemic gene delivery.* Journal of Controlled Release, 2002. **78**(1): p. 259-266.
4. Wagner, E. and J. Kloeckner, *Gene delivery using polymer therapeutics,* in *Polymer Therapeutics I*. 2006, Springer. p. 135-173.
5. Thomas, C.E., A. Ehrhardt, and M.A. Kay, *Progress and problems with the use of viral vectors for gene therapy.* Nature Reviews Genetics, 2003. **4**(5): p. 346-358.
6. Godbey, W.T., K.K. Wu, and A.G. Mikos, *Poly(ethylenimine) and its role in gene delivery.* Journal of Controlled Release, 1999. **60**(2–3): p. 149-160.
7. Boussif, O., et al., *A versatile vector for gene and oligonucleotide transfer into cells in culture and in vivo: polyethylenimine.* Proceedings of the National Academy of Sciences, 1995. **92**(16): p. 7297-7301.
8. Moghimi, S.M., et al., *A two-stage poly (ethylenimine)-mediated cytotoxicity: implications for gene transfer/therapy.* Molecular Therapy, 2005. **11**(6): p. 990-995.
9. Fischer, D., et al., *In vitro cytotoxicity testing of polycations: influence of polymer structure on cell viability and hemolysis.* Biomaterials, 2003. **24**(7): p. 1121-1131.
10. Dash, P., et al., *Factors affecting blood clearance and in vivo distribution of polyelectrolyte complexes for gene delivery.* Gene therapy, 1999. **6**(4).
11. Ogris, M., et al., *The size of DNA/transferrin-PEI complexes is an important factor for gene expression in cultured cells.* Gene therapy, 1998. **5**(10).
12. Sharma, V.K., M. Thomas, and A.M. Klibanov, *Mechanistic studies on aggregation of polyethylenimine-DNA complexes and its prevention.* Biotechnology and bioengineering, 2005. **90**(5): p. 614-620.
13. Kircheis, R., L. Wightman, and E. Wagner, *Design and gene delivery activity of modified polyethylenimines.* Advanced Drug Delivery Reviews, 2001. **53**(3): p. 341-358.
14. Kichler, A., *Gene transfer with modified polyethylenimines.* The journal of gene medicine, 2004. **6**(S1): p. S3-S10.
15. Pun, S.H., et al., *Cyclodextrin-modified polyethylenimine polymers for gene delivery.* Bioconjugate Chemistry, 2004. **15**(4): p. 831-840.
16. Morille, M., et al., *Progress in developing cationic vectors for non-viral systemic gene therapy against cancer.* Biomaterials, 2008. **29**(24–25): p. 3477-3496.
17. Necas, J., et al., *Hyaluronic acid (hyaluronan): a review.* Veterinarni medicina, 2008. **53**(8): p. 397-411.
18. Laurent, T.C. and J. Fraser, *Hyaluronan.* The FASEB Journal, 1992. **6**(7): p. 2397-2404.
19. Ossipov, D.A., *Nanostructured hyaluronic acid-based materials for active delivery to cancer.* Expert Opinion on Drug Delivery, 2010. **7**(6): p. 681-703.
20. Sy, M.S., et al., *Interactions Between CD44 and Hyaluronic Acid: Their Role in Tumor Growth and Metastasis,* in *Attempts to Understand Metastasis Formation III*, U. Günthert, P. Schlag, and W. Birchmeier, Editors. 1996, Springer Berlin Heidelberg. p. 129-153.

21. Bartolazzi, A., et al., *Interaction between CD44 and hyaluronate is directly implicated in the regulation of tumor development.* The Journal of experimental medicine, 1994. **180**(1): p. 53-66.
22. Oh, E.J., et al., *Target specific and long-acting delivery of protein, peptide, and nucleotide therapeutics using hyaluronic acid derivatives.* Journal of Controlled Release, 2010. **141**(1): p. 2-12.
23. Choi, K.Y., et al., *Hyaluronic acid-based nanocarriers for intracellular targeting: interfacial interactions with proteins in cancer.* Colloids and Surfaces B: Biointerfaces, 2012. **99**: p. 82-94.
24. Sun, X., et al., *Positive hyaluronan/PEI/DNA complexes as a target-specific intracellular delivery to malignant breast cancer.* Drug delivery, 2009. **16**(7): p. 357-362.
25. Hornof, M., et al., *Low molecular weight hyaluronan shielding of DNA/PEI polyplexes facilitates CD44 receptor mediated uptake in human corneal epithelial cells.* The journal of gene medicine, 2008. **10**(1): p. 70-80.
26. Wang, Y., et al., *A facile approach to construct hyaluronic acid shielding polyplexes with improved stability and reduced cytotoxicity.* Colloids and Surfaces B: Biointerfaces, 2011. **84**(1): p. 259-266.
27. Ito, T., et al., *DNA/polyethyleneimine/hyaluronic acid small complex particles and tumor suppression in mice.* Biomaterials, 2010. **31**(10): p. 2912-2918.
28. Ghosh, K.S., B.K. Sahoo, and S. Dasgupta, *Spectrophotometric studies on the interaction between (−)-epigallocatechin gallate and lysozyme.* Chemical Physics Letters, 2008. **452**(1): p. 193-197.
29. Maiti, T.K., K.S. Ghosh, and S. Dasgupta, *Interaction of (−)-epigallocatechin-3-gallate with human serum albumin: Fluorescence, fourier transform infrared, circular dichroism, and docking studies.* Proteins: Structure, Function, and Bioinformatics, 2006. **64**(2): p. 355-362.
30. Zheng, X., et al., *Electrochemical studies of (−)-epigallocatechin gallate and its interaction with DNA.* Analytical and bioanalytical chemistry, 2006. **386**(6): p. 1913-1919.
31. Lee, F., et al., *Synthesis and bioactivity of conjugate composed of green tea catechin and hyaluronic acid; In preparation.*
32. Kuo, J.W., D.A. Swann, and G.D. Prestwich, *Chemical modification of hyaluronic acid by carbodiimides.* Bioconjugate Chemistry, 1991. **2**(4): p. 232-241.
33. Homma, A., et al., *Novel hyaluronic acid–methotrexate conjugates for osteoarthritis treatment.* Bioorganic & Medicinal Chemistry, 2009. **17**(13): p. 4647-4656.
34. Luo, X.-h., et al., *A strategy to improve serum-tolerant transfection activity of polycation vectors by surface hydroxylation.* Biomaterials, 2011. **32**(36): p. 9925-9939.
35. Ito, T., et al., *Hyaluronic acid and its derivative as a multi-functional gene expression enhancer: Protection from non-specific interactions, adhesion to targeted cells, and transcriptional activation.* Journal of Controlled Release, 2006. **112**(3): p. 382-388.
36. Godbey, W., K.K. Wu, and A.G. Mikos, *Tracking the intracellular path of poly (ethylenimine)/DNA complexes for gene delivery.* Proceedings of the National Academy of Sciences, 1999. **96**(9): p. 5177-5181.
37. Pack, D.W., et al., *Design and development of polymers for gene delivery.* Nature Reviews Drug Discovery, 2005. **4**(7): p. 581-593.

Chapter 5: Conclusions and Future Directions

5.1. Conclusions

With the advent of nanotechnology, we have witnessed immense progress in the design of DDS for anticancer drugs. However, out of the many DDS reported in literature, few have been successfully translated into clinical therapies. Some of the limitations include lack of treatment efficacy and toxic side effects, which may arise as a result of failure to achieve optimal stability. Intermolecular interactions between the carrier and therapeutic cargo play a key role in influencing the stability of DDS. Green tea catechin, EGCG has the ability to interact with variety of bioactive molecules. Thus the objective of my thesis is to develop polymeric carriers based on EGCG for cancer therapy. Three different types of payloads were investigated – small molecule drug, Dox, cytotoxic protein GzmB as well as DNA. Two different EGCG based conjugate designs – PEG-EGCG and HA-EGCG were synthesized for the delivery of these payloads. In this thesis, the polymeric carriers were characterized extensively and evaluated in terms of their delivery efficiency.

In Chapter 2, the formation of Dox-loaded PEG-EGCG micelles for tumor delivery was reported. Strong interactions between EGCG and Dox facilitated the formation of highly stable, nanosized micelles with a remarkably high drug loading capacity (~ 86 %). As a result of the high stability and minimal drug leakage in circulation, Dox-loaded PEG-EGCG micelle demonstrated reduced toxicity *in vivo* and a much elevated maximum tolerated dose compared to two clinically relevant Dox formulations - Dox and DOXIL. Most notably, Dox-loaded PEG-EGCG micelle at 50 mg/kg achieved greater significant tumor growth inhibition as compared to optimal dosages of both Dox and DOXIL. This demonstrated that PEG-EGCG micelle can provide for an effective and safe carrier to deliver Dox for cancer therapy.

In Chapter 3, HA-EGCG conjugates were utilized for the targeted cancer cell eradication by intracellular delivery of the cytotoxic protein GzmB. Nanogel complexes comprising HA-EGCG and GzmB were prepared based on self-assembly in aqueous solution, triggered by the interactions between EGCG moieties and GzmB. The nanogel complexes demonstrated targeted toxicity against CD44 overexpressing HCT-116 colon cancer cells. The toxicity was due to GzmB mediated apoptosis, thus confirming the successful delivered GzmB into the cytoplasm of the cancer cells.

Besides small molecule drug and protein, EGCG could also interact favorably with DNA. Thus HA-EGCG conjugates were employed for the targeted intracellular delivery of DNA to cancer cells in Chapter 4. HA-EGCG nanogel complexes achieved significant enhancement in gene transfection than PEI/DNA binary complexes and HA complexes in CD44 overexpressing HCT-116 cancer cells. The improvement in transfection was attributed to increased cellular uptake imparted by CD44-mediated endocytosis. High stability of the nanogel complexes also facilitated efficient internalization and gene transfection.

In summary, this thesis has clearly demonstrated that our design of EGCG based polymeric carriers could be used for the efficient and safe delivery of various types of drugs. These carriers provide a novel strategy in advancing cancer therapy.

5.2. Future Directions

- In Chapter 2 we observed that highly stable DOX-loaded PEG-EGCG micelles could inhibit tumor growth at elevated dosages without side effects. While high stability was advantageous in reducing leakage and nonspecific toxicity during circulation, it also inhibited free drug liberation upon carrier extravasation into the tumor vasculature,

contributing to poor antitumor activity. Hence, engineering tumor environment-responsive Dox-loaded PEG-EGCG micelle is a useful strategy worth examining. Such a micelle carrier design could allow the triggered release of the drug once it has reached the tumor site. Many stimuli specific to the tumor environment have been identified. In particular, pH-responsive polymeric drug carriers, which could degrade in the acidic pH of the extracellular tumor environment, have been studied extensively. With respect to the PEG-EGCG conjugates, a pH-sensitive linker can be introduced in between PEG chain and EGCG moiety to facilitate micelle disintegration and on-site drug release. Such pH-responsive PEG-EGCG carriers have great potential to realize the ideal goal of tumor site specific delivery for cancer therapy.

- Thus far we have examined the intracellular delivery of protein and DNA by HA-EGCG nanogel complexes *in vitro*. For practical cancer therapy applications, it is imperative to evaluate the therapeutic efficacy of this nanogel carrier using *in vivo* tumor models. One possible issue that may arise in the process of systemic administration is the preferential uptake of HA in organs such as the liver, where abundant HA receptors are expressed. To overcome this potential problem, the surface of the HA-EGCG nanogel complex could be appropriately PEGylated. It has been well-documented that PEG can impart a steric hindrance effect to repel attachment of proteins and other molecules, thus reducing the uptake and accumulation at liver site. In our experiment setting, the desired PEG surface coating may be achieved by adding various amounts of PEG-EGCG conjugates to the HA-EGCG nanogel complexes. These PEGylated nanogel complexes may provide a solution for bringing forward the *in vitro* delivery efficacy to *in vivo* therapeutic outcome.